FINAL REPORT

Mobile Platform III: Characterizing Spatially Inhomogeneous Non-Criteria Pollutants in the Los Angeles Air Basin

Principal Investigator:
S.E. Paulson
[a]Dept. of Atmospheric and Oceanic Sciences
405 Hilgard Ave., University of California, Los Angeles, CA 90095-1565, USA.
(310)206-4442. Fax: (310)206-5219. paulson@atmos.ucla.edu.

Co-Principal Investigator:
A.M. Winer[b]

Lead Researcher:
W. Choi[a]

Researchers:
M. He[c]
V. Barbesant[a,d]
S. Hu[e]
K.H. Kozawa[e]
S. Mara[e]

[b]Environmental Health Sciences Department, School of Public Health, 650 Charles E. Young Drive South, University of California, Los Angeles, CA 90095-1772.
[c]Now at: Department of Mechanical and Aeronautical Engineering, Clarkson University, Potsdam, NY.
[d]Department of Mechanics, Ecole Polytechnique, 91128 Palaiseau Cedex, France.
[e]California Air Resources Board, Research Division, 1001 I St., Sacramento, CA 95814.

November 2012

Table of Contents

1.0 List of Tables

2.0 List of Figures

3.0 List of Abbreviations

ARB	Air Resources Board
BH	Boyle Heights
CO	Carbon Monoxide
CARB	California Air Resources Board
CART	Classification and Regression Tree
CPC	Condensation particle sizer
DoLA, DTLA	Downtown Los Angeles
EPA	Environmental Protection Agency
FMPS	Fast mobility particle sizer
GIS	Global Information System
GPS	Global Positioning System
HDDT	Heavy Duty Diesel Truck
HEV	High emitting vehicles
HEGV	High emitting gasoline vehicles
LAX	Los Angeles International Airport
KS	Kolmogorov-Smirnov
MMP	Mobile Measurement Platform
NCEP	National Centers for Environmental Prediction
NO	Nitric Oxide
NO_x	Oxides of Nitrogen
PAH	Poly Aromatic Hydrocarbons
PAS	Photoelectric Aerosol Sensor
PB	Particle Bound
PeMS	Freeway Performance Measurement System
PIU	Particle Instrumentation Unit, located in downtown Los Angeles
PM2.5	Particulate matter mass for particles smaller than 2.5 µm
PNEF	Particle Number Emission Factor
R_i	Richardson Number
SoCAB	South Coast Air Basin
SCAQMD	South Coast Air Quality Management District
SMA, SMO	Santa Monica Airport
UCLA	University of California at Los Angeles
UFP	ultrafine particles
WLA	West Los Angeles
WD_{rel}	Wind Direction Relative to a Reference Point

4.0 Abstract

A number of epidemiological studies have shown that exposure to elevated levels of fresh vehicular emissions causes a wide range of adverse human health effects. Fresh vehicular emissions contain a wide range of particle- and gas-phase species. Because such emissions are emitted and diluted together, their individual impacts are difficult to separate. Ultrafine particles (UFP) might contribute to the degradation of health associated with exposure to elevated levels of fresh vehicular emissions, but they are also an excellent tracer for fresh vehicle emissions, and are one of the foci of this study.

In urbanized areas, a large fraction of households are commonly located near freeways. In a highly urbanized area such as the California South Coast Air Basin (SoCAB), approximately 50% of the population lives within 1.5 km of freeways. An earlier mobile measurement platform study under the direction of Drs. Winer and Paulson demonstrated a large pollutant impact zone, extending beyond 2.5 km downwind of a freeway in Santa Monica, California during pre-sunrise hours.

The current study explores the variability of extended freeway plumes at several locations in Southern California. The ARB mobile measurement platform (MMP) was employed to measure vehicle-related pollutant concentrations on transects running upwind and downwind perpendicular to four freeway segments in the coastal, central and eastern areas (downtown Los Angeles, Paramount, Carson and Claremont) of the California South Coast Air Basin (SoCAB) during the pre-sunrise period (04:30-06:30).

Extended freeway plumes were observed for ultrafine particles, nitric oxide and particle-bound polycyclic aromatic hydrocarbons (PAH), at all four sites during stable pre-sunrise periods. Plume lengths were measured to be ~2 km or more with a dilution rate coefficient about a factor of ten lower than commonly observed for daytime. An average of 39 and 19% (±8–9%) of freeway plume peak concentrations of UFP remained 500 and 1500 m downwind from the freeways, respectively, for the four transects studied here. Because a large fraction of UFP and other vehicle related pollutants typically penetrate into indoor environments, and nocturnal surface inversions are widespread across the globe, our findings have significant implications for more extensive human exposures to vehicle-related pollutants than previously indicated based on daytime measurements of roadway plumes.

Factors controlling pollutant plume length downwind of freeways under stable conditions were background-subtracted peak concentration (which is a function of traffic flows and temperature) as well as meteorological parameters, such as wind direction and speed. Vertical stability (Richardson number) plays a minor role in dispersion coefficient variations within stable boundary layer conditions. A curve fit using a Gaussian dispersion model solution described excellently the observed UFP profiles both at the peak and far downwind (> 2 km) with R^2 ~0.9 or larger for all measurement sites.

The measurements of detailed plume shapes offer several additional insights about the details of pollutants near roadways. The geometry of the intersection of the secondary roadway (or, presumably, other components of the built environment) with the freeway geometry is an important parameter controlling the position of the plume peak concentration. The maximum concentration of the pollutant plume is closer to the centerline of the freeway if the freeway passes under the roadway, and it moves further downwind, by about 100 m, if the freeway passes above the secondary road. In the second case, the maximum concentration also tends to be lower.

Particle size is a factor in health impacts because it determines how much and where airway deposition occurs. As particles are diluted, they also undergo coagulation, deposition, evaporation and/or condensation. We explore the interplay of these factors, and demonstrate that as particle size decreases, UFP decay rates increase with distance from freeway.

Mobile measurement platform measurements are by their nature conducted at single places and times and thus are challenging to compare. With an aim toward making comparisons quantitative, we have developed an objective and systematic classification scheme of meteorological conditions affecting atmospheric primary pollutant levels in the (SoCAB). The method used is a classification and regression tree (CART) modeling approach. Previous CART approaches have been applied to secondary pollutants such as ozone. Here, we develop regression trees to predict the levels of traffic-related primary air pollutants such as NO and CO, based on combined upper air and surface meteorological conditions for 2007–09. The resulting regression trees perform well, providing excellent correlations between the regression classifications developed for different primary pollutant metrics, such as daily CO and NO maxima, as well as between monitoring sites. The spatial variations in primary pollutant concentrations between East-West monitoring sites in the SoCAB are more significant than those between North-South monitoring sites. The regression trees indicate these East-West variations are at least partly caused by Santa Ana Winds during winter and spring seasons. The meteorological parameters that determine the variability in primary pollutant concentrations, in approximate order of importance, are the mean surface wind speed, geopotential heights at 925 mbar, the upper air north-south pressure gradient, the daily minimum temperature, relative humidity at 1000 mbar, and vertical stability.

Here we apply the CART analysis to an inter-comparison of MMP measurements collected in several locations and times within Southern California. Daytime UFP concentrations in neighborhoods showed strong inter-community variations between West Los Angeles (1.1×10^4 particles·cm^{-3}), downtown Los Angeles (2.2×10^4 particles·cm^{-3}) and Boyle Heights (3.3×10^4 particles·cm^{-3}) in 2008. Intra-community pollutant variations were less intense but significant as an air mass experiences emissions from major freeways (I-405 and I-10).

Pollutant concentrations including UFP were highly elevated in close proximity to major freeways, as well as Santa Monica Airport. Impacts of high emitting vehicles on UFP distributions both on arterial roadways and in neighborhoods were also significant. About 70% reductions of UFP and $PM_{2.5}$ were observed during the I-405 closure event (so called "Carmageddon") in 2011 with 20 - 85% decreases in nearby traffic flows in West Los Angeles.

Several lines of evidence point to the reduction in fleet averaged per-vehicle ultrafine particle emissions. By fitting freeway plumes using a formulation of the Gaussian plume dispersion model together with traffic data, we estimated a particle number emission factor of 7.5×10^{13} particles·vehicle^{-1}·km^{-1}, about one seventh of an estimate for nearby freeways made in 2001 in the published literature. For measurements in neighborhoods and on the freeways and arterials in West and downtown Los Angeles, ultrafine particle concentrations declined by between 10 and 70% between 2008 and 2011, depending on the location (neighborhood interiors, arterials, freeways etc.) and the contribution of high emitters. These comparisons demonstrate in-use motor vehicle UFP concentrations have significantly declined and suggest in-use motor vehicle emissions in general have declined as well.

5.0 Executive Summary

The project described here is comprised of a detailed analysis of plumes from freeways that occur in the early morning. Additionally a statistical approach to compare measurements made at different locations and times is developed. Finally, the comparison of primary pollutant concentrations in several neighborhoods within the Los Angeles area is presented.

Because a large fraction of UFP and other vehicle related pollutants typically penetrate into indoor environments [1], and nocturnal surface inversions are widespread across the globe, our findings have significant implications for more extensive human exposures to vehicle-related pollutants than previously indicated based on daytime measurements of roadway plumes.

5.1 Presunrise

Pre-sunrise (or nocturnal) extension of freeway plumes occurs far downwind (> 2 km) compared to daytime plume length (<300 m). This study showed this is a general phenomenon in California's South Coast Air Basin (SoCAB) and explored the variability of the large downwind pollutant impact zone observed by Hu et al. [2] in the pre-sunrise hours on a wider geographic scale.

Transect measurements using the instrumented mobile measurement platform (MMP) were conducted for pre-sunrise hours (04:30–06:30) at four different locations, each aligned as close to perpendicular as possible to straight sections of freeway: Downtown LA (101 freeway), Paramount (91 freeway), Carson (I-110 freeway), and Claremont (I-210 freeway) during the winter and early summer seasons (Table 1, Figure 1).

Table 1. Summary of the location of sampling transects and freeways, and measurement periods.

Transect street	Location	Freeway (Lat./Lon.)	Freeway over /under transect	Distance from coast / length	Sampling period (2011)
Coronado	Downtown LA	101 (34.074N /118.272W)	Over-pass	~ 22 km / 1.2 km up-2.2 km / downwind	2/24, 3/9, 3/14, 3/17
Obispo	Paramount	91 (33.877N /118.156W)	Over-pass	~ 13 km / 2 km up-1.8 km downwind	1/27, 2/1, 3/10, 3/18
228th	Carson	I-110 (33.819N /118.287W)	Under-pass	~ 6 km / 1.3 km up-2.2 km downwind	1/21, 2/3/ 3/8, 3/11, 3/29
Mountain	Claremont	I-210 (34.120N /117.729W)	Under-pass	~ 70 km / 0.8 km up-2.6 km downwind	5/19, 5/24, 5/25, 5/26, 6/1, 6/2, 6/7

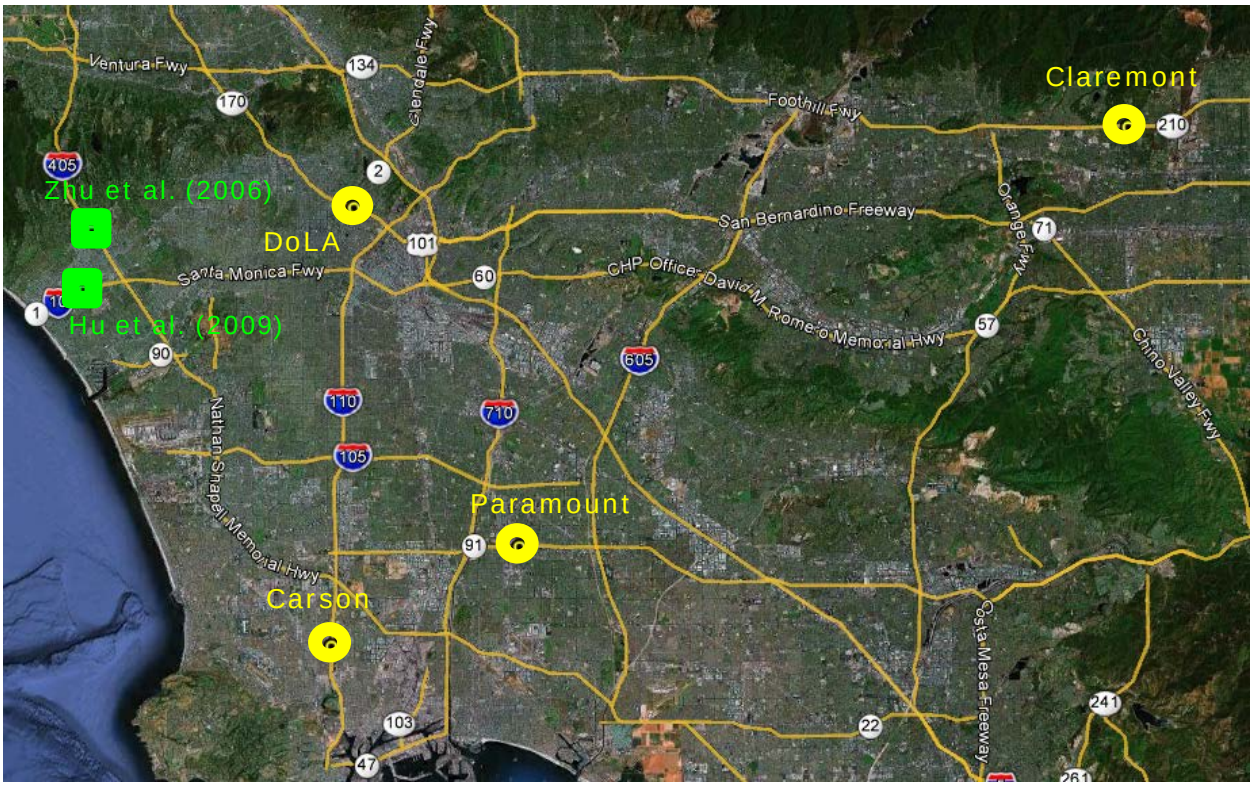

Figure 1. Map of transects where pre-sunrise measurements were conducted in the South California Air Basin (SoCAB). Yellow circles indicate the location of transects in this study and green squares denote the location of previous studies conducted by Zhu et al. (2002; 2006) in West LA and Hu et al. [2] in Santa Monica. Google Earth map. Additional measurements were made during 2011 surrounding the 405 closure as part of this study.

Extended freeway plumes were observed for ultrafine particles (UFP), nitric oxide and particle-bound polycyclic aromatic hydrocarbons (PAH), at all four sites during stable pre-sunrise periods. Plume lengths were measured to be ~2 km or more with a dilution rate coefficient about a factor of ten lower than commonly observed for daytime.

Figure 2 shows several interesting features of UFP spatial profiles. First, significant extensions of freeway plumes compared to daytime length were observed at all four locations, consistent with the results first reported by Hu et al. [2] in Santa Monica. Thus, our results confirm that pre-sunrise extension of freeway plumes (>2 km) is a common phenomenon, at least from the coastal plain to inland valleys in the SoCAB. An average of 39 and 19% (±8–9%) of freeway plume peak concentrations of UFP remained 500 and 1500 m, respectively downwind from the freeways for the four transects studied here.

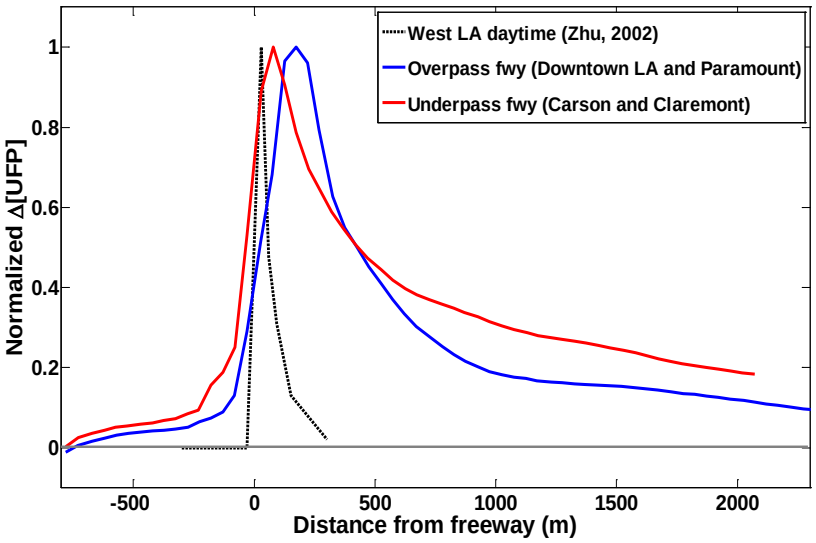

Figure 2. Variations in background-subtracted UFP concentrations with respect to distance from the freeway. Values are smoothed after being normalized to peak concentrations. The blue line: mean concentration profiles of overpass freeways (the Downtown LA and Paramount transects); red line: mean profiles of underpass freeways (the Carson and Claremont transects); black dashed line: daytime observations in West LA reported by Zhu et al.[3]. The horizontal gray solid line represents upwind background concentrations. Negative and positive distance indicates upwind and downwind locations, respectively.

Second, the peak concentrations of pollutant plumes for overpass freeways were located at farther distance downwind from freeways compared to underpass freeways. We attribute these differences to different patterns of plume transport. For overpass freeways (6–8 m above the ground), it takes time for the freshly emitted plume to reach the ground and hence, a more diluted plume was encountered in the ground. In contrast, the instruments immediately experience a freeway plume freshly emitted below when the MMP crosses over a freeway (Underpass freeway, Figure 3).

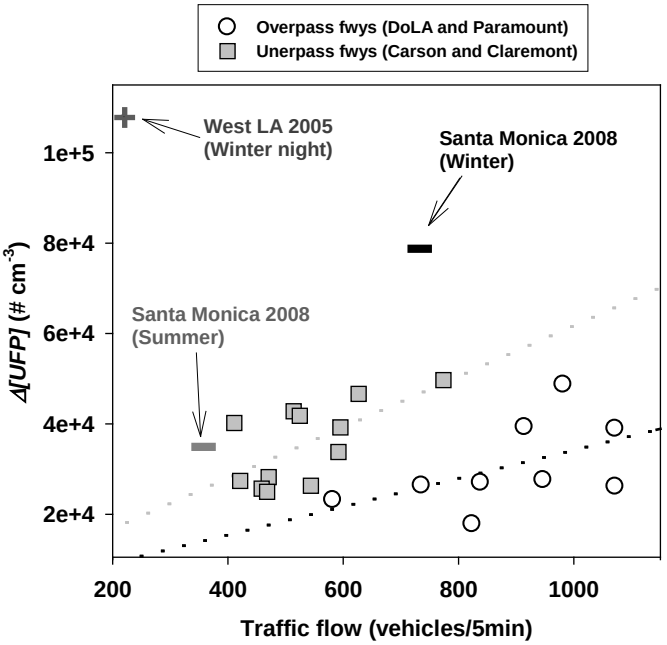

Figure 3. Net UFP concentrations from freeway emissions as a function of traffic flow on freeways. Black circles denote daily average data for overpass freeways (DoLA and Paramount), and gray squares represent data for underpass freeways (Carson and Claremont). Gray and black dashed lines are linear fits for gray squares and black circles, respectively. Black and gray thick horizontal bars are the averaged values observed for the 2008 Santa Monica winter and summer seasons, respectively [2]. The cross shows the averaged nighttime data for the 2005 West LA winter night period [4].

Third, the plume decay rate with distance from freeways was much slower under pre-sunrise conditions than those of daytime with one order of magnitude smaller decay rate constant near the freeway (<700m downwind from the freeway). The decay rate constant, *K(x)* was obtained using exponential fit, $e^{-K(x)}$. Estimated *K(x)* ranged 0.0014–0.0033 for the four transects in this study, which were comparable to Santa Monica measurements [2] in 2008 (0.0014 for winter and 0.0021 for summer) and one order of magnitude smaller than daytime constant (0.011) of West LA in 2001 [3]. In addition, we did not find seasonal variations in *K(x)*; the smallest *K(x)* was observed in May–June in Claremont.

5.2 Mathematical Description of Early Morning Plumes

A curve fit method using a Gaussian dispersion model solution (Eq. 1) was successfully applied to obtain both the dispersion coefficients and particle number emission factor (PNEF) directly from ultrafine particle (UFP) concentration profiles observed downwind of major roadways in the SoCAB for pre-sunrise hours. The best fit curves and range of pollutant concentrations are shown in Figure 4. For all four transects, curve fits describe well the observed profiles of UFP number concentrations both at the peak and far downwind (R^2 ~0.9 or larger) (Figure 4). The Briggs' formulation for vertical dispersion parameter σ_z (Eq. 2) was adopted in this study due to the better performance among others examined in describing the observed profiles.

$$C(x,z) = \frac{Q_c}{\sigma_z}\left[\exp\left(-\frac{(z+H)^2}{2\sigma_z^{\,2}}\right) + \exp\left(-\frac{(z-H)^2}{2\sigma_z^{\,2}}\right)\right] \quad \text{(Eq. 1)}$$

$$\sigma_z(x) = \frac{\alpha \cdot x}{1+\beta \cdot x} \quad \text{(Eq. 2)}$$

Where C is the concentration, z is height, H is the height of emission source, σ_z is the standard deviations of the time-averaged concentration distributions in the vertical directions at distance x from the source, and α and β are free variables described below. In Eq. (1), Q_c is a wind speed-corrected emission rate. The mean particle number emission factor (PNEF) estimated from this expression for the mixed fleets containing less than 3–5 % trucks on observed freeways was 7.5×10^{13} particles·vehicles^{-1}·km^{-1}. This estimated PNEF is just ~15% of that (5.2×10^{14} particles·vehicles^{-1}·km^{-1}) previously estimated for I-405 (with similar truck contribution) in 2001 by Zhu et al. [5], supporting the notion that the UFP emissions and concentrations are dropping dramatically.

A curve fit using a Gaussian dispersion model solution described excellently the observed UFP profiles both at the peak and far downwind (> 2 km) with R^2 ~0.9 or larger for all measurement sites. Estimated particle number emission factor (PNEF) using a curve fit method was 7.5×10^{13} particles·vehicle^{-1}·km^{-1}, which is 7 times smaller than an estimate (5.2×10^{14} particles·vehicle^{-1}·km^{-1}) made in 2001 for the I-405 freeway by Zhu et al. [5].

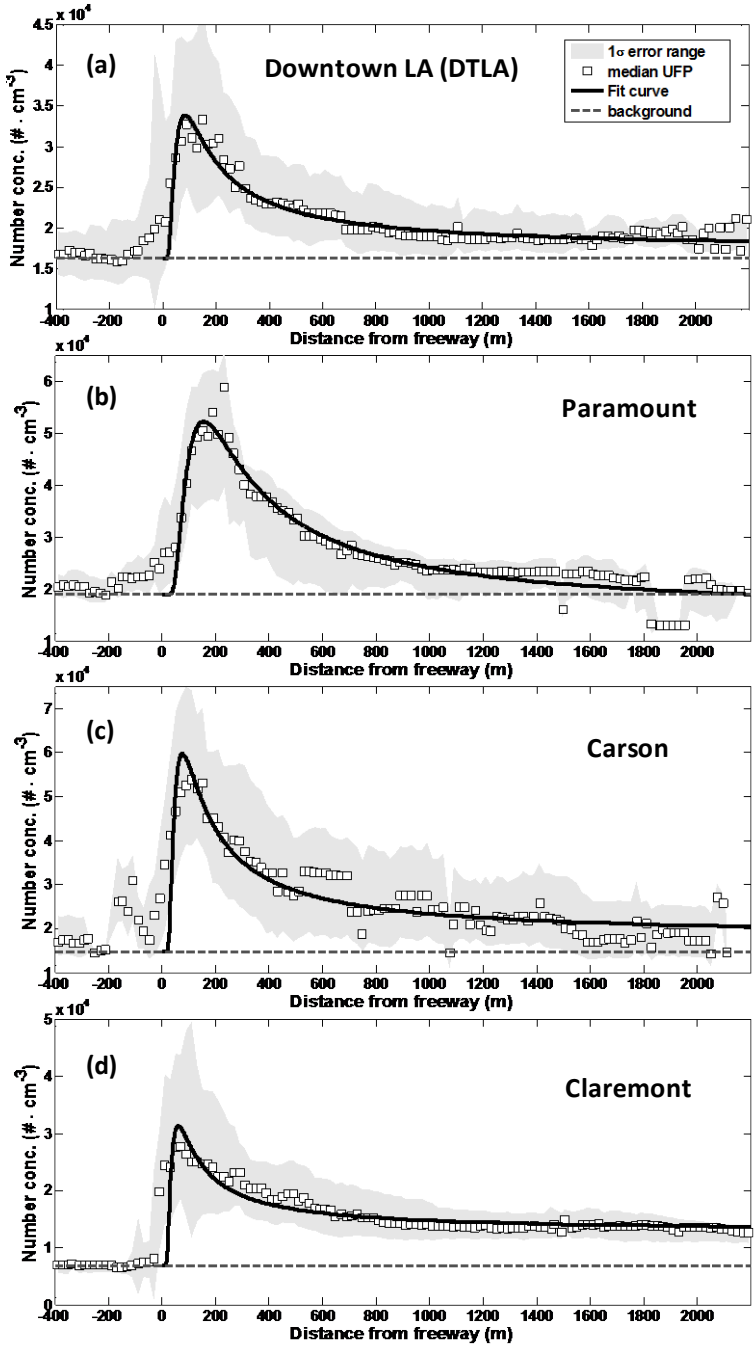

Figure 4. Observed median UFP number concentrations with distance downwind of freeways (white squares), 1σ error ranges (gray areas), upwind background concentrations (horizontal dark gray dashed lines), and curve fits to the observations with Gaussian dispersion model form (black lines) for (a) the Downtown Los Angeles, (b) Paramount, (c) Carson, and (d) Claremont transects.

Dispersion coefficients, α and β (Eq. 2) showed a strong positive correlation with respect to freeway geometry (underpass vs. overpass freeways) (Figure 5), which suggests overlap in the factors controlling α and β. α is related to the peak position and plume width (advection), and β to plume dilution rates (eddy diffusion or entrainment). Based on above findings, we can hypothesize that a positive correlation between α and β was caused by (1) meteorological conditions (advection and turbulence; *hypothesis 1*) and/or (2) plume intensity (*hypothesis 2*).

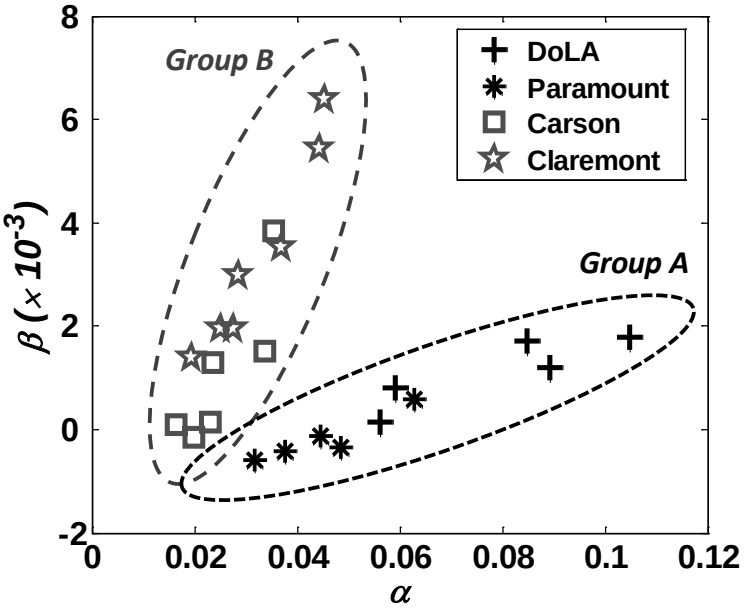

Figure 5. Relationship between α and β obtained from the curve fits to daily mean spatial profiles of UFP in the DoLA (black crosses), Paramount (black asterisks), Carson (gray squares), and Claremont (gray stars) transects. Black dotted line represents a group A, where freeways overpass the transects and gray dashed line a group B, where freeways pass under the transects.

Hypothesis 1 emphasizes the role of wind speeds and directions in determining α and β, and hence plume decay rates, stating that faster winds perpendicular to the freeway transport a plume more effectively (smaller α) under stable conditions. At the same time, stronger turbulence caused by faster winds disperses pollutant more rapidly (smaller β). Indeed, we found meaningful relationships between wind direction and vector averaged wind speeds vs. α. Nonetheless, stronger relationships were found between dispersion coefficients vs. background-subtracted UFP peak concentrations and temperature (Figure 6). These stronger relationships suggest an importance of hypothesis 2 in controlling dispersion coefficients, and hence a plume length. *Hypothesis 2* states more intensive plumes tend to have smaller α and β because dilution rate in a plume is a function of both dilution coefficient and concentration differences from the background [6]. A strong positive correlation between ambient temperature and α supports this hypothesis in that lower temperature leads to higher UFP emissions [7, 8]. Nonetheless, faster decay does not necessarily mean smaller impact of pre-sunrise freeway plume, because the plume magnitude is more intensified under conditions with faster decay rates.

From strong correlations of Q_c, α and β with surface wind speeds/directions, temperature, and traffic density, this curve fit method provides a potential to parameterize those plume parameters and ultimately, to predict them under stable pre-sunrise conditions using statistical tools such as multivariate regressions. However, more observation data are needed for a definite conclusion, because freeway interchange geometry alters the effects of meteorology and traffic flows on plume parameters.

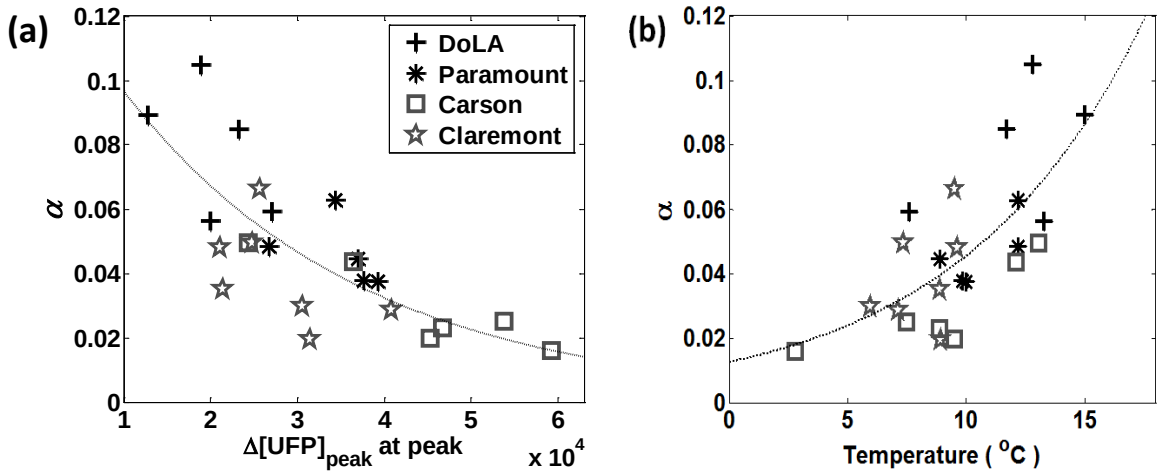

Figure 6. Plots of the relationships of dispersion coefficient α with (a) concentration gradient ($\Delta[UFP]_{peak}$) at the peak and (b) ambient temperature. Dotted lines in plots indicate exponential curve fits; (a) α=0.14·exp(-3.64×10^{-5}·$\Delta[UFP]_{peak}$) (R^2=0.59), and (b) α = 1.27×10^{-2}·$e^{0.13 \cdot T}$ (R^2=0.48).

In addition to the several conclusions outlined above, we have also been able to demonstrate that decay rates of UFP increase as particle size decreases with distance from freeway. This has little effect on the decay curve for particles larger than 35 nm, but has a modest effect on the decay curves for particles smaller than this size (Figure 7).

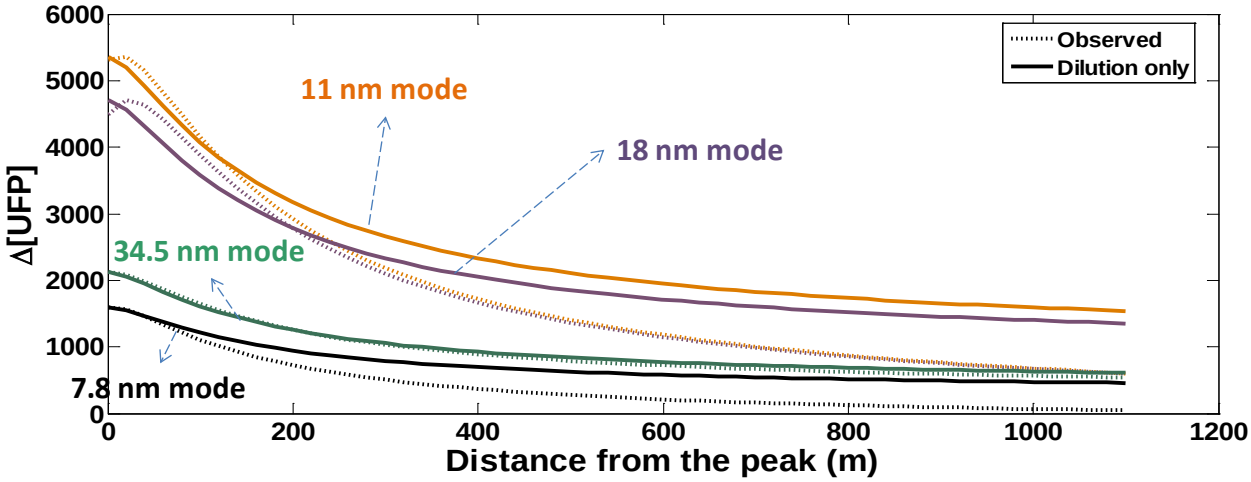

Figure 7. Comparisons of Δ[UFP] profiles between observations (solid lines) and expected one when only dilution was considered (dotted lines) for each size bin.

Because a large fraction of UFP and other vehicle related pollutants typically penetrate into indoor environments [1], and nocturnal surface inversions are widespread across the globe, our findings have significant implications for more extensive human exposures to vehicle-related pollutants than previously indicated based on daytime measurements of roadway plumes.

5.3 Classification of Days Based on Meteorology

In addition to MMP measurements and analysis, we have also developed an objective and systematic classification scheme of meteorological conditions affecting atmospheric primary pollutant levels for the South Coast Air Basin (SoCAB). This approach, based on a statistical technique known as *Classification and Regression Trees* (CART) developed for primary pollutants can be useful in objectively comparing MMP data obtained across different days in the same location as well as for MMP data obtained at different locations for various monitoring periods, as long as the locations are within the same overall synoptic meteorology regime, e.g. the California South Coast Air Basin.

Highly specialized measurements of air quality, including MMP measurements generally cannot be made simultaneously in more than one area due to limited resources. In many cases, comparing this data is desirable. At present, we are not aware of any studies that have produced quantitative and systematic assessment criteria to classify the degree of similarity of meteorological conditions with respect to traffic-related primary pollutants. In this study, we develop an objective classification scheme of meteorological conditions for the SoCAB using a classification and regression tree (CART) method.

The CART method explains the distribution or variation of a target pollutant using a number of explanatory meteorological variables. The variables can have a linear or non-linear relationship with the target variable. The CART model makes a hierarchy of binary decisions, each of which splits a pollutant distribution into two statistically exclusive, significantly different groups, based on the meteorological variables that yield the largest reduction in pollutant variability after split. Each split group is then divided again into two sub-groups by the same or a different meteorological variable. These splits continue until a set of terminal nodes is reached. Each final node represents a combination of several specific meteorological conditions related to a certain level of a target pollutant observed. Because the CART approach is based on a simple split by the most important meteorological variable, it allows complicated links between a target variable and various explanatory variables to be clear, easier to interpret, and quantitatively compared, regardless of their relationship (linear or non-linear). Explanatory meteorological variables considered in the model were 18 upper air meteorological variables obtained from National Centers for Environmental Prediction (NCEP) reanalysis database [9] and 11 surface meteorological variables obtained at LAX. Study periods were confined to 2007–2009 to insure reasonably consistent emissions so that we can assume variations in pollutant concentrations were controlled solely by meteorology.

A resulting regression tree with 11 final nodes created for $[CO]_{max}$ at downtown LA is shown in Figure 8. The most important variable related to $[CO]_{max}$ variations was surface wind speeds (1st split), followed by geopotential height at 925 mbar (Φ_{925mb}), north-south gradient of geopotential heights ($\Delta\Phi_{N\text{-}S}$), daily min. surface temperature (T_{min}), and atmospheric stability (S_{925}). The resulting splits are reasonable: for example, lower wind speeds are related to higher concentrations due to lower dispersion, higher geopotential heights and lower minimum surface temperatures are more common in the winter, which is characterized by a shallower boundary layer (due to less surface heating by the sun and intense surface radiative cooling) and more stable atmosphere. Lower values for S_{925}, defined as temperature differences between 1000 mbar and 925 mbar represents less stable conditions, yielding lower pollution days (Figure 8).

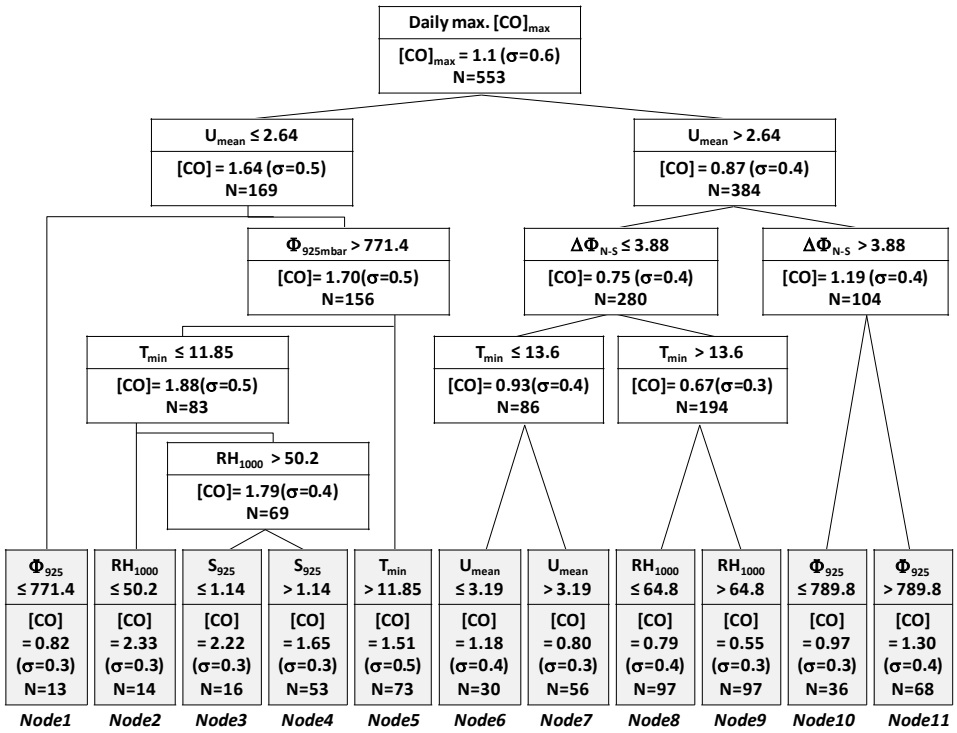

Figure 8. Regression tree for daily *[CO]$_{max}$* at Downtown LA (N. Main St.) for 2007–2009. The split criterion of explanatory variables is shown at the top of each box (node). The bottom layer of each node indicates the mean *[CO]$_{max}$* and standard deviation (σ) as well as the number of data in each node (*N*). Gray boxes represent the terminal nodes.

In order to evaluate the comparability of the regression trees between the primary pollutants, mean $[NO_x]_{max}$ were obtained for days that fall into each final node of the $[CO]_{max}$ regression tree. An excellent linear correlation between nodal mean $[CO]_{max}$ and $[NO_x]_{max}$ (R^2=0.99) implies that atmospheric concentrations of primary pollutants, CO and NO_x were controlled by similar meteorological conditions as expected (Figure 9).

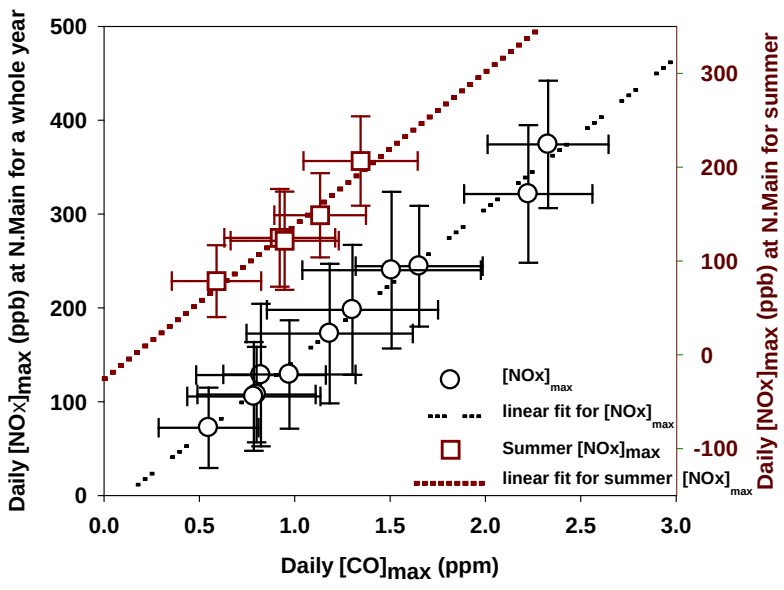

Figure 9. Comparison plots of the mean *[CO]$_{max}$* in each final node vs. mean *[NO$_x$]$_{max}$* for days falling in the corresponding nodes. Black circles: entire year regression tree and dark red squares: summer season regression tree. Red dotted and black dotted-dashed lines denote linear regression fit.

We also investigate the meteorological comparability between locations where differences might be expected due to different prevailing surface meteorology. For example, coastal areas generally experience stronger winds and cooler surface temperatures compared to non-mountainous inland areas. The data however support the hypothesis that the mesoscale weather system governs regional surface meteorology in a similar way throughout SoCAB. We can verify this hypothesis by comparing the mean nodal $[CO]_{max}$ at downtown LA with the mean concentrations for days that fall into the corresponding nodes at several different locations (Figure 10). Five monitoring sites were chosen for this comparison: Long Beach, Pomona, Rubidoux, San Bernardino, and Upland as farther distant east from downtown LA. For all locations, correlations were excellent (R^2 = 0.91–0.98) with the exception of node 2. Node 2 represents conditions known as "Santa Anas", strong winds from the high desert well known to bring very different weather to the SoCAB. Consequently, we believe that the regression tree developed for Downtown LA has good applicability for establishing meteorological comparability between different locations in the SoCAB.

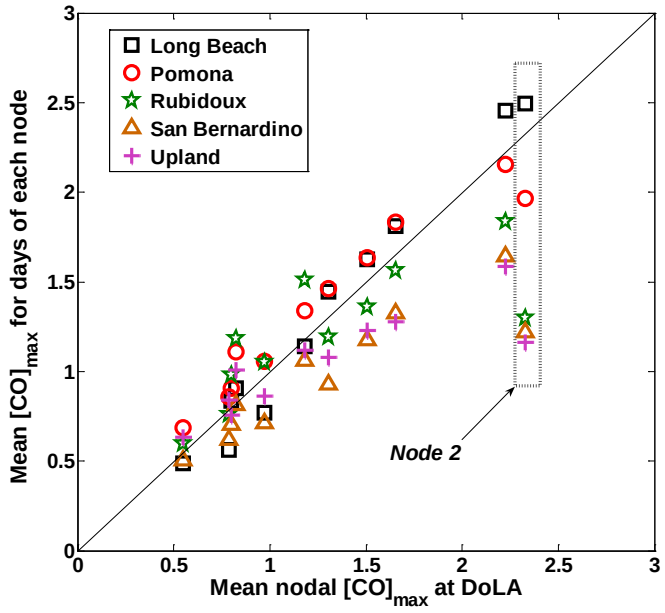

Figure 10. 1:1 comparison plot between the mean nodal $[CO]_{max}$ at downtown LA vs. the mean concentrations for days that fall into the corresponding final nodes at five different monitoring sites (Long Beach, Pomona, Rubidoux, San Bernardino, and Upland).

5.4 Neighborhood Comparison

The CART analysis was applied to compare the meteorological similarity between measurement days. Measurements of traffic-related air pollutants were conducted using a mobile measurement platform (MMP) in West LA (WLA), downtown LA (DoLA), and Boyle Heights (BH) in California in the summer afternoon (12:00–17:00) of 2008 and 2011. Each route consists of various environments: dense residential neighborhoods; several major arterial roadways; areas immediately upwind and downwind streets of freeways and residential neighborhoods near Santa Monica Airport (SMA). Of the total 15 measurement days, 13 days were classified to be under meteorologically comparable conditions with regard to dispersion of primary pollutants. Two days fell into meteorologically different nodes, for which representative primary pollutant levels were slightly higher compared to the others. Nonetheless, all three nodes encountered for the sampling dates are similar and fall into three adjacent nodes containing similar pollutant concentrations.

Observations showed significant inter-community variations between Downtown Los Angeles, Boyle Heights, and West Los Angeles in 2008 with the mean (±1σ) particle number concentrations (PNC) of $3.3(\pm2.2)\times10^4$, $2.2(\pm1.7)\times10^4$, and $1.1(\pm1.4)\times10^4$, respectively (Figure 11). However, we note that standard deviations are large due to strong impacts from individual

high emitting vehicles (HEV). After removing the local spikes from high emitting vehicles (HEV) encountered during the measurements, application of the Kolmogorov-Smirnov (KS) test verified that inter-community variations in UFP concentrations are statistically significant ($p<<0.01$) at 99% confidence level. Similar inter-community variations in UFP distributions were observed on arterial roadways between West Los Angeles, downtown Los Angeles, and Boyle Heights. We attribute these differences to larger number of old high emitting vehicles, denser road networks, and weaker wind speeds in Boyle Heights and downtown Los Angeles than West Los Angeles.

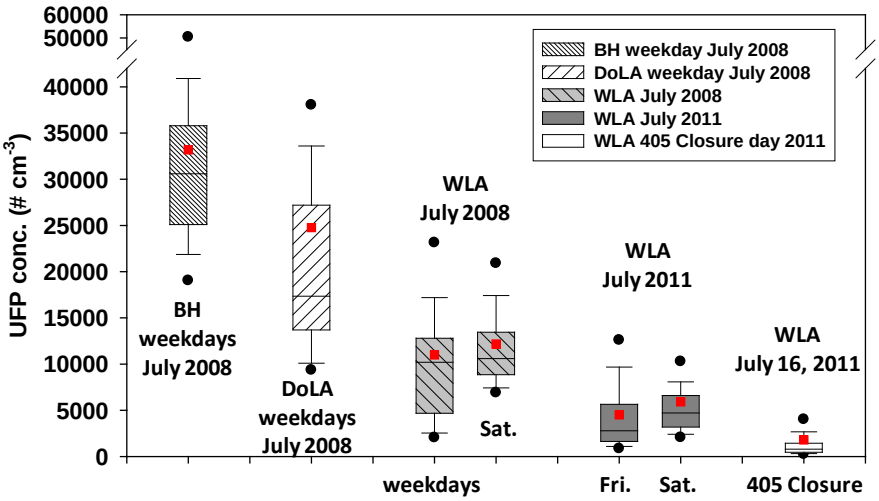

Figure 11. Box plot of UFP concentration variations sampled in residential neighborhoods of Boyle Heights, Downtown LA, West LA in 2008 , WLA in 2011, and WLA on I-405 closure Saturday. Red squares represent the mean values.

5.5 Freeway Closure

Finally, a striking and valuable feature from the present study is that the 36-hour I-405 closure event provided a superb opportunity to investigate the air-quality benefits of traffic emission reductions on a larger neighborhood scale (several kilometers) not just at near-roadway scales (several hundred meters). During the I-405 closure Saturday, more than 95% and 65% reductions in traffic densities were observed on the I-405 and I-10 freeways, respectively, compared to the preceding and following non-closure Saturdays. Although not quantitatively measured, significant drops in vehicle numbers on nearby arterial roads were also observed during the closure Saturday. We conclude voluntary restraints on vehicle use occurred extensively throughout the WLA area in response to the intensive and long-running warnings in the media of potential chaotic congestion, i.e. "Carmageddon". With the assumption that observed traffic flows on the I-10 freeway and Sepulveda Blvd. on the I-405 closure Saturday represent overall traffic patterns throughout the WLA areas, a 30–40% reduction in traffic flows on freeways accomplished about a 70-80% decrease in both UFP and $PM_{2.5}$ concentrations both in the neighborhoods and on arterial major roads (Figure 11). This case study makes clear the potential benefits for public health of achieving significant vehicle emission reductions. This study also showed the significant impact of HEV on total UFP concentrations.

6.0 Introduction

Numerous epidemiological studies have shown that exposure to elevated levels of fresh vehicular emissions and/or living in close proximity to roadways has been associated increased rates of reduced lung function (e.g., [10], cancer [11, 12], respiratory symptoms [13-15], asthma [15, 16], general mortality [17], depressed immune function [18], type II diabetes [19], mortality in heart failure patients [20], heart attacks [21], autism [22] and pre-term birth [23, 24]). Fresh vehicular emissions contain a wide range of particle- and gas-phase species. These individual impacts are difficult to separate because such emissions are emitted and diluted together. Ultrafine particles (UFP) appear to have the potential to be a 'causative agent' in fresh vehicular emissions responsible for degrading health in a variety of ways. For example, recent results of a European expert panel elicitation study on UFP health effects suggested a high likelihood of an association between UFP exposure and cardiovascular or respiratory hospital admissions [25].

The results from these health studies are useful because a large fraction of households are located near freeways. For example, Brugge et al. [26] estimated about 11% of US households are located within 100 m of 4-lane highways. And, in a highly urbanized area such as the California South Coast Air Basin (SoCAB), as much as 50% of the population lives within 1.5 km of freeways [27]. For these reasons, numerous air quality studies have been conducted near major roads and freeways. Karner et al. [28] synthesized the findings from 41 near-roadway monitoring studies published between 1978 and 2008. The studies collectively examined concentration–distance relationships for 14 pollutants with experiments conducted during both daytime and the evening, a period when vigorous atmospheric turbulence enhances the dilution/dispersion of emitted pollutants in a relatively deep, unstable convective boundary layer. In these studies, essentially all pollutants decayed to background levels 115–570 m away from the edge of road. Some pollutants quickly decreased within 150 m followed by a gradual decay toward background (CO and UFP number concentrations), another group decayed consistently throughout the entire distance range (benzene and NO_2), while PM_{10} and $PM_{2.5}$ showed no trend with distance [28]. The trends all likely resulted from the interplay between urban background concentrations, emissions from traffic, other emissions sources, and aerosol size distribution dynamics.

In addition, in the near-roadway environment, pollutants such as those from motor vehicles, can find their way into homes, which are not airtight [1]. This has important implications for early morning exposures to near-roadways. To date, however, only a small handful of near-roadway studies have been conducted under the stable nocturnal conditions generally encountered at night or especially in the early morning hours before and shortly after sunrise. Under those conditions, weak turbulence and a stratified boundary layer significantly suppress dispersion processes, leading to an extension of freeway/roadway plumes. Zhu et al. [4] sampled at six fixed locations within 500 m downwind of a freeway and found that nighttime number concentrations of UFP (*[UFP]*) reached 80% of daytime peak values in West Los Angeles with just 25% of daytime traffic volumes on the I-405 freeway. To map highly resolved spatial and temporal variations in *[UFP]* over longer distances downwind of a freeway in Santa Monica, California under stable pre-sunrise conditions, Hu et al. [2] were the first to report a much wider impact area of elevated *[UFP]* (more than 2 km downwind). However, the generality of this result for other roadways and locations, as well as the major factors determining the spatial scales of extended plumes in the early morning near major roads, remained to be determined.

As toxicological and epidemiological data related to UFP have developed, so has instrumentation for high time resolution monitoring of UFP and related pollutants. UFP are an attractive tracer for fresh emissions because they typically exhibit the highest dynamic concentration range of the combustion-related primary pollutants, a by-product of their short lifetimes [29], resulting in a relatively low urban background. The background varies widely in urban areas, depending on location and time of day, but it consistently provides a clear, steady baseline for the small spatial and time scales of interest here.

7.0 Instrumentation and Measurements

7.1 Mobile Measurement Platform: Instrumentation, sampling, and data analysis

The mobile measurement platform (MMP) used in this study, a Toyota RAV4 electric sub-SUV with no pollution of its own, was equipped with a suite of fast response instruments for various air pollutants. These included UFP size distributions and number concentrations, nitric oxide (NO), carbon monoxide (CO), particle-bound polycyclic aromatic hydrocarbon (PB-PAH), particulate matter with aerodynamic diameters less than 2.5 μm ($PM_{2.5}$), and black carbon (BC) (Table 2). Particle and gas instruments (FMPS, CPC, and DustTrak $PM_{2.5}$, Teledyne API 300e for CO and 200e for NO, and PAS for PAHs) were calibrated by their respective manufacturers just before field measurements began. Calibration checks for gas-instruments were also conducted before each sampling campaign. Flow and zero checks were conducted on a daily basis. More detailed information about calibration and flow checks is available in Hu et al. [2], Kozawa et al. [30], and Westerdahl et al. [31]. Data were recorded using a data-logger (Eurotherm Chessell Graphic DAQ Recorder) with 1 second time resolution.

Measurements were conducted during the pre-sunrise period (04:30 – 06:30) for the four transects described above. For the DoLA, Paramount, and Carson transects, sampling was conducted in the winter-to-spring seasons (January to March), and for the Claremont transect, sampling occurred in the transition period between spring and summer (May to June) in 2011. Of the total 25 measurement days, 5 days of data were excluded in this analysis due to inconsistent wind directions (e.g., opposite direction to normal days) or to inclement weather conditions (fog/rain). With the exception of stop signs and traffic lights, the mobile platform was driven at consistent speeds (~ 10 to 15 mph) over each transect (5 to 7 m spatial resolution).

The instruments employed have different response times due to the characteristics of the instruments themselves, as well as differences in inlet length and flow rates. Furthermore, response times sometimes varied slightly from day to day. To account for any differences, measurement data were synchronized on a daily basis using a time-lag correlation method using the equation below (Eq. 3):

$$r = \frac{1}{T\sigma_a\sigma_b}\int_{t_0}^{t_0+T}\left(a(t)-\bar{a}\right)\left(b(t+\tau)-\bar{b}\right)dt \qquad \text{Eq. (3)}$$

where a and b are simultaneously measured species, t is time, τ is a time-lag applied to time series in b, σ is the standard deviation for the two pollutants a and b, and T is the number of data

points in the time-series. For two co-emitted vehicle related pollutants *a* and *b*, the instruments for *a* and *b* should respond in concert and be well correlated with each other if the instrumental response times are identical. The best estimate of the difference in response time between instruments due to all factors combined corresponds to the τ with the maximum correlation coefficient. The ultrafine particle number concentration measured with the CPC or FMPS was used as the reference because these instruments have the fastest response times (~1 s), resulting in the clearest and sharpest responses to vehicular sources. Several smoke tests were also conducted to measure the response times of instruments from the inlet of the sampling manifold (Table 2). When the correlation between ultrafine particles and other specific species was poor (usually because there was no clear freeway peak for a pollutant which was sometimes the case for the DustTrak PM measurements and occasionally for other pollutants), averaged smoke test results were applied to synchronize the instrumental response times.

Table 2. Monitoring instruments on the mobile platform operational during the PSR measurements.

Instrument	Measurement Parameter	Response time[a] (Inlet to record)
TSI Portable CPC, Model 3007	UFP Count (10 nm-1μm)	4 s
TSI FMPS, Model 3091	UFP Size (5.6-560 nm)	9 s
TSI DustTrak, Model 8520	PM2.5 Mass	5 s
EcoChem PAS 2000	Particle-bound PAH	10 s
Teledyne API Model 300E	CO	21 s
LI-COR, Model LI-820	CO_2	7 s
Teledyne-API Model 200E	NO	22 s
Vaisala Sonic Anemometer and Temperature/RH sensor	Surface winds, temperature, and relative humidity (*RH*)	-
Garmin GPSMAP 76CS	Distance and relative speed	-
SmartTether™	Vertical profiles of temperature, *RH*, and winds	-

a. Response time is an averaged value for smoke test results

Distances from the freeways were computed using the mobile platform position data recorded every second by a Garmin GPSMAP and the latitude/longitude information of the center of freeway obtained from Google Earth software. Traffic flow data were collected for the 101 (DoLA), 91 (Paramount), I-110 (Carson), and I-210 (Claremont) freeways from the Freeway Performance Measurement System (PeMS) operated by the Institute of Transportation at University of California, Berkeley. Data were obtained from the freeway sensors located 100 m northeast of the DoLA transect (VDS ID: 717452, 34.075 °N/118.273 °W), 550 m east of the Paramount transect (VDS ID: 765467, 33.877 °N/118.150 °W), 850 m south of the Carson

transect (VDS ID:763522, 33.811 °N/118.287 °W), and 60 m east of the Claremont transect (VDS ID:767984, 34.120 °N/117.728 °W).

A balloon tether sonde (SmartTether™, Anasphere Inc.) was used to probe the vertical temperature, humidity and wind gradients to determine atmospheric stability. Vertical profiles (up to ~ 100 m a.g.l.) for temperature, humidity and winds were obtained on a daily basis (about 30 minutes before the MMP measurements) near the transects (560 m away from the Downtown LA transect, 1.2 km from the Paramount transect, 3.7 km from the Carson transect, and 3.8 km from the Claremont transect). It was not possible to launch the balloon immediately adjacent to the transects due to air safety regulations (balloon launches are prohibited within 5 miles of any airport) as well as the requirement for adequate open space to launch a balloon. In addition surface meteorological data were collected with a 2D sonic anemometer and temperature/humidity sensors on the MMP (Table 2), before and after every transect run for ~5 minutes.

7.2 Presunrise Measurements Description

7.2.1 Sampling areas and transects

For the pre-sunrise measurements, four sampling routes ("transects") were chosen, each aligned as close to perpendicular as possible to straight sections of freeway (Table 3 and Table 4). They were themselves roughly perpendicular to prevailing winds, and away from interchanges with other freeways or major arterials. Each transect followed a quiet, residential streets as much as possible. None of the chosen transects had direct freeway access, which greatly reduces interference from local high-emitting vehicles. Locations were chosen perpendicular to: the 101 freeway in Downtown Los Angeles (DoLA), the 91 freeway in Paramount, the I-110 freeway in Carson, and the I-210 in Claremont (Figure 12). DoLA is highly urbanized area, Paramount and West Carson are semi-urban, and Claremont is a suburban inland area at the foot of the San Gabriel Mountains.

The DoLA transect, near downtown Los Angeles, along N. Coronado St. is a small two lane street, and runs north–south in direction. The entire upwind and first 1500m of downwind area is residential. The farthest 1500–2200 m on the downwind side traverses a commercial district with tall buildings. The Paramount transect is located 11 km from the coast in a flat area of the coastal plain and is surrounded entirely by residential areas. The Carson transect is also on the coastal plain, ~ 6 km northwest of the Ports of Los Angeles and Long Beach. The transect is mostly surrounded by residential areas, but the upwind and downwind ends (> 850 m from the freeway) are adjacent to industrial/commercial areas. We did not find evidence of pollutant emissions from these industrial areas in our measurements as would be expected particularly in the pre-sunrise hours. Finally, the Claremont transect is located in an inland valley, ~70 km from the coast at the foot of steeply rising San Gabriel Mountains, and is entirely surrounded by quiet residential areas.

The DoLA transect is crossed by several arterial streets downwind of the freeways: Temple St., Beverly Blvd., 3rd St., 6th St., and Wilshire Blvd. The Carson, Paramount and Claremont transects are each crossed by just one or two major streets: Figueroa St. and Main St. for the Carson transect, Artesia Blvd. for the Paramount transect, and Foothill Blvd. for the Claremont transect. However, only small numbers of vehicles were observed on the cross streets during the pre-sunrise measurement periods. Nonetheless, to avoid possible interference from local

vehicular emissions on these cross streets, data obtained in the vicinity (several tens meters on the downwind side) of these streets were excluded from our analyses.

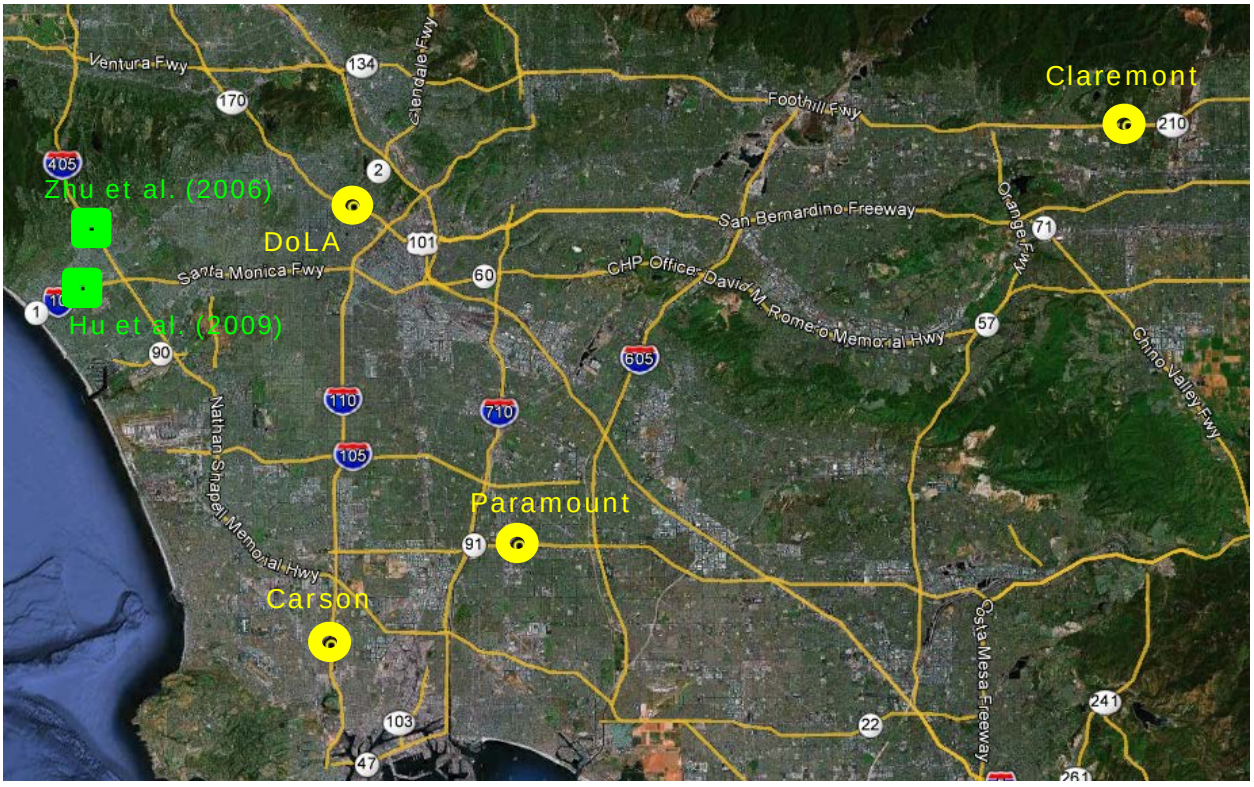

Figure 12. Map of transects where pre-sunrise measurements were conducted in the South California Air Basin (SoCAB). Yellow circles indicate the location of transects in this study and green squares denote the location of previous studies conducted by Zhu et al. (2002; 2006) in West LA and Hu et al. [2] in Santa Monica. Google Earth map. Additional measurements were made during 2011 surrounding the 405 closure as part of this study.

Table 3. Summary of the location of sampling transects and freeways, and measurement periods.

Transect street	Location	Freeway (Lat./Lon.)	Freeway over /under transect	Distance from coast / length	Sampling period	Refs
Constitution	West LA	I-405 (34.060N/ 118.455W)	Over-pass	~ 7 km / 0.3 km up-0.5 km down-wind	9 days for May through July, 2001 (daytime) 7 days for February, 2005 (Nighttime)	Zhu et al. (2002) Zhu et al. (2006)
Stewart	Santa Monica	I-10 (34.026N/ 118.463W)	Over-pass	~ 4 km / 1 km up-2.6 km down-wind	3/7, 3/12, 3/18 2008 (Winter) 6/30, 7/2 2008 (Summer)	Hu et al. (2009)
Coronado	Downtown LA	101 (34.074N/ 118.272W)	Over-pass	~ 22 km / 1.2 km up-2.2 km down-wind	2/24, 3/9, 3/14, 3/17 2011	this study
Obispo	Paramount	91 (33.877N/ 118.156W)	Over-pass	~ 13 km / 2 km up-1.8 km down-wind	1/27, 2/1, 3/10, 3/18 2011	
228th	West Carson	I-110 (33.819N/ 118.287W)	Under-pass	~ 6 km / 1.3 km up-2.2 km down-wind	1/21, 2/3/ 3/8, 3/11, 3/29 2011	
Mountain	Claremont	I-210 (34.120N/ 117.729W)	Under-pass	~ 70 km / 0.8 km up-2.6 km down-wind	5/19, 5/24, 5/25, 5/26, 6/1, 6/2, 6/7 2011	

Table 4. Surface meteorology, vertical temperature gradients (dΘ/dz), and traffic flows on the freeway during the measurement periods.

Transect	Sampling time	Temp. (°C)	RH (%)	Wind speed ($m \cdot s^{-1}$)	Wind direction relative to freeway[d] (°)	dΘ/dz ($\times 10^{-2}$ $K \cdot m^{-1}$)	Traffic flow (truck flow) on the freeways during measurements ($veh \cdot 5min^{-1}$)
West LA[a] (daytime)	10:30 – 16:00	34[b]	-	1 – 2[e]	78 (>62%) [f]	-	979
West LA[b] (night 2001)	23:00 – 04:00	10	-	< 1[e]	~ 35	-	221
Santa Monica (summer 2008)[c]	04:00 – 06:30	17	86	0.9	47	-	340
Santa Monica (winter 2008)[c]	06:00 – 07:30	11	69	0.7	49	-	715
DoLA	05:00 – 06:30	12	77	0.7	73	0.73	797 ± 215 (48 ± 6)
Paramount	05:00 – 06:30	10	76	0.5	82	0.67	1020 ± 112 (24 ± 4)
West Carson	05:00 – 06:30	8	67	0.6	76	0.40	627 ± 136 (24 ± 10)
Claremont	04:30 – 06:00	8	82	0.6	58	1.23	465 ± 79 (23 ± 4)

a. Zhu et al. [3].
b. Zhu et al. [4].
c. Hu et al. [2].
d. Wind direction is relative to the freeway direction. 90° is normal and 0° is parallel to the freeway.
e. Mostly wind speeds were 1-2 $m \cdot s^{-1}$ for daytime measurements and below 1 $m \cdot s^{-1}$ at night.
f. More than 62% of observations were recorded with this value with an interval of 22.5°.

7.2.3 High emitters

High emitting vehicles encountered on transects confound extraction of the freeway plume shape and extent, so it is desirable to remove their signatures from the data. After the measurement data were synchronized, a running low 25% quantile method was applied to remove the local impacts of individual high-emission vehicles encountered on a transect. The window sizes of the running low 25% quantile were 53 s (26 s before and after the center data point) when the distance from a freeway was farther than 1 km, 31 s (15 s before and after) for distances from a freeway between 300 m to 1 km, and 3 s (1 s before and after) within 300 m of a freeway. This method successfully removed the short-lived, individual, local, high- emitting

vehicle effects without altering remaining data. We additionally examined any remaining local effects, particularly near freeways, by reviewing video and audio records to verify proximity of high emitting vehicles before removing corresponding data.

7.3 Neighborhood Routes and related meteorological and traffic data

7.3.1 Study Locations and routes

Measurements of traffic-related air pollutants were conducted using a mobile measurement platform (MMP) in West Los Angeles (WLA) and Downtown Los Angeles (DTLA) in California (Figure 13). Each route driven consisted of various environments: dense residential neighborhoods in which light traffic volumes were encountered by the MMP during sampling periods; several major arterial roadways; upwind and downwind streets that run parallel and adjacent to the freeways (~ 30 m from the edge of freeways); residential neighborhoods near Santa Monica Airport (SMA). WLA and DTLA are located in a coastal plain, ~4 km and ~21 km east of the Pacific Ocean, respectively. Both areas are, in general, influenced by consistent onshore sea-breezes (south-westerlies) during the day (10:00–18:00). Thus, air masses arriving at the WLA route from the ocean are relatively unpolluted, whereas air masses at the DTLA route have incorporated more pollution during transport across the city.

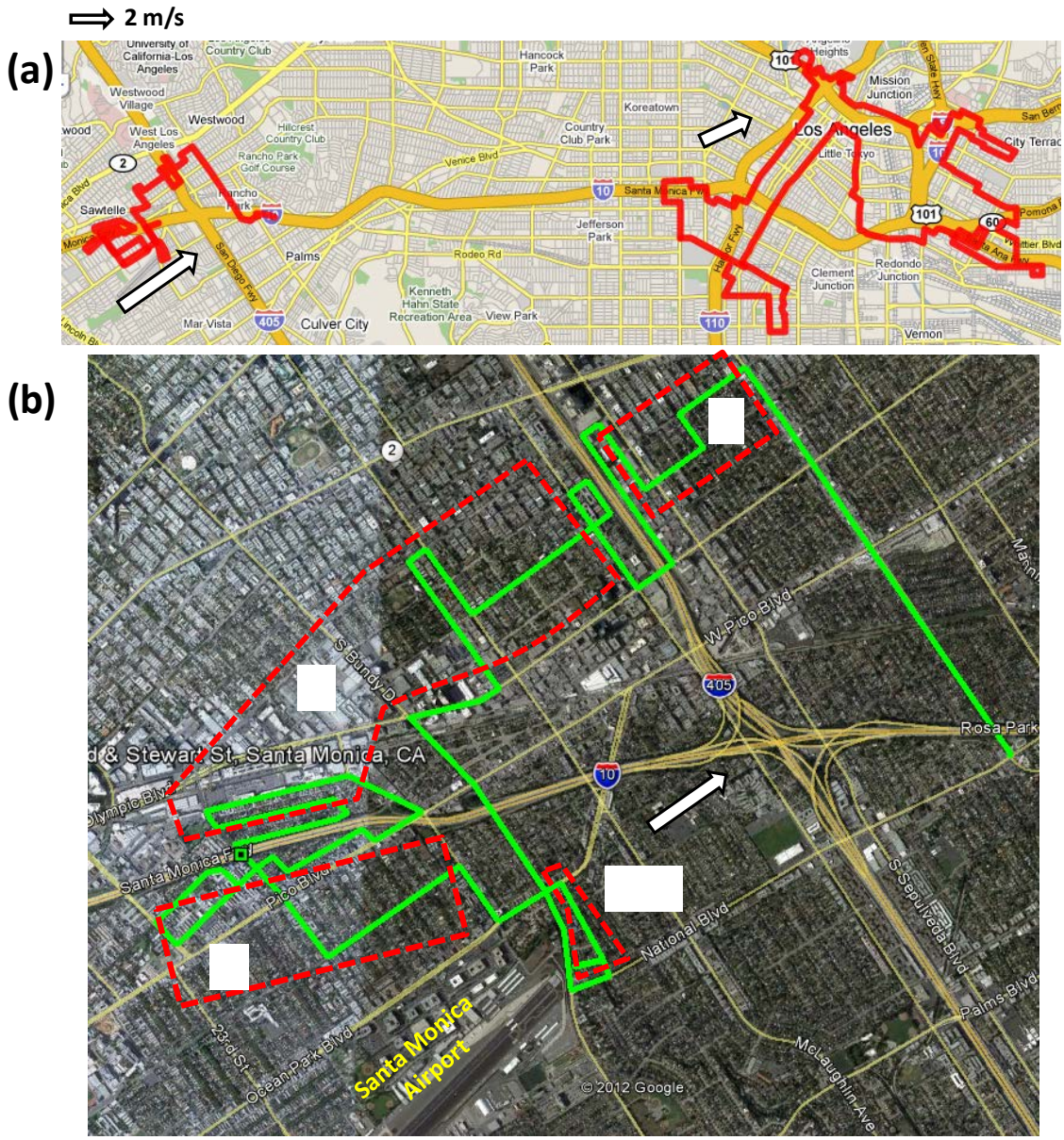

Figure 13. (a) Map of Downtown LA (red line in east of the map) and West LA routes (red line in west of the map). White arrows represent mean wind speeds and direction during the sampling periods. (b) Map of WLA route (green line). Red dotted lines confine neighborhood sub-areas (*A*, *B*, *C*, and *SMA*). White arrow represents prevailing winds. (*Map sources: (a) Google Map and (b) Google Earth*). Areas outside the boxes are not included in the neighborhood analyses.

WLA is traversed by two major freeways (I-10 and I-405), and DTLA is surrounded by numerous freeways (e.g., I-10, 101, I-110, 60, and I-5). In Los Angeles (LA) county, mobile sources (e.g., on-road traffic, aircraft, trains, ships, and off-road vehicles) account for 96%, 90%, 36%, and 18% of total emissions in CO, NOx, $PM_{2.5}$, and PM_{10}, respectively [32]. Because the study areas are traversed and surrounded by many arterial roads and freeways, pollutant emissions depend strongly on nearby on-road traffic volumes. The number of registered vehicles

in LA county has not changed significantly since 2004 (e.g., less than ± 1% changes based on 2004) [33]. at the time of this study in 2011 the vehicle fuel consumption in LA county also had changed little, less than ± 2.5%, compared to 2005 [34].

Sampling was conducted in the summer of 2008 (DTLA and WLA) and in 2011 (WLA), two times a day in the afternoon (between 12:00 and 17:00) (Table 5). In 2008, measurements were conducted on three weekdays and one Saturday in WLA and three weekdays in DTLA. In 2011, sampling was conducted for three consecutive weeks (pre-, post-, and during I-405 closure) on three contiguous days (Friday–Sunday) from 8 to 23 July in WLA. Of the measurement periods in 2011, the I-405 freeway was closed for the whole day of July 16 and until 12:00 of July 17 due to the demolition of the Mulholland Drive Bridge. The I-405 closure covered 16 km between the I-10 and 101 freeways for the northbound lanes, and 8 km between Getty Center Dr. and the 101 freeway for the southbound lanes. Only a single lane was permitted to drive southbound during the closure period.

Summary data for the 405 closure measurements are shown in Table 6 [35]. The study site lies 6.4 km east of Santa Monica Bay and the Pacific Ocean (indicated as "Zhu et al., 2006" in Figure 12 above). I-405 runs generally north and south (actual orientation 330^{o}) in west Los Angeles, CA with a 1% upgrade heading north. At this location, 5 km north of I-10, and 11 km south of US-101, the freeway is elevated ~4.5 m above the surrounding terrain. Sepulveda Boulevard is located immediately adjacent and runs parallel to I-405. Measurements were taken on Constitution Avenue, which adjoins the Los Angeles National Cemetery to the east and Los Angeles Veterans Administration to the west.

During the closure, the northbound lanes were completely closed for 16 km between I-10 and U.S. 101, southbound lanes for 8 km from U.S. 101 to Getty Center Drive. Traffic was permitted to enter I-405 southbound at Getty Center Drive and Sunset Boulevard, but travel was restricted to a single lane. Sepulveda remained open through the duration of the campaign. Constitution was closed to local access for July 16 and 17 only.

Table 5. Measurement dates, mean surface meteorological conditions, and the CART classification results for meteorological comparability.

Area	Measurement Date (Time)	Day of week	Temp. (°C)	Relative humidity (%)	Wind speeds ($m \cdot s^{-1}$)	Wind direction (°)	CART final node[a]
DTLA	07/14/2008 (14:00 – 17:00)	Mon.	27.6	41	2.6	240	2
	07/16/2008 (14:00 – 17:00)	Wed.	26.7	49	2.4	260	2
	07/18/2008 (14:00 – 17:00)	Fri.	24.6	61	2.9	250	2
	Mean (Std.)		26.3 (1.5)	50 (9)	2.6 (0.7)	250 (10)	
WLA	06/30/2008 (14:00 – 16:30)	Mon.	21.9	60	4.1	243	2
	07/08/2008 (14:00 – 16:30)	Tue.	20.7	73	5.1	240	5
	07/10/2008 (14:00 – 16:30)	Thu.	23.4	63	4.4	227	2
	07/12/2008 (14:00 – 16:30)	Sat.	23.9	63	4.3	240	2
	Mean (std.)		22.5 (1.5)	65 (5)	4.5 (0.6)	238 (13)	
WLA	07/08/2011 (12:00 – 14:00)	Fri.	22.6	70	3.9	240	2
	07/09/2011 (12:00 – 13:30)	Sat.	21.5	72	3.8	233	2
	07/10/2011 (12:00 – 13:30)	Sun	21.8	68	4.1	240	2
	07/15/2011 (13:30 – 15:00)	Fri.	21.3	57	4.6	247	2
	07/16/2011 (14:30 – 16:00)	Sat.	20.3	67	5.1	245	1
	07/17/2011 (13:15 – 14:45)	Sun	20.9	68	4.3	240	2
	07/22/2011 (14:20 – 16:00)	Fri.	20.9	66	4.8	233	2
	07/23/2011 (13:30 – 15:00)	Sat.	21.1	66	4.4	245	2
	Mean (std.)		21.3 (0.7)	67 (4)	4.4 (0.4)	240 (5)	

a. CART classifications were made based on daily maximum CO data obtained at N. Main monitoring station operated by South Coast Air Quality Management District as described in detail in Section 11.

7.3.2 Traffic and meteorological data

Freeway traffic data were obtained from the Freeway Performance Measurement System (PeMS) operated by the Institute of Transportation at University of California, Berkeley. Data were collected from sensors located at Pico station (VDS ID: 717794-5, 34.038°N/-118.439°W) for I-405 freeway and Cloverfield station (VDS ID: 737246, 34.025°N/-118.467°W) for I-10 freeway in WLA. In DTLA, traffic data were collected from three sensors near the sampling route (VDS ID: 718335, 34.037°N/-118.289°W for I-10 freeway; VDS ID: 764032, 34.026°N/-118.275°W for I-110; VDS ID: 764853, 34.065°N/-118.251°W for 101 freeway).

Meteorological data were obtained from a weather station located at Santa Monica Airport (< 1 km from the route) in WLA and at University of Southern California (< 2 km from the route) in DTLA. Data from both stations were collected through the MesoWest website operated by the Department of Atmospheric Sciences at University of Utah. To determine regional meteorological comparability among measurement days in 2011 and 2008, a classification and regression trees (CART) method for primary pollutants, developed to evaluate meteorological comparability in air quality studies in California's South Coast Air Basin [36], was applied. The CART method yields statistically exclusive groups (*nodes*) of a target variable based on a number of explanatory variables (meteorological variables in this case, such as pressure, temperature, wind speeds, relative humidity, and pressure gradients in both the upper air and surface). Thus, individual final nodes created by the CART model are associated with specific meteorological conditions for a specific level of traffic-related primary pollutants. More details about the CART method and regression trees developed for the study areas are found elsewhere [36].

7.3.3 405 Freeway Closure Dates, Sampling Times and Traffic Flows

Table 6. Summary of meteorological and traffic conditions during I-405 closure sampling campaign. Data displayed as: average value from 10:00-20:00 (standard deviation).

	pre-closure			closure				post-closure	
day in July 2011	8	9	10	15	16	17	22	23	24
	Fri	Sat	Sun	Fri	Sat	Sun	Fri	Sat	Sun
meteorology									
Temperature (ºC)	23 (2)	22 (1)	22 (1)	21 (1)	21 (1)	22 (1)	21 (1)	21 (1)	20 (1)
Wind Speed (m s^{-1})	3.0 (0.7)	3.0 (0.8)	3.0 (1.0)	5.2 (2.9)	4.3 (2.4)	5.0 (3.2)	5.2 (3.2)	4.9 (3.1)	5.4 (3.4)
Wind Direction (º)	195 (25)	199 (28)	196 (36)	216 (27)	204 (45)	191 (30)	208 (35)	210 (30)	190 (24)
Relative Humidity (%)	74 (5)	78 (4)	77 (4)	68 (4)	74 (7)	75 (2)	79 (5)	76 (5)	80 (3)
traffic volume (10^2 /hr)									
I-405 Freeway.	160 (35)	180 (25)	188 (13)	150 (35)	16 (2)	63 (20)	151 (32)	177 (19)	184 (22)
Sepulveda Boulevard	16 (5)	11 (3)	7 (2)	10 (4)	9 (2)	6 (3)	15 (5)	11 (3)	9 (3)
Density (vehicles km^{-1})	280 (90)	240 (25)	190 (15)	240 (105)	35 (5)	75 (15)	315 (85)	315 (85)	230 (42)
Average Speed (km h^{-1})[a]	69 (22)	82 (13)	102 (6)	80 (29)	75 (1.6)	90 (3)	53 (22)	64 (21)	86 (18)

[a] Averaged speed of I-405 and Sepulveda combined, weighted by magnitude of traffic flow from each roadway.

8.0 Prevalence of Wide Area Impacts Downwind of Freeways under Pre-sunrise Stable Atmospheric Conditions

The objectives of the present study are to: (1) investigate the generality of the Hu et al. (2009) results; (2) investigate variability of pollutant plumes under stable meteorological conditions during the early morning hours in inland and coastal areas of the SoCAB; (3) identify the major factors contributing to the extension of freeway plumes in the pre-sunrise period; and (4) assess how freshly-emitted UFP evolve in their characteristics during transport downwind.

8.1 Meteorology and traffic flow

The averaged surface meteorology for each transect is summarized in Table 4. The mean temperature ranged from 8–12 °C and relative humidity from 67–82 % during the measurement periods. Although the measurements in Claremont were conducted May through June, the mean temperature and humidity were similar to those for other transects. The daily mean wind speeds were less than 1 $m \cdot s^{-1}$ for all four transects indicating calm and stable conditions during the pre-sunrise period.

The usual prevailing wind direction was approximately perpendicular to the freeway for the DoLA, Paramount, and Carson transects with mean directions in the 73–82° range relative to the freeways (90° being normal to the freeway orientation). For the Claremont transect, winds were more askew to the freeway with a mean direction of 58°. Winds for this transect were the least variable, however, due to the adjacent mountains to the north which produce a strong, thermally-induced, mountain-valley wind system.

Static atmospheric stability can be represented with a vertical potential temperature gradient ($d\Theta/dz > 0$ for stable, $d\Theta/dz \sim 0$ for neutral, and $d\Theta/dz < 0$ for unstable). During the measurement periods, $d\Theta/dz$ was slightly positive for all transects representing slightly stable conditions. The vertical temperature gradient was highest near the Claremont transect (1.23×10^{-2} $K \cdot m^{-1}$) although the differences by location were not significant.

Mobile platform measurements were conducted during the period of sharply increasing traffic flow on the freeways due to the onset of the morning commute. The mean traffic flows on the freeway in the vicinity of the transects during the measurement period were 800, 1,000, 630, and 470 vehicles per 5 minutes on the 101 (DoLA), 91 (Paramount), I-110 (Carson), and I-210 freeways (Claremont), respectively. The fleet mixes on the transects were not characterized in detail, however they were not obviously different from one another. Truck flows accounted for a small fraction of the total traffic flows, falling in a similar range for all transects (2.4 to 6%, Table 4, PeMS). The differences in truck contribution should result in modest differences in mixed-fleet emission rates for each transect, as well as between our measurements and those in the literature.

8.2 Prevalence of a wide UFP impact area downwind of freeways under stable conditions

Figure 14 and Figure 15 show the normalized average profiles of background-subtracted UFP concentrations with distance from the freeway. Profiles have been normalized to peak concentrations. This normalization allows us to clearly see how far downwind freeway emissions impact adjacent areas and directly compare decay of freeway plumes.

Interesting features are observed in the variations in UFP concentrations with distance from freeways. First, significant extensions of freeway plumes compared to daytime length were observed at all sites during the pre-sunrise period, an observation that is consistent with the results reported by Hu et al. [2] for Santa Monica. Our results confirm that pre-sunrise (or nocturnal) extension of freeway plumes far downwind is a general phenomenon, at least from the coastal plain to the inland valleys in the SoCAB. Second, in many cases, UFP concentrations did not return to the upwind background concentrations at 2 km or more downwind, indicating plume impacts could extend farther than 2 km, although it is difficult to completely rule out potential influence of local sources at extended distances. In addition, it appears that UFP concentrations farther than 1 km downwind decay much more slowly and are often gradually stabilized above the upwind background concentrations. This observation suggests that freeway emissions might increase the background concentrations in the downwind areas by up to 10–30% of the peak concentrations (Figure 14 and Figure 15).

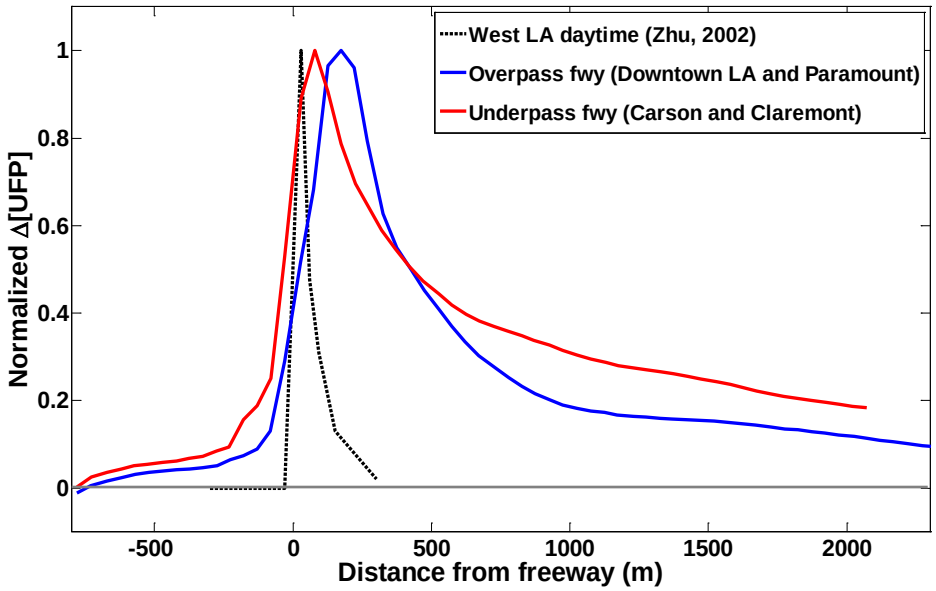

Figure 14. Variations in background-subtracted UFP concentrations with respect to distance from the freeway. Values are smoothed after being normalized to peak concentrations. The blue line: mean concentration profiles of overpass freeways (the Downtown LA and Paramount transects); red line: mean profiles of underpass freeways (the Carson and Claremont transects); black dashed line: daytime observations in West LA reported by Zhu et al.[3]. The horizontal gray solid line represents upwind background concentrations. Negative and positive distance indicates upwind and downwind locations, respectively.

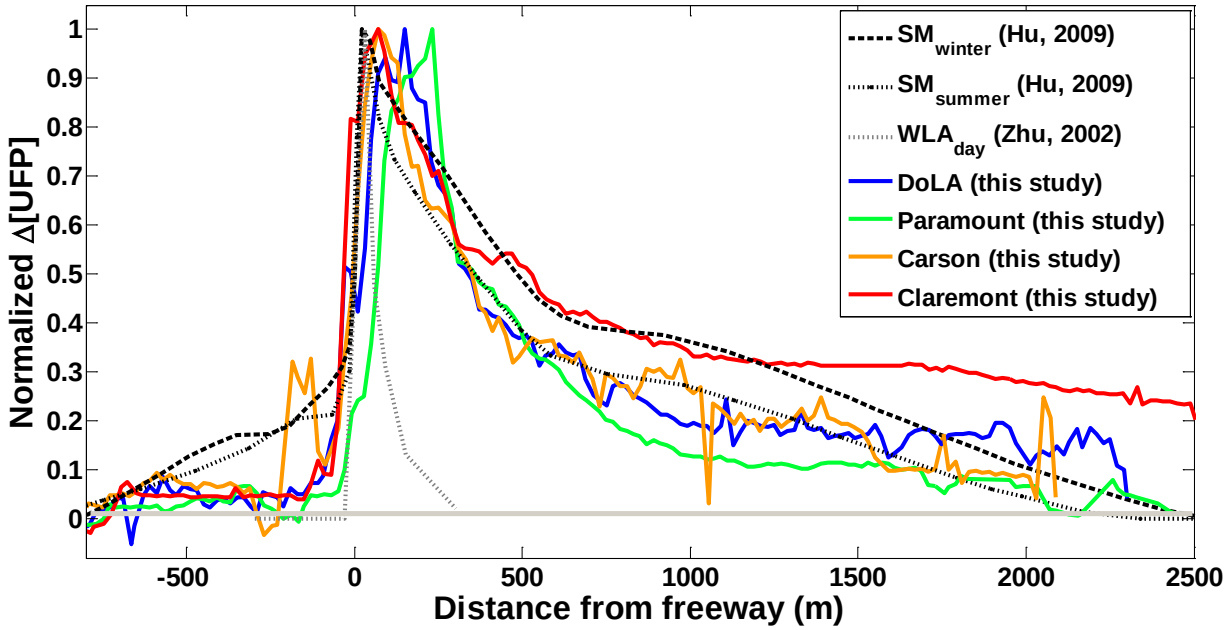

Figure 15. Variations in background-subtracted UFP concentrations with respect to distance from the freeway. Values are normalized to peak concentrations. The blue line: Downtown LA (DoLA) transect; green line: Paramount; orange line: Carson; and red line: Claremont (this study). Black dashed and dotted lines represent observations in winter and summer, respectively, as reported by Hu et al. (2009) in Santa Monica (SM). The gray dotted line represents daytime observations in West LA (WLA) reported by Zhu et al. (2002). The horizontal gray solid line represents upwind background concentrations. Negative distance indicates upwind locations and positive indicates downwind locations.

We note that the Hu et al. [2] averaged downwind concentration profile appears to decay more rapidly starting at ~1200 m. We believe the new data presented here are more representative. The shape of the curve in Hu et al. [2] was somewhat influenced by an artifact resulting from averaging several days with higher concentrations on which the sampling route extended only 1200 m south of the freeway with several lower concentration days on which the sampling route was extended to 2500 m.

8.3 Comparisons of UFP concentrations at various downwind distances between locations in SoCAB

In Figure 16, the spatial distributions of UFP number concentrations with downwind distance from the freeways measured in 2011 are summarized and compared with those of the previous studies conducted in West LA and Santa Monica (Hu et al., 2009b; Zhu et al., 2002a; Zhu et al., 2006). Background upwind UFP concentrations were low in Claremont (5,300 particles·cm^{-3}), and much higher in the other three areas (15,000, 19,000, and 16,000 particles·cm^{-3} in DoLA, Paramount, and Carson, respectively). These latter levels are comparable to the winter background level in Santa Monica in 2008 while the summer background UFP concentration in Santa Monica (7,000 particles·cm^{-3}) was similar to that of Claremont.

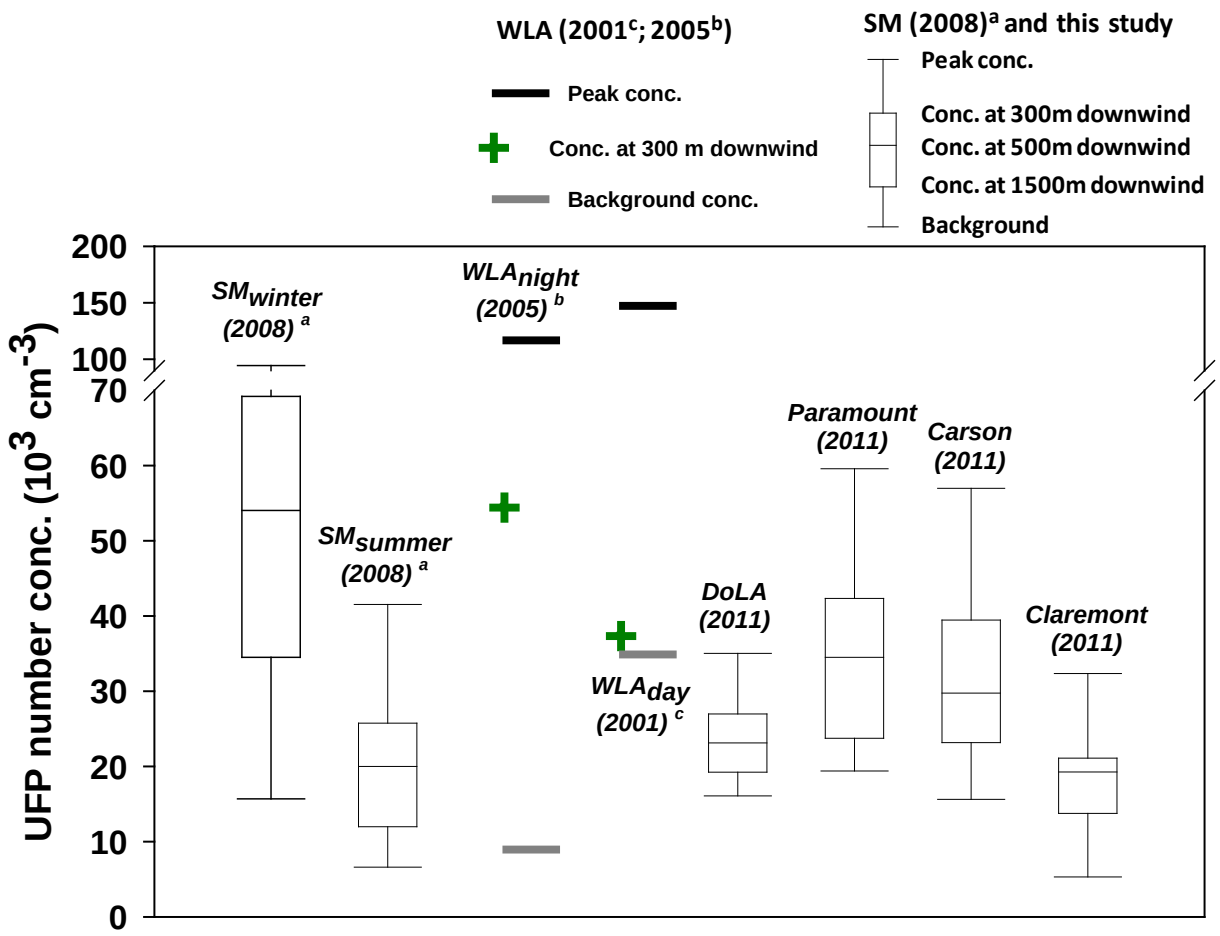

Figure 16. Concentrations of UFP (#×10^3· cm^{-3}) observed at several distances from the freeway. Top and bottom horizontal bars denote peak plume concentration and the upwind background concentration, respectively. The horizontal lines of the box (from the top) represent the concentrations at 300m, 500m, and 1500m, respectively, downwind from the freeway. For Zhu et al. (2002a; 2006), top and bottom horizontal bars denote the freeway peak and upwind concentrations, and green crosses denote the concentrations at 300m downwind. We note that the measurements in this study were made earlier in the morning than those of Hu et al. (2009), and thus somewhat lower absolute concentrations are expected, although many other factors also play a role. [a]Hu et al. [2]; [b]Zhu et al. [4]; [c]Zhu et al. [3].

The net UFP due to freeway emissions, *Δ[UFP]*, defined as the difference between the peak and background concentrations (the concentration measured on the upwind portion of the transect), also varied significantly by location. In this study, *Δ[UFP]* values were 1.9, 4.0, 4.1, and 2.7×10^4 particles·cm^{-3} in DoLA, Paramount, Carson, and Claremont, respectively, which are comparable to the summer season value in Santa Monica in 2008 (3.5×10^4 particles·cm^{-3}; Hu et al., 2009) and 2–4 times lower than the winter season Santa Monica value (7.9×10^4 particles·cm^{-3}; Hu et al., 2009). Nighttime *Δ[UFP]* in West LA in 2005 reported by Zhu et al. [4] was about

3–5 times higher (1.1×10^5 particles·cm^{-3}). These differences are likely to be attributable to both differences in traffic flows, vehicle fleet mix and resulting emission rates on the freeways as well as differences in freeway geography and orientation (discussed below).

The relationship between the daily $\Delta[UFP]$ and traffic flows on the freeways during the measurement periods falls into two distinct groups; freeways that pass over the transect (DoLA and Paramount) and those passing under the transect (Carson and Claremont) (Figure 17). Within each group, it appears $\Delta[UFP]$ increases with traffic flow. The linear fit results for overpass and underpass freeways are shown in Eq. (4) and (5), respectively:

$$\Delta[UFP] = 31\times(Traffic\ \ flow) + 2700\ \ (r^2 = 0.27)\ \ (\text{overpass freeways}) \qquad \text{Eq. (4)}$$

$$\Delta[UFP] = 56\times(Traffic\ \ flow) + 5600\ \ (r^2 = 0.42)\ \ (\text{underpass freeways}) \qquad \text{Eq. (5)}$$

These relationships also show that $\Delta[UFP]$ is larger for underpass freeways and better correlated with the traffic flow. When the mobile platform crosses over a freeway (gray squares in Figure 17), the instruments immediately experience a freeway plume freshly emitted from below. In contrast, it takes time for a freshly emitted plume to reach the ground when the freeway source is elevated above the transects by 8 m. In the latter case, the mobile platform encounters a somewhat aged and diluted freeway plume (black circles in Figure 17) with a less intense peak. In addition, the relationship between the peak concentrations and traffic flows is expected to be more scattered for overpass freeways because, while a plume is diluted somewhat before reaching the ground, it is also more affected by atmospheric stability and turbulence at that moment. Consistent with this, the UFP peak appeared ~ 65 m from the center of the freeway for the underpass freeways (Carson and Claremont). Conversely, for the overpass freeways, UFP peak distances were ~ 150 m from the centerline of the freeway for DoLA and ~ 230 m for Paramount as shown in Figure 14 and Figure 15. Moreover, the ratio of the $\Delta[UFP]_{peak}$ (particles·cm^{-3}) to the traffic flow (vehicles·5min^{-1}) was greater for the underpass freeway transects, 66 (Carson) and 58 (Claremont) than for the overpass freeway transects, 24 (DoLA) and 39 (Paramount). This also supports the influence of freeway geography on UFP and other primary pollutant spatial distributions. However, in the previous study of the Stewart St. transect across the I-10 freeway in Santa Monica [2], the response of $\Delta[UFP]_{peak}$ to traffic flow was closer to that of the underpass freeways in the present study despite the I-10 freeway crossing over the transect (horizontal bars in Figure 16). This might be explained by the downwind topography of the Santa Monica transect as the transect reaches the same elevation as the freeway at ~70 m downwind. Thus, the plume center line can directly reach the ground as in the underpass freeway case. A significant difference in $\Delta[UFP]_{peak}$ response to traffic flow (gray cross in Figure 16) was found for the West LA transect studied by Zhu et al. [4]. This difference may result from differences in a number of factors including atmospheric stability and winds associated with time of day (evening vs. early morning), vehicle types/driving patterns on the I-405 freeway, and different instrumentation.

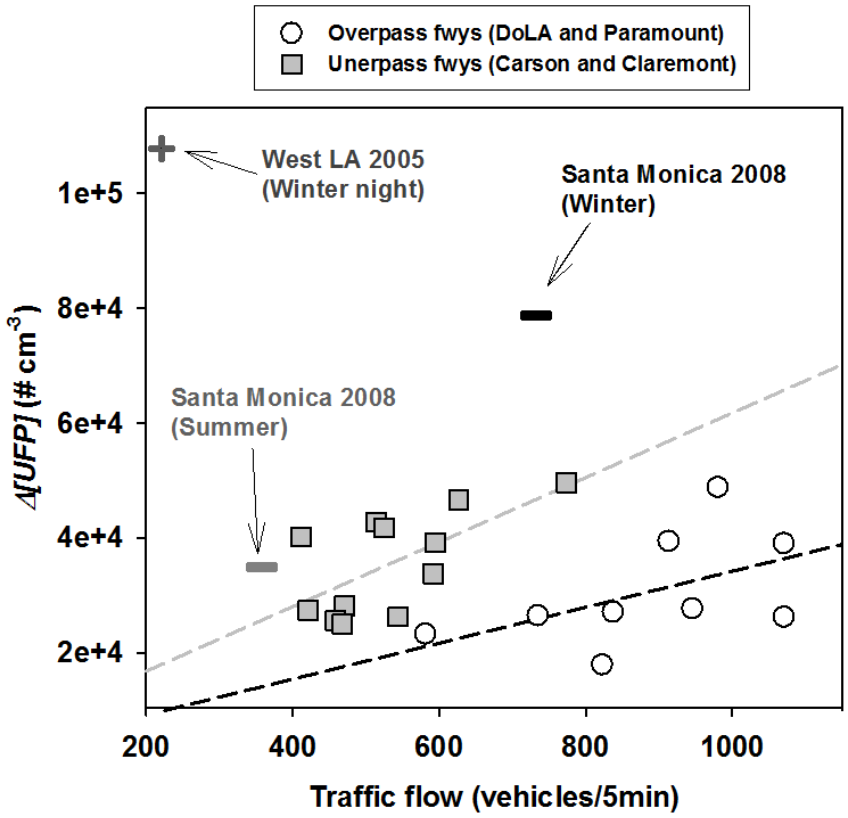

Figure 17. Background subtracted peak UFP concentrations (*Δ[UFP]*) as a function of traffic flow on freeways. Black circles denote daily average data for the DoLA and Paramount transects, where the freeway passes over the transect, and gray squares represent data for the Carson and Claremont transects, where the freeway passes under the transect. Gray and black dashed lines are linear fits for gray squares and black circles, respectively. Black and gray thick horizontal bars are the averaged values observed for the 2008 Santa Monica winter and summer seasons, respectively (Hu et al., 2009). The cross shows the averaged nighttime data for the 2005 West LA winter night period (Zhu et al., 2006).

8.3.1 Comparisons of plume decay rates near freeways

The impact distance of freeway plumes on downwind areas is of great interest for both human exposure assessments and dispersion model applications. However, direct comparisons of decay rates are difficult because of varying peak and background concentrations; to reduce this effect, we normalized *Δ[UFP]* to the peak concentration as shown in Figure 18. If we assume dilution is the major process decreasing pollutant concentrations with distance [37-39] and other processes are negligible, we can describe the temporal evolution of UFP using Eq. (6) which describes an air parcel released from the freeway in a Lagrangian system [40]:

$$\frac{d\left([UFP]_t - [UFP]_{bkgnd}\right)}{dt} = -K(t)\cdot\left([UFP]_t - [UFP]_{bkgnd}\right) \qquad \text{Eq. (6)}$$

$$\frac{\left([UFP(x)]-[UFP]_{bkgnd}\right)}{\left([UFP]_{peak}-[UFP]_{bkgnd}\right)}=e^{-K(x)\cdot x} \qquad \text{Eq. (7)}$$

where $[UFP]_t$ and $[UFP]_{bkgnd}$ are UFP concentrations at time t and the upwind background, respectively, and $K(t)$ is the time-dependent rate of entrainment of background air in the plume. Integrating Eq. (6) and assuming consistent wind speed and direction normal to the freeway (air travel distance, $x=U\times t$, where U is mean wind speed), we can convert the time basis to air parcel travel distance ($K(x) = K(t)/U$) to yield Eq. (7). Note that the left hand side of Eq. (7) is the background-subtracted $\Delta[UFP]$ at downwind distance x, normalized to $\Delta[UFP]_{peak}$ at the peak (this is the y-axis in Fig 18). We also assume K is constant with distance, an assumption that should break down as a plume disperses farther downwind due to the increases in the vertical length scale of the plume. The length scale of our analysis is constrained to within 700 m downwind from the freeway after which Eq. (7) no longer describes the plume shapes well.

The resulting exponential fits successfully describe the observations for all transects in the present and previous studies, with r^2 values of 0.93–0.96 (this work), 0.91–0.99 (Santa Monica; Hu et al., 2009), and 0.77 (daytime West LA (WLA); Zhu et al., 2002) (Figure 18). The entrainment rate constant, $K(x)$, estimated from the fits were $2.2(\pm0.1)\times10^{-3}$ (DoLA), $3.3(\pm0.1)\times10^{-3}$ (Paramount), $2.3(\pm0.1)\times10^{-3}$ (Carson), $1.7(\pm0.04)\times10^{-3}$ (Claremont), $1.4(\pm0.03)\times10^{-3}$ (Winter Santa Monica), $2.1(\pm0.1)\times10^{-3}$ (Summer Santa Monica), and $2.0(\pm0.1)\times10^{-2}$ m^{-1} (daytime WLA). Consistent with Hu et al. [2]'s conclusion, the daytime $K(x)$ in WLA reported by Zhu et al. [3] is higher by a factor of 6 – 14 than the pre-sunrise $K(x)$, and pre-sunrise $K(x)$ does not appear to indicate a clear seasonal variation.

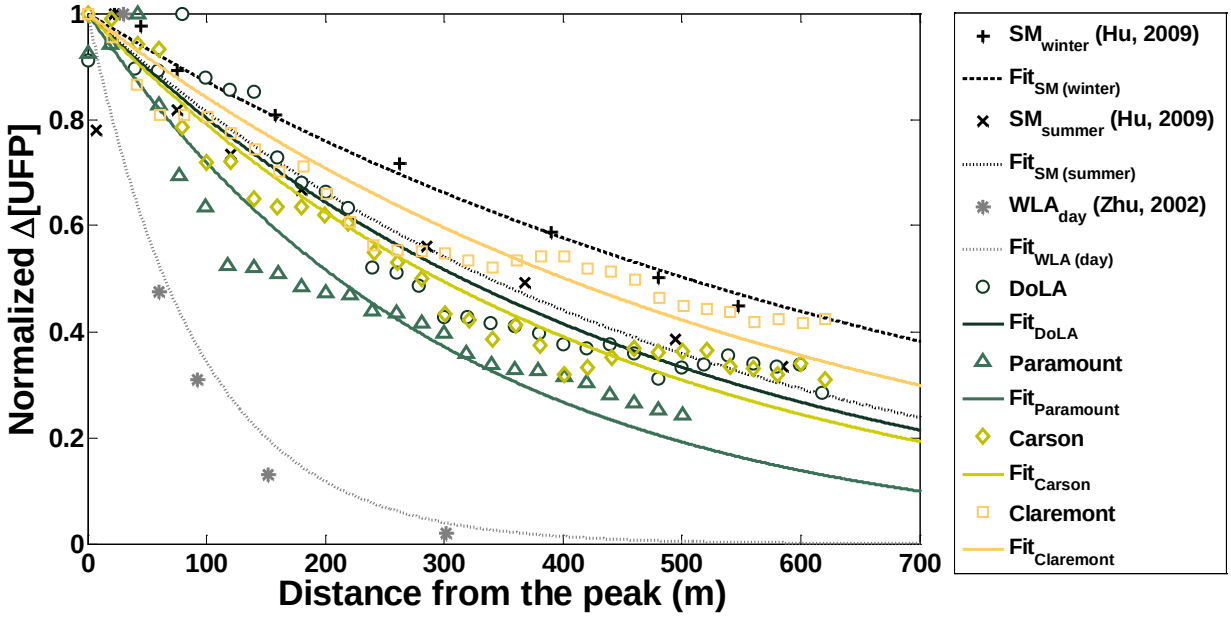

Figure 18. Normalized *Δ[UFP]* with downwind distance from the freeway and exponential fits. SM: Santa Monica (black cross and x) and WLA: West LA (gray asterisk). Symbols indicate observations for each transect and the line with the same color as a symbol shows an exponential fit to those symbols.

8.4 Variations in size distribution of UFP with downwind distance from freeways

Averaged size distributions of particle number concentrations with distance downwind from the freeways were obtained using a fast mobility particle sizer (FMPS) (Figure 19). The mean size distributions (for number concentrations) for all transects had similar features: (1) the dominant peak appeared at 11 nm diameter, (2) a distinct secondary peak appeared around 34 nm diameter, and (3) two shoulder peaks were observed at 17 nm and 52 nm. Similar four-mode size distributions were observed near the I-405 freeway [3, 37] although the exact peaks were slightly shifted, perhaps due to differences in instrumentation and wind conditions. The low levels of particles less than 20 nm in diameter in upwind background size distributions clearly indicates that UFP smaller than 20 nm in diameter are attributable to fresh emissions from freeway vehicles. It is also apparent that particles in the 11 nm mode decline much faster than those in the 34 nm or 52 nm mode.

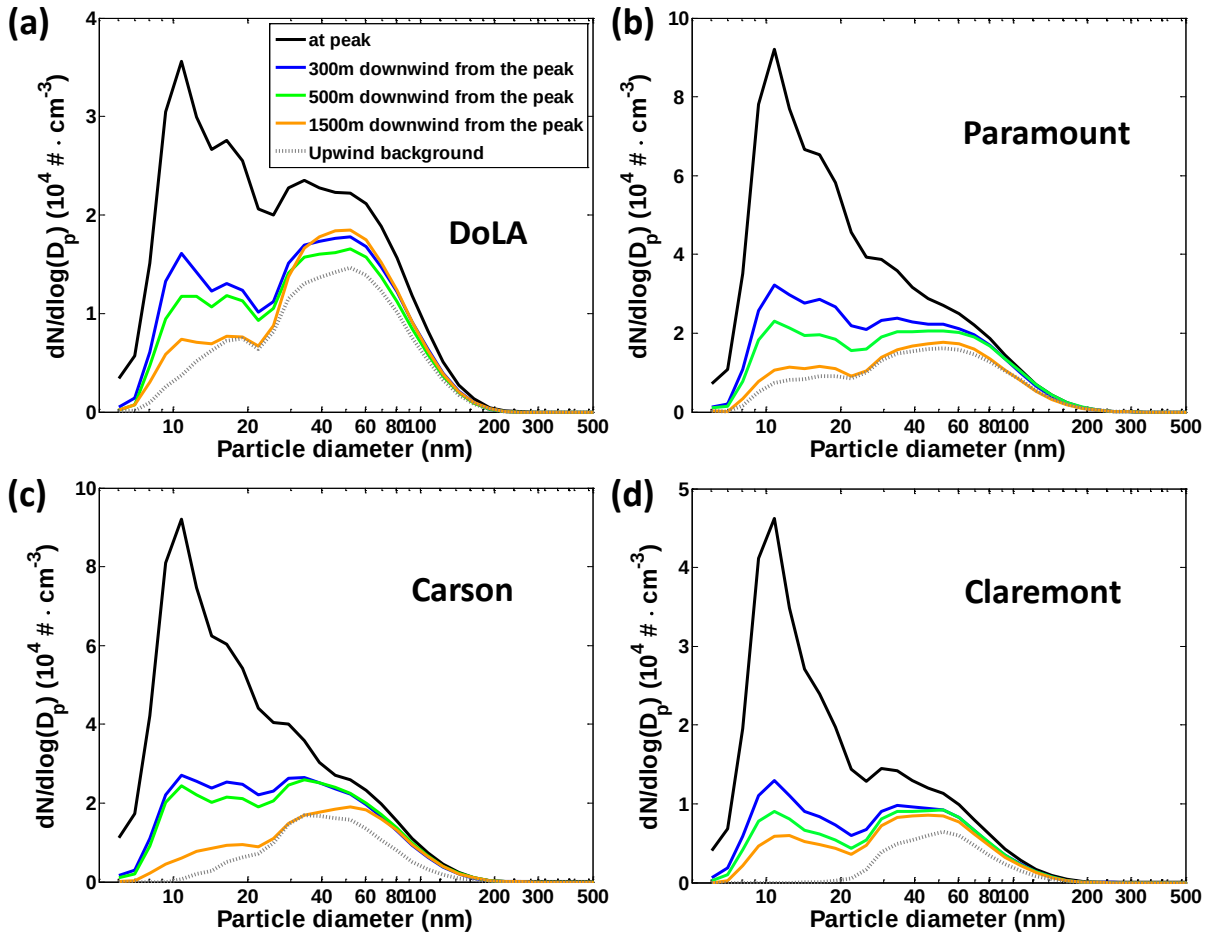

Figure 19. Size distributions of UFP number concentrations at the peak location (black solid line), 300 m (light purple), 500 m (green), and 1500 m (gray solid line) downwind from the peak as well as averaged upwind background (gray dotted line) for the (a) DoLA, (b) Paramount, (c) Carson, and (d) Claremont transects.

Although the particle number in all size bins decreased with distance, the decay rates decrease as particle size increases resulting in a shifting size distribution (Figure 21). By 500 m downwind, about 90% of the smallest particles (5.6–7.5 nm) disappeared (not shown), whereas 70%, 63%, 37% and 18% of particles in the 9–12 nm (*mode 1*), 15–21 nm (*mode 2*), 27–37 nm (*mode 3*), and 49–65 nm (*mode 4*) size bins disappeared, respectively. Consequently, the contributions of these four size bins to the total UFP number decreased at *mode 1* (20% → 12%) and *2* (13% → 10%) and increased at *mode 3* (9% → 12%) and *4* (7% → 12%) (Figure 20).

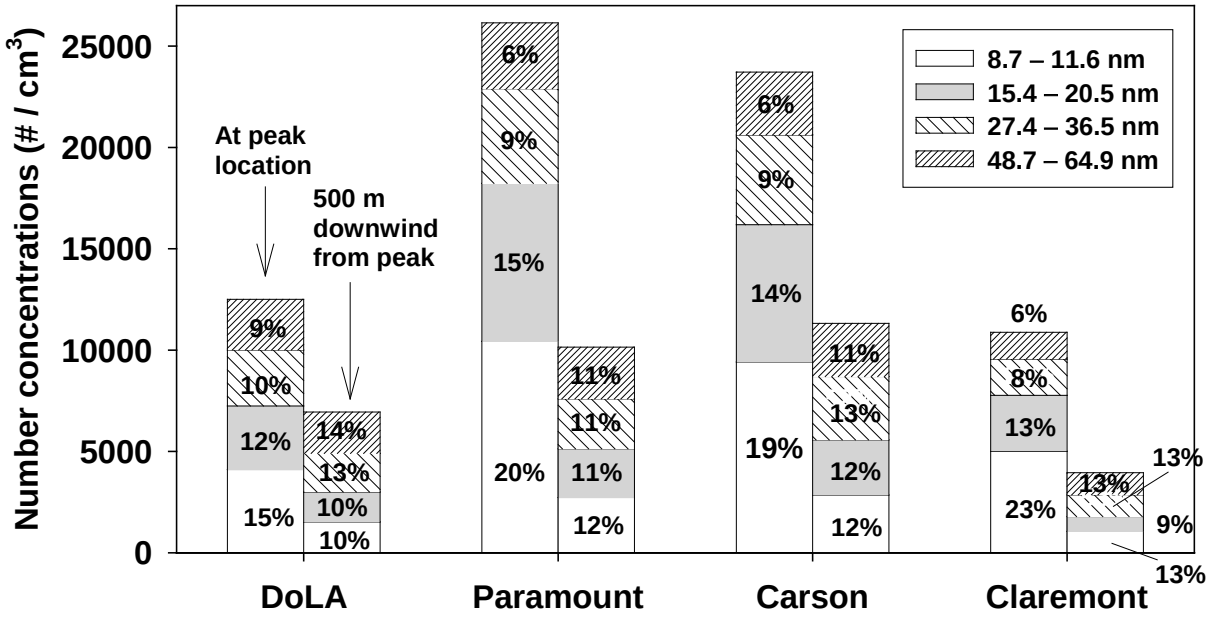

Figure 20. Number concentrations (particles·cm^{-3}) in four size-segregated bins (8.7–11.6 nm, 15.4–20.5 nm, 27.4–36.5 nm, and 48.7–64.9 nm), where mode-like peaks appeared in the mean size distributions (Figure 19). Their contributions to the total number concentrations are shown inside the bars (%). Left stacks for each transect are for the peak location of the plume and right stacks are for 500 m downwind from the peak.

As expressed in Eq. (6), the decay rates of particle numbers from dilution result from both the entrainment coefficient (*K*) and the particle number gradient between a plume and surrounding background (*Δ[UFP]*). Although it is reasonable to assume the same *K* can be applied to particles in *modes 1 – 4* [41], *Δ[UFP]* varied significantly among size modes (*Δ[UFP]* were inversely related to size) possibly causing changes in dilution rates for different modes. However, this hypothesis does not exclude the possibility that other particle dynamics, such as evaporation/condensation, coagulation, and/or dry deposition, contribute to the spatial variations in UFP near the freeway under calm and stable pre-sunrise conditions.

8.5 Concentration variations in other pollutants with distance downwind from the freeways

A summary of concentrations of other pollutants at several downwind distances from freeway peaks is shown in Table 7. Concentration profiles of NO and PB-PAH, pollutants simultaneously measured with UFP, showed clear and significant freeway emissions (Figure 21).

Although the upwind background concentrations of NO and PB-PAH ranged widely (0.7 to 75 ppb and 0.6 to 26 ng·m^{-3} for NO and PB-PAH, respectively), the difference between the peak and background concentrations ($\Delta[NO]_{peak}$) was much narrower (23 to 63 ppb and 23 to 31 ng·m^{-3} for NO and PB-PAH, respectively). Because concentrations normalized to the background are strongly influenced by the background levels, the difference between the plume and background appears to be more representative of fresh freeway emissions. For example, the ratios of NO peak concentration to the background for the Carson and Claremont transects are 1.8 and 33, respectively, while $\Delta[NO]_{peak}$ for the Carson transect (63 ppb) is three times bigger than that for the Claremont transect (23 ppb), much more consistent with the difference in freeway traffic flows for the Carson transect (Table 7).

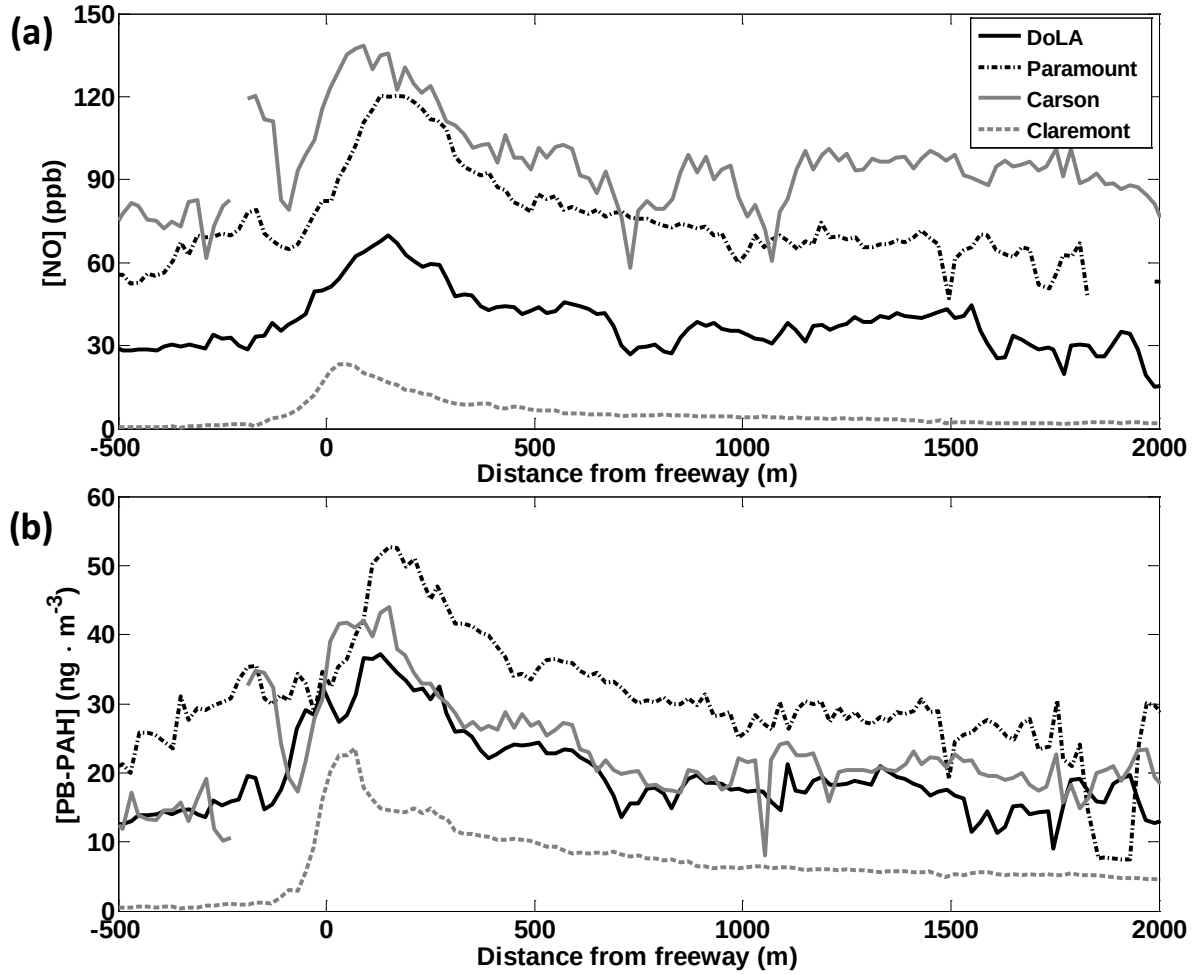

Figure 21. Averaged spatial variations in (a) [NO] and (b) [PB-PAH] near the freeways for the DoLA (black solid line), Paramount (black dash-dotted line), Carson (gray solid line), and Claremont transects (gray dashed line).

Table 7. Mean concentrations in the upwind area, at the plume peak location, and 300m, 500m, and 1500m downwind from the peak of NO, PB-PAH, CO, and $PM_{2.5}$. Background-subtracted concentrations at the peak location are also provided.

Species	Transect	Background Conc.	Peak Conc.	$\Delta[C]_{peak}$ [a]	Conc. at 300m downwind[b]	Conc. at 500m downwind[b]	Conc. at 1500m downwind[b]
NO (ppb)	DoLA	28.8	69.7	40.9	47.7	43.8	40.0
	Paramount	59.6	120.4	60.8	98.2	84.7	47.0
	West Carson	75.4	138.3	62.9	109.6	93.8	99.0
	Claremont	0.7	23.4	22.7	9.2	6.7	2.2
PB-PAH ($ng \cdot m^{-3}$)	DoLA	14.0	37.2	23.2	25.9	24.3	16.8
	Paramount	25.8	52.7	26.9	41.6	35.1	19.1
	West Carson	13.2	44.0	30.7	28.6	26.8	22.6
	Claremont	0.6	23.6	23.0	11.5	9.8	5.3
CO (ppm)	DoLA	1.14	1.65	0.51	1.33	1.36	1.12
	Paramount	1.19	2.01	0.83	1.59	1.29	0.76
	West Carson	1.17	2.02	0.85	1.69	1.61	1.37
	Claremont	0.55	0.64	0.09	0.55	0.54	0.51
$PM_{2.5}$ ($\mu g \cdot m^{-3}$)	DoLA	15.6	18.4	2.8	16.5	16.1	16.0
	Paramount	24.0	29.9	5.9	27.23	25.2	21.2
	West Carson	11.5	15.4	3.9	13.7	12.8	12.3
	Claremont	10.0	12.2	2.2	11.2	10.9	10.1

a. Background subtracted concentration at the freeway peak location.
b. Concentrations at the downwind distance from the freeway peak position.
∗ Corresponding UFP data is shown in Figure 3.

The dilution rate coefficients, *K(x)* for NO estimated with Eq. (7) were $3.0(\pm 4\%)\times 10^{-3}$ (DoLA), $2.7(\pm 3\%)\times 10^{-3}$ (Paramount), $2.5(\pm 4\%)\times 10^{-3}$ (Carson), and $3.2(\pm 2\%)\times 10^{-3}$ (Claremont), similar to the dilution rates for UFP (above). *K(x)* values for PB-PAH were similar to those for NO and UFP, at $2.7(\pm 4\%)\times 10^{-3}$ (DoLA), $2.7(\pm 3\%)\times 10^{-3}$ (Paramount), $2.9(\pm 4\%)\times 10^{-3}$ (Carson), and $2.2(\pm 3\%)\times 10^{-3}$ (Claremont). The *K(x)* value for NO for Claremont is significantly higher than those for UFP and PB-PAH. This may result from the extremely low concentration of background NO which, in turn, may result from higher nighttime ozone levels for that transect facilitating chemical NO loss with ozone. The surface ozone levels from California Air Resource Board monitoring sites were 23 (±6) ppb in the near Claremont site (Glendora-Laurel), whereas ranged 0–4 ppb in the near the other three transects during the measurement periods [42]. The very low upwind background levels of traffic-related pollutants on the Claremont transect (Table 7) is likely due to increased ambient ozone and the fact that the upwind area is unpopulated. Nearby ozone concentrations were 44 (±15) ppb during the measurement periods, supporting this hypothesis.

CO and $PM_{2.5}$ are relatively long-lived pollutants and have higher urban backgrounds. As a result, freeway peaks were less pronounced; freeway peaks for CO and $PM_{2.5}$ were ~51% and ~25% higher for CO and $PM_{2.5,}$ respectively, compared to a factor of > 2–3 for NO and PB-PAH (Table 7).

9.0 Predicting freeway plume lengths during the stable early morning.

9.1 Introduction

Although a number of studies on UFP emissions from major roadways and their spatial impacts have recently been conducted, the sampling conditions in most studies were limited to the daytime unstable convective boundary layer [28]. However, Hu et al. [2] found a wide UFP impact up to 2 km downwind of the I-10 freeway during stable pre-sunrise hours in Santa Monica, California. Subsequently, in Section 8 we confirm the prevalence of wide area impacts downwind of freeways under stable pre-sunrise conditions in the South California Air Basin (SoCAB) and found the decay constant of UFP concentrations with distance under stable conditions is one order of magnitude smaller than that of daytime. Although the dominant factor that results in differences in dispersion/dilution rates between nocturnal (or stable) and daytime conditions is clearly atmospheric stability combined with different boundary layer heights [2, 4, 43, 44], quantitative and systematic meteorological dependencies of the decay of primary pollutants with distance downwind of major roads have yet to be developed, particularly for stable atmospheres. This gap prevents the prediction of the extent and magnitude of roadway plumes under stable conditions.

Many studies have attempted to predict the pollutant concentrations from vehicular emissions near roadways using various dispersion models [45]. However, most studies have focused on predicting elevated pollutant concentrations at a specific distance in the vicinity of the sources rather than describing concentration profiles. A few studies attempted to reproduce UFP concentration profiles obtained during daytime conditions within short distance ranges [< 300 m, 5, 46], however, these studies focused only on decay rates during daytime at several discrete distances.

Gaussian dispersion models have been commonly used to explain the spatial concentration variations from line sources [e.g., 38, 45, 46-48]. In this model, parameterization of dispersion coefficients is critical to calculate pollutant concentrations at specific distances from the source. Existing parameterizations of the dispersion coefficients are based on Pasquill stability classes [49]. However, the Pasquill parameterization has only two classes for stable conditions (Table 8), and thus has limited ability to explain the variations in concentration profiles under stable conditions.

Table 8. Parameterizations of σ_z for Gaussian and K-theory dispersion models

References	Equation form	Land use	Stability Class	σ_z or γ^* formula
Chock [50]	$\sigma_z = (a + b \cdot x)^c$	N/A	Stable	a=1.49, b=0.15, c=0.77
Briggs [51]	$\sigma_z = \frac{\alpha \cdot x}{(1 + \beta \cdot x)}$	Rural	E[a] (slightly stable)	α = 0.03 β = 0.3×10^{-3}
			F[a] (moderately stable)	α = 0.016 β = 0.3×10^{-3}
		Urban	E– F[+] (stable)	α = 0.08 β = 1.5×10^{-3}
Sharan and Yadav [52]	$\gamma = (\sigma_w/U)^2$	N/A	Stable or unstable	$\sigma_w = \sqrt{\overline{(w - \bar{w})^2}}$

[+] E and F are Pasquill stability classes for nighttime conditions [49].

[*] γ represents a turbulence parameter used in Sharan and Yadav (1998), where σ_w is turbulence intensity in vertical direction, w is vertical wind component, and U is the mean wind speed.

In the present study, the effectiveness of the Gaussian dispersion model solution to fit observed UFP concentration profiles, and estimations of dispersion coefficients as well as emission factors directly from the observations, are discussed. In addition, the quantitative effects of meteorological parameters and the role of background-subtracted plume concentrations on plume extensions are investigated. Appropriate parameterization of dispersion coefficients and emission factors based on observable variables can provide predictive capability for the extent of freeway plumes under stable conditions.

9.2 Development of a curve fit equation

Although particle number concentrations are influenced by particle dynamics such as coagulation, deposition, and condensation/evaporation, a common conclusion from previous studies is that dilution is the most important process controlling particle number [e.g., 38]. Particularly near emission sources, such as the curbside of a major road, the dilution timescale is approximately one to two orders of magnitude faster than deposition and coagulation, respectively [38]. Thus, in this study, it is assumed dispersion is a dominant contributor to changes in UFP number concentrations within about 2 km from freeways.

A Gaussian dispersion model solution assuming an infinite line source was applied as a basic equation for curve fits to the observed concentration profiles (Eq. 8):

$$C(x,z) = \frac{Q}{\sqrt{2\pi}\sigma_z(x) \cdot U_e}\left[\exp\left(-\frac{(z+H)^2}{2\sigma_z^2(x)}\right) + \exp\left(-\frac{(z-H)^2}{2\sigma_z^2(x)}\right)\right] \quad \text{(Eq. 8)}$$

where Q (particles·m^{-1}·s^{-1}) is an emission rate, U_e is an effective wind speed (ambient wind + speed correction due to traffic wake), z is height, H is the height of emission source, and σ_z is the standard deviations of the time-averaged concentration distributions in the vertical directions at distance x from the source [53]. An infinite line source assumption is considered reasonable for the present study due to the long length of freeways (more than 20 km) compared to relatively short downwind length scale of transects (~ 2 km). Equation (8) is additionally simplified to obtain a final curve fit equation (Eq. 9), where Q_c represents a bulk emission parameter including emission rate (Q) combined with wind effects (U_e), and remains as a free variable to be determined from observed concentration profiles.

$$C(x,z) = \frac{Q_c}{\sigma_z}\left[\exp\left(-\frac{(z+H)^2}{2\sigma_z^{\,2}}\right)+\exp\left(-\frac{(z-H)^2}{2\sigma_z^{\,2}}\right)\right] \qquad \text{(Eq. 9)}$$

The final step to formulate a curve fit equation is to parameterize σ_z, and two common methods were examined: Chock's [50] and Briggs' [51] formulas, which were used by Luhar and Patil [53] and Briant et al. [48], respectively, for their model evaluations. However, we note both Chock's and Briggs' formulas have just one or two equations for stable atmospheres, based on land use (e.g., urban and rural). Thus, neither formula is sufficient to explain the meteorology-dependent variations in observed freeway plume decays during stable pre-sunrise hours. To account for these limits, two coefficients in Chock's and Briggs' formulas remained as free variables in the curve fit equation (e.g., α and β for Briggs formula in Eq. 10), and we found the best results to describe the observed concentration profiles were obtained with the Briggs' formula form. Curve fit results with Chock's formula tended to underestimate the peak concentrations near freeways.

$$\sigma_z(x) = \frac{\alpha \cdot x}{1+\beta \cdot x} \qquad \text{(Eq. 10)}$$

We additionally examined a K-theory model, which was developed by Sharan and Yadav [52] for dispersion of pollutants from a point source under stable conditions with light winds (Table 8). Zhu and Hinds [5] modified the K-theory model for a line source to explain the decay of a freeway plume during daytime. The curve fits with the K-theory model yielded poorer fits to our observations in the far downwind areas than did the Gaussian model with the Briggs formulation for σ_z. Consequently, Eq. (9) combined with Eq. (10) was used to fit the observed data using least squares in the MATLAB environment.

9.3 Curve fit parameters (Q_c, α, and β)

The emission parameter, Q_c, which represents the wind speed-corrected emission factor, influences only the magnitude of the peak and the overall pollutant concentrations. Thus, this method allows us to estimate an emission factor for a mixed vehicle fleet on major roads directly from the observed concentration profiles.

Pollutant profiles simulated with Eqs. (9) and (10) clearly show that as α decreases, holding β constant, the freeway plume peak appears farther downwind of the emission source, allowing pollutants to be transported farther downwind (Figure 22a). With a fixed α, decreasing β results in more rapid dissipation of the plume, but the peak location is unaffected (Figure 22b).

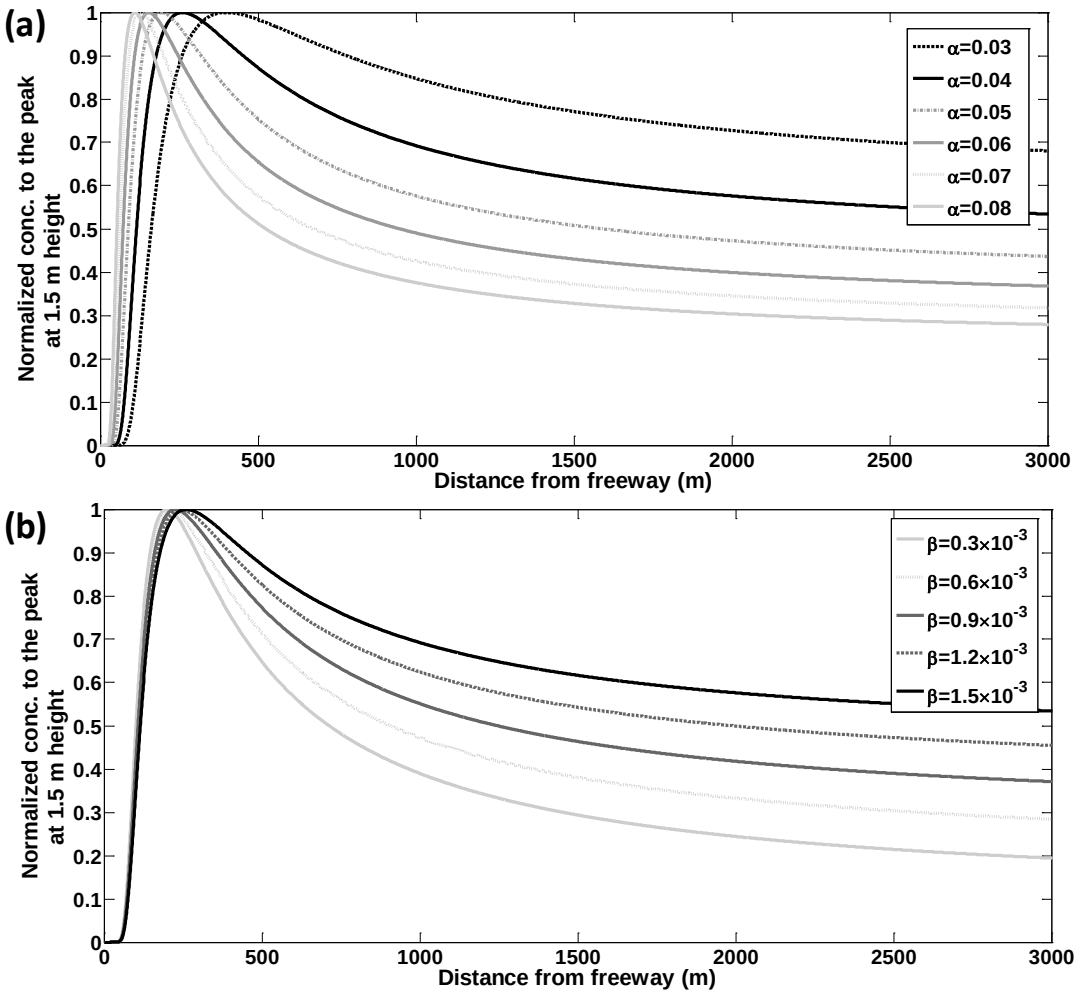

Figure 22. Variations in spatial profiles of pollutants calculated with Eq. (9) and (10) varying α or β. *X*-axis is distance downwind from freeway and y-axis is normalized concentrations to the peak at 1.5 m height (z = 1.5 m). (a) Results were obtained with fixed Q_c and $\beta = 1.5\times10^{-3}$ and varying α from 0.03 to 0.08, and (b) with a fixed Q_c and α = 0.04, changing β from 0.3 – 1.5×10^{-3}.

Here, we explore the values for α and β derived by fitting Eqs. (9) and (10) to the daily averaged data, in order to quantitatively investigate the effects of both meteorology and traffic density on the magnitude of peak concentrations and decay rates of freeway plumes. If α and β are properly parameterized with measurable properties such as surface meteorology, it is possible to predict how widely freeway plumes influence neighborhoods downwind of freeways under stable atmospheric conditions.

We note that the peak concentrations can be directly influenced by vehicle number and type (and other characteristics), passing on the freeway at the moment when the mobile platform crosses the freeway, whereas the long early morning plume tails result from rather slow transport. For example, with consistent winds of 0.5 m/s, air travel time is about 30 seconds and 1 hour at 15 m and 2 km downwind of freeway, respectively. Because traveling a transect with the mobile platform usually requires 10 to 15 minutes, and traffic flows on freeways often show

patchy distributions, individual scans are complicated to interpret due to different time scales between the peak and tails of plumes. For this reason, we use daily averaged profiles for the present study.

9.4 Ability of Gaussian to fit to the observations

In this section, the effectiveness of curve fitting to the observations and comparisons of the mean dispersion coefficients (α and β) to those commonly used in the model (Briggs' formula, Table 8) are discussed.

For all four transects, curve fits describe well the observed profiles of UFP number concentrations both at the peak and far downwind (R^2 ~ 0.9 or better) (Figure 23). Curve fits, however, do not explain a slight increment in UFP concentrations in close proximity to the freeways in upwind directions. These discrepancies are likely to result from both wind variability on a short timescale and eddy diffusion in the direction opposite to the prevailing winds. The mean values of α obtained from the observations were 0.07, 0.03, 0.02, and 0.03 for the DoLA, Paramount, Carson, and Claremont transects, respectively, and of β were 0.4×10^{-3}, -0.5×10^{-3}, 0.6×10^{-3}, and 2.8×10^{-3} for DoLA, Paramount, Carson, and Claremont, respectively (Table 9).

Table 9. Summary of measurements, estimated emission parameter, Q_c, and dispersion coefficients (α and β) from the curve fits.

Measurement area (transect street)	Date	Backgnd[a] conc. ($\times 10^3$)	Q_c ($\times 10^4$)	α	β ($\times 10^{-3}$)	Transect averaged Q_c, σ_z and R^2 for curve fit	Model fit condition
Downtown LA (Coronado St.)	2/24/11	16.1	1.34	0.059	0.81	$Q_c = 8.7\times10^4$	H = 6 m
	3/7/11	4.7	0.93	0.105	1.79	$\sigma_z = \frac{0.07x}{(1+0.4\times10^{-3}x)}$	z =1.5 m
	3/9/11	14.7	0.99	0.056	0.15		
	3/14/11	13.0	1.15	0.085	1.72	R^2 =0.96	
	3/17/11	16.1	0.63	0.089	1.21		
Paramount (Obispo St.)	1/27/11	19.3	1.86	0.038	-0.19	$Q_c = 16.5\times10^4$	H = 6 m
	2/1/11	18.3	1.83	0.045	-0.12	$\sigma_z = \frac{0.034x}{(1-0.5\times10^{-3}x)}$	z =1.5 m
	3/10/11	12.4	1.32	0.048	-0.34		
	3/15/11	6.1	1.70	0.063	0.58	R^2 =0.96	
	3/18/11	19.8	1.94	0.038	-0.43		
West Carson (228th St.)	1/21/11	23.6	0.63	0.024	1.29	$Q_c = 5.6\times10^3$	H = 0 m[b]
	2/3/11	21.6	0.74	0.016	0.09	$\sigma_z = \frac{0.02x}{(1+0.6\times10^{-3}x)}$	z =1.5 m
	3/8/11	11.0	0.43	0.034	1.51		
	3/11/11	14.2	0.56	0.020	-0.14	R^2 =0.91	
	3/16/11	15.3	0.27	0.035	3.85		
	3/29/11	12.3	0.58	0.023	0.14		
Claremont (Mountain Ave.)	5/19/11	4.8	0.38	0.030	3.42	$Q_c = 3.0\times10^3$	H = 0 m[b]
	5/24/11	6.4	0.26	0.035	5.37	$\sigma_z = \frac{0.03x}{(1+2.8\times10^{-3}x)}$	z =1.5 m
	5/25/11	7.2	0.32	0.066	7.29		
	5/26/11	7.0	0.39	0.020	1.44	R^2 =0.87	
	6/1/11	5.1	0.31	0.050	5.18		
	6/2/11	7.4	0.50	0.029	2.27		
	6/7/11	7.1	0.26	0.048	4.55		

[a] Background concentrations are defined as a lower 25% quantile point in the upwind area.

[b] Actual height of the freeway surface is about 5 m below the transect. However, it is assumed that a freeway plume is well mixed within freeway area due to mechanical turbulence produced by vehicle wakes and then rolls up to the measurement transect.

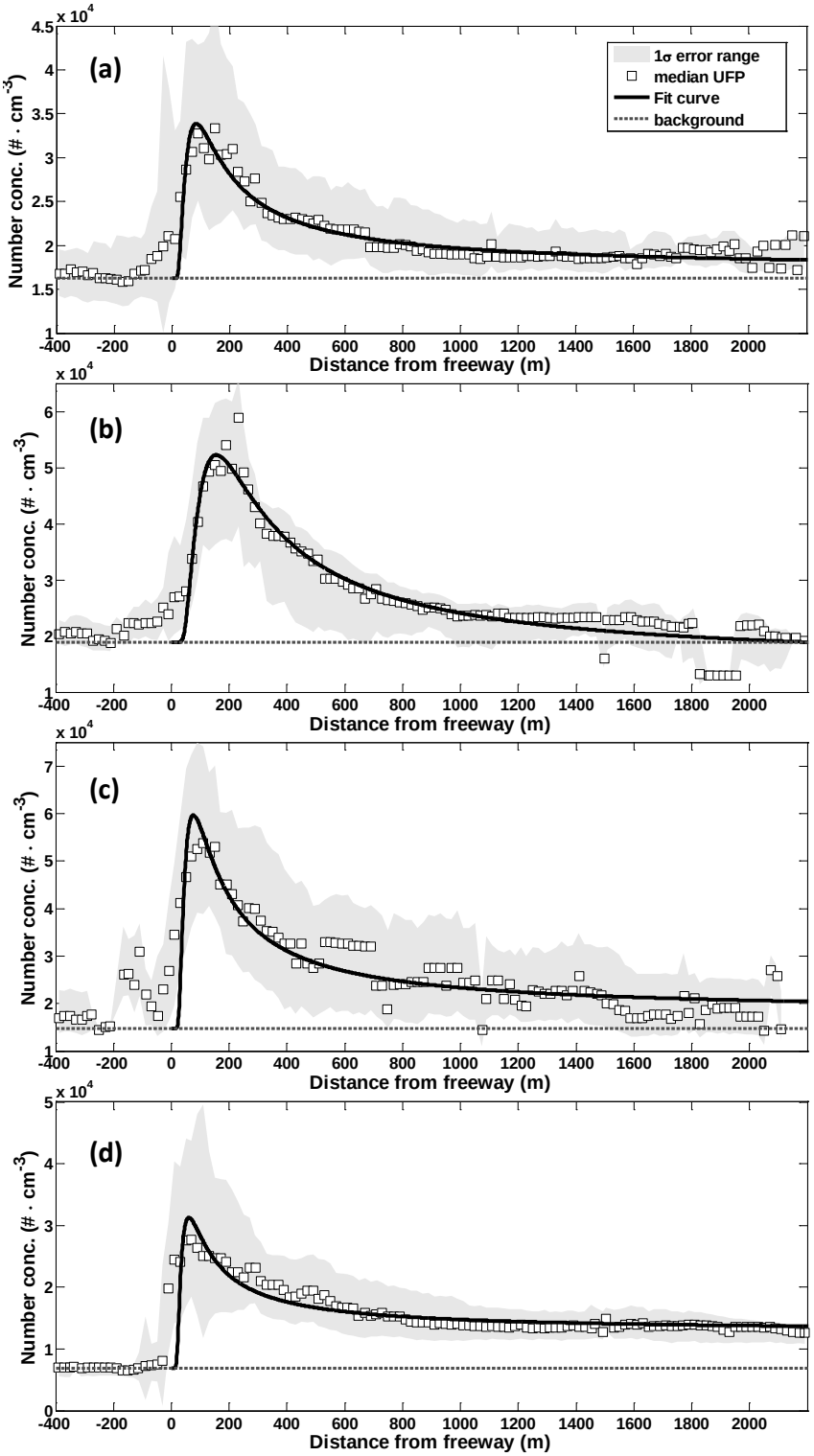

Figure 23. Observed median UFP number concentrations with distance downwind of freeways (white squares), 1σ error ranges (gray areas), upwind background concentrations (horizontal dark gray dashed lines), and curve fits to the observations with Gaussian dispersion model form (black lines) for (a) the DoLA, (b) Paramount, (c) Carson, and (d) Claremont transects.

The Briggs' [51] α and β values are listed in Table 8. The mean α for the DoLA transect (0.07) is similar to Briggs' value for urban areas under stable conditions (α = 0.08), and α for the other three transects are comparable to Briggs' constant for rural areas under slightly stable conditions (α = 0.03) or between urban and rural values under moderately stable conditions (α = 0.08 and 0.016 for urban and rural, respectively). The DoLA transect is located in a highly urbanized area, with tall buildings on the downwind side, while the Paramount, Carson, and Claremont transects are in less urbanized areas, surrounded mostly by residential neighborhoods [6].

The mean β for the DoLA and Paramount transects were smaller than the Briggs' value for urban (1.5×10^{-3}) and rural areas (0.3×10^{-3}), respectively. On the contrary, β observed in Claremont was higher than the Briggs' β value even for urban areas. Curve fits for the Carson transect yielded a β between the Briggs' β for urban and rural areas. Physically, these results suggest UFP emitted from freeways dispersed more quickly in DoLA and Paramount, where the freeways pass over the transect, than reported decay rates in the literature

Table 8,[Table 1; 51]. UFP decays for the Claremont transect were slower than expected and for the Carson transect comparable to those in the literature. Freeways in Carson and Claremont pass 6–8 m under the transect streets. Overall, both α and β ranged widely by location when compared to the generalized Briggs' formula. Those differences might be caused in part by freeway topographic features and/or other processes such as particle dynamics. In any case, the curve fit methods provide an effective tool to estimate dispersion coefficients directly from the observations.

9.4.1 Impacts of dispersion coefficients and freeway-street interchange geometry on plume shapes

The dispersion coefficients α and β show a strong positive correlation with one another, but clearly fall into two exclusive groups, apparently the result of the freeway-street interchange geometry (Figure 24). This outcome resulted from the different inputs in the curve fit equation (Eq. 9) for the two cases: source height H = 6 m for group *A* (freeway passes over the transect) and H = 0 m for *B* (freeway passes below). Compared to group *B*, group *A* values for α ranged more widely and β varied less. For group *A* (overpass freeways), it takes more time for the vehicular plume to disperse before reaching the ground from the elevated freeway height, thus the location of the peak, which depends on α, may vary depending on topographic and atmospheric conditions. In contrast, for group *B* (underpass freeways), the peak will appear adjacent to the freeway regardless of atmospheric conditions because a plume rises directly from the freeway, which may lead to smaller variations in α, and relatively larger variations in β. These results suggest the importance of freeway–street interchange geometry in determining dispersion coefficients.

A positive correlation between α and β suggests overlap in the factors controlling α and β. Figure 24 illustrates that α is related to the peak position and plume width (advection), and β to plume dilution rates (eddy diffusion or entrainment). Based on above findings, we can hypothesize that a positive correlation between α and β was caused by (1) meteorological conditions (advection and turbulence; *hypothesis 1*) and/or (2) plume intensity (*hypothesis 2*). In the following sections, these two hypotheses are discussed in detail.

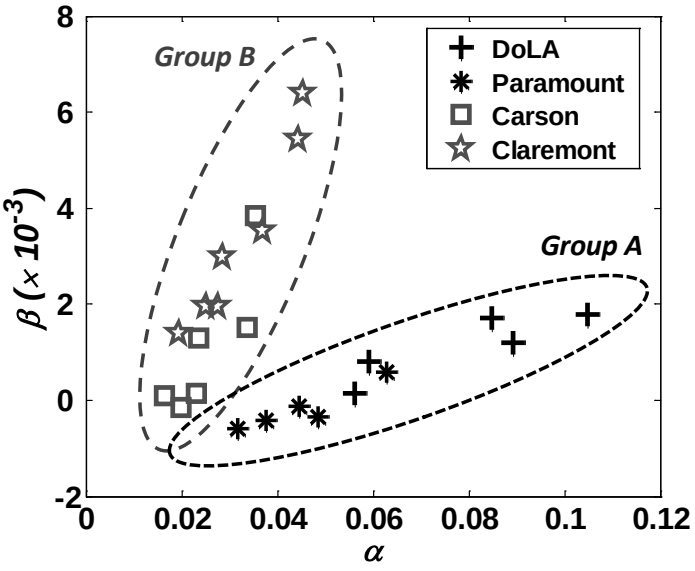

Figure 24. Relationship between α and β obtained from the curve fits to daily mean spatial profiles of UFP in the DoLA (black crosses), Paramount (black asterisks), Carson (gray squares), and Claremont (gray stars) transects. Black dotted line represents a group A, where freeways pass over the transects and gray dashed line a group B, where freeways pass under the transects.

9.5 Meteorological effects on plume characteristics (hypothesis 1)

For hypothesis 1, pollutants can be effectively advected farther with relatively moderate and consistent winds in one direction in stable environments. On the other hand, stronger winds may produce more vigorous turbulence to disperse pollutants more rapidly. Thus, for stable pre-sunrise hours, moderate and consistent winds may be able to effectively transport plumes (smaller α), but would result in faster decay rates (smaller β), compared to weaker winds.

9.5.1 Wind direction

Hypothesis 1 focuses on the role of meteorology such as wind speed and direction in variations in the dispersion coefficient, α and β. As expected, in addition to determining the upwind and downwind side, wind direction was a determinant of plume length. The dispersion coefficient, α, generally showed a negative relationship with relative wind direction to the freeway (WD_{rel}, 90° = normal to freeway), suggesting plumes are more effectively transported with winds perpendicular to the freeway (Figure 24a). A positive correlation of elevated $\Delta[UFP]_{1km}$ (background subtracted UFP number concentration, $[UFP]_{1km} - [UFP]_{bkgnd}$) at 1km downwind of freeway with WD_{rel} supports the effects of WD_{rel} on plume transport (Figure 24b). However, the high scatter observed indicates the importance of other factors. Dispersion coefficient β does not show an observable relationship with WD_{rel} (not shown), because wind direction is not directly related to the dilution process.

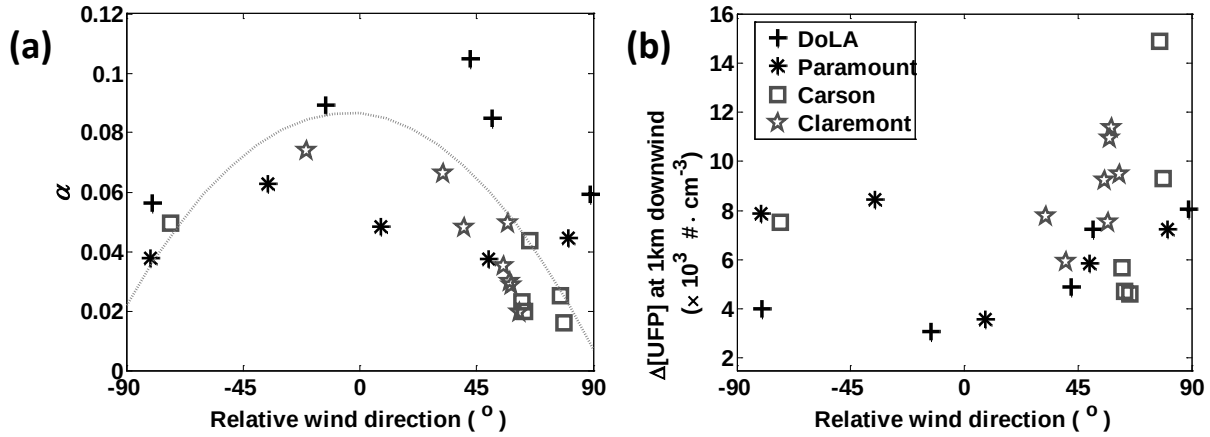

Figure 25. Wind direction effects on (a) dispersion coefficient, α, and (b) background subtracted UFP concentrations at 1 km downwind of freeway. Black crosses, black asterisks, gray squares, and gray stars represent daily mean values for the DoLA, Paramount, Carson, and Claremont transects, respectively. Relative wind direction is daily mean wind direction relative to freeway orientation (90 ° = normal to freeway). Gray dotted line in (a) represents 2nd order polynomial fits (R^2=0.48).

9.5.2 Wind speeds

Under convective boundary layer conditions, higher wind speeds enhance the instability of the air, producing mechanical turbulence energy in addition to thermally induced turbulence. However, at the same time, consistent winds also effectively transport air masses via advection. At night, statically stable air suppresses turbulent energy production, thus under calm stable conditions, moderate consistent winds can help transport an air mass farther. *Hypothesis 1* suggests that both α and β would decrease (more transport and faster dispersion) as wind speeds increase under calm conditions, assuming a consistent wind direction. α is likely to be more related to vector averaged resultant wind speeds because the hypothesis concerns transport, whereas β should more depend on scalar wind speeds, which should most directly affect dispersion rate.

Figure 26a shows that α responds differently to resultant wind speeds according to freeway–street interchange geometry. For the underpass freeways (Carson and Claremont), α appears to increase with resultant wind speeds, although the trend is largely driven by one data point obtained on 6/8/2011, represented as a light gray star in Figure 26. On that day, winds were unusually strong, the prevailing wind direction was reversed, and a fog formed in the uphill downwind area. For the underpass freeway transects, the peak concentration location might not be significantly influenced by wind speeds, since a plume is directly emitted below the transects. Therefore, wind speeds might more strongly impact the dissipation rate (β) of a plume, creating faster decays and narrower peaks as the wind speed increases (Figure 26b). In contrast, clear negative relationships between α and resultant wind speeds were observed for the overpass freeway transects (DoLA and Paramount). Different scales of α in DoLA and Paramount are likely to result from differences in land use (e.g., urbanized or semi-urbanized) as discussed below. Plumes emitted above the transects will be transported farther with higher resultant wind speeds before reaching the ground (smaller α), explaining the negative correlation between α and resultant wind speeds.

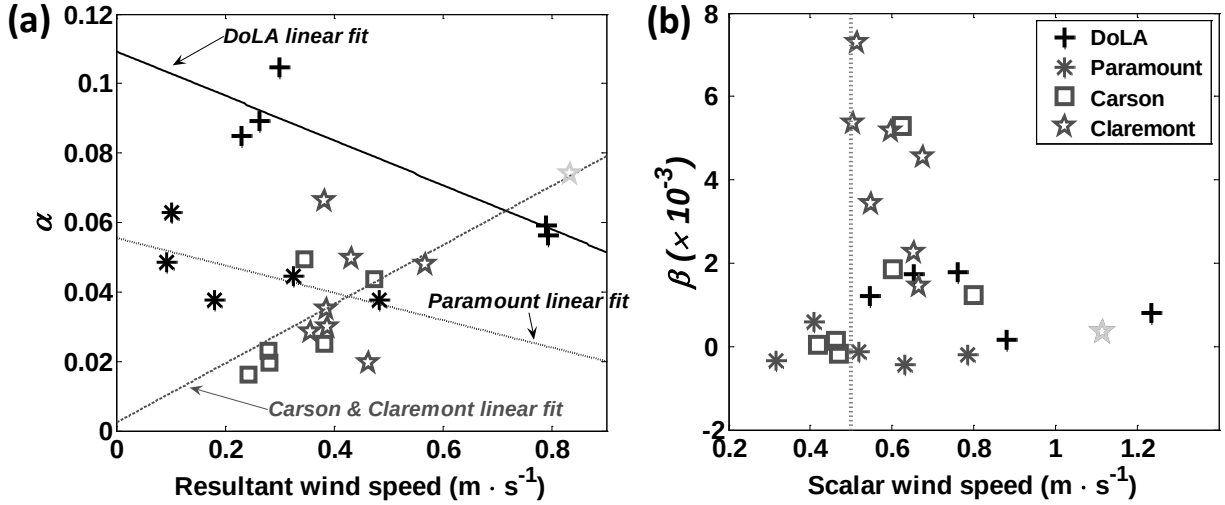

Figure 26. Variations in dispersion coefficients as a function of wind speeds. (a) α vs. vector averaged resultant wind speeds (R^2=0.81 for DoLA; 0.41 for Paramount; 0.49 for Carson & Claremont). (b) β vs. scalar averaged wind speeds. Black solid line is a linear fit for the DoLA data points, black dotted line for Paramount, and gray dashed line for Carson and Claremont. Vertical dotted line in (b) represents scalar wind speed of 0.5 m·s^{-1}. Light gray star denotes Claremont data obtained on 6/8/2011 when wind was strong with reversed prevailing wind direction and fog in the uphill downwind area.

Scalar wind speeds (WSS) and β were, in general, negatively correlated (Figure 26b) when wind speeds were larger than 0.5 m·s^{-1}. In contrast to the α–resultant wind speeds relationships, the overpass freeway transects (DoLA and Paramount) were more weakly correlated than underpass freeway sites. It appears that wind speeds influence α more strongly for the overpass freeway transects, whereas for the underpass freeway transects β is more affected by wind speeds. This negative correlation is not valid under extremely light wind conditions (WSS < 0.5 m·s^{-1}). Under these calm stable conditions, other parameters are likely to govern the dilution rate of a plume, such as concentration gradient, discussed in *Section 3.4*. Overall, winds alone are not likely the dominant factor in determining dispersion coefficients α and β, during the stable pre-sunrise hours. Consequently, *hypothesis 1* by itself cannot explain entirely the variations in plume decays with distance.

9.6 Effects of freeway emissions on plume extension (hypothesis 2)

For hypothesis 2, we found higher concentration plumes tend to have smaller α. As discussed in above, a dilution rate in a plume is a function of both dilution coefficient and concentration differences ($\Delta[UFP]$) between the background and plumes [40, 54]. If $\Delta[UFP]$ is larger, a plume will decay faster. Interestingly, we found α and β have stronger correlations with $\Delta[UFP]$ than winds as described below.

9.6.1 Effects of Δ[UFP] on plume decay rates

In order to verify *hypothesis 2*, the effects of $\Delta[UFP]_{peak}$, which is defined as differences between background and plume peak concentrations, on dispersion coefficients α and β were investigated. Larger $\Delta[UFP]_{peak}$ values relate to smaller α and β (Figure 27). Dillon et al. [40] and LaFranchi et al. [54] used Eq. (11) to express dilution rates during the urban plume transport, and in Section 8 we showed a dilution rate coefficient (K) near the peak of freeway plumes can be determined by integrating Eq. (11):

$$\frac{d\left([C]_t - [C]_{bkgnd}\right)}{dt} = -K \cdot \left([C]_t - [C]_{bkgnd}\right) \qquad \text{(Eq. 11)}$$

where t is time, $[C]_t$ and $[C]_{bkgnd}$ are pollutant concentrations at time t in a plume and in the background, respectively. Because dilution rate is a function of $\Delta[C]$ between the background and plumes as well as the dilution rate coefficient (K), differences in decay rates of individual pollutants and among UFP numbers for different size bins can be observed in the same plume [6, 28]. In addition, because $\Delta[UFP]$ decreases with distance, the decay rate would be dampened as a plume ages. This pattern is clearly shown in the observed spatial profiles of UFP for all transects (Figure 23).

Dependencies of β on $\Delta[UFP]_{peak}$ fall into two groups according to freeway-street interchange geometry, as discussed in *Section 3.2* (Figure 27b). Although α and $\Delta[UFP]_{peak}$ seem to follow a single trend line, the transects populate different parts of the curve, larger $\Delta[UFP]_{peak}$ corresponding to the underpass freeway transects. Due to different slopes in these two groups, the overall trend line has an exponential form ($\alpha=0.14\cdot exp(-3.64\times10^{-5}\Delta[UFP]$), R^2=0.59). From the above discussions, we conclude the decay rates are strongly influenced by not only wind speeds and directions but also concentration difference relative to the background, i.e. $\Delta[UFP]_{peak}$.

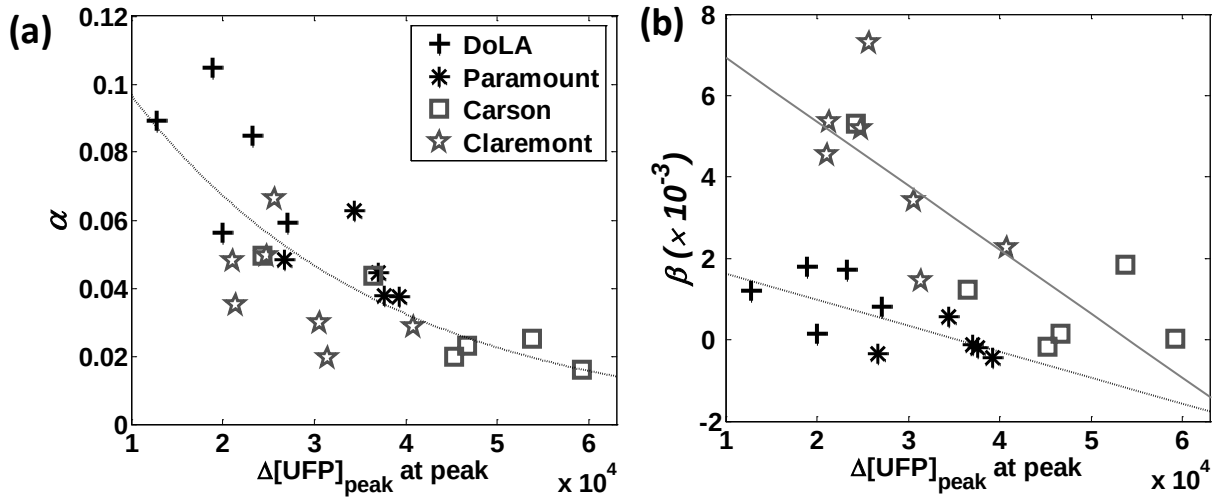

Figure 27. Plots of the relationships of concentration gradient ($\Delta[UFP]_{peak}$) at the peak with (a) α and (b) β. Dotted line in plot (a) is an exponential curve fits: $\alpha=0.14\cdot exp(-3.64\times10^{-5}\Delta[UFP]$) ($R^2$=0.59). Black dotted line and gray solid line in plot (b) are linear fits for over-pass (R^2=0.63) and under-pass (R^2=0.67) freeway transects, respectively.

9.6.2 Temperature, atmospheric stability, and emission factor

Although temperature does not directly affect the dissipation rates of plumes, we found a clear positive correlation between the temperature and the dispersion coefficient, α (Figure 28a; R^2 = 0.48). As discussed in *Section 3.4.1*, $\Delta[UFP]$ is an important factor in determining the dispersion coefficients. Because higher UFP emissions from vehicle tailpipes are strongly related to colder temperature particularly for the nucleation mode (10–20 nm) [7, 8, 55], colder temperatures might indirectly lower dispersion coefficients by elevating UFP concentrations from vehicular sources, and increasing $\Delta[UFP]_{peak}$ (Figure 27a). Supporting the emissions studies [7, 8, 55], higher $\Delta[UFP]_{peak}$ normalized to the traffic density were indeed observed at lower ambient temperatures for all transects in this study (Figure 28b). Zhu et al. [4] also showed the same inverse relationship between temperature and UFP concentrations corrected for traffic volume at the edge of the I-405 freeway.

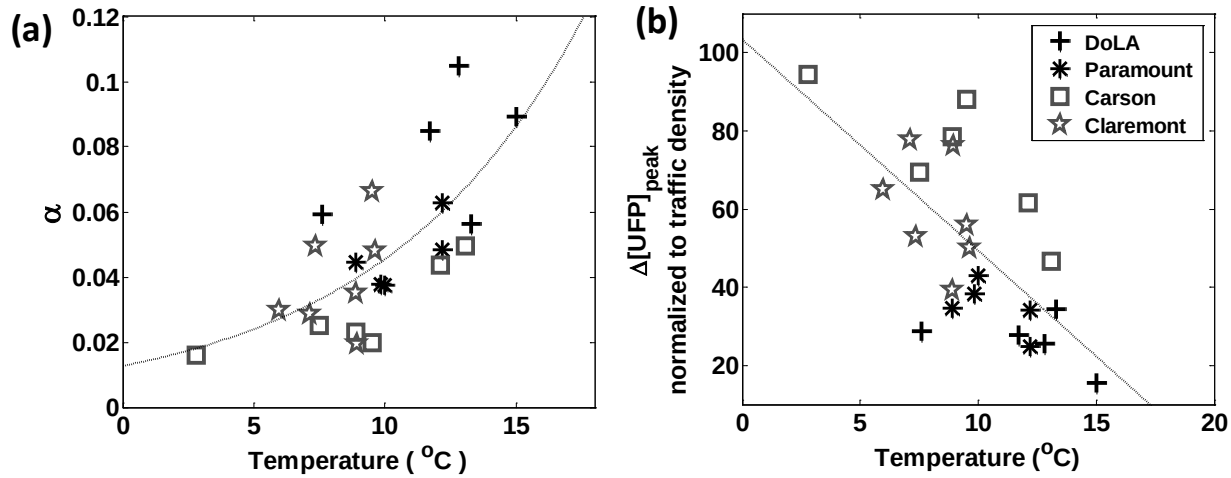

Figure 28. Temperature effects on (a) dispersion coefficient, α, and (b) peak concentration gradient from the background ($\Delta[UFP]_{peak}$ = $[UFP]_{peak}$ − background $[UFP]_{bkgnd}$) corrected by traffic density. Black dotted lines are curve fits: (a) $\alpha = 1.27\times10^{-2}\cdot e^{0.13\cdot T}$ (R^2=0.48) and (b) $\Delta[UFP]_{peak}\cdot(Traffic)^{-1} = -5.41\cdot T+103.4$ (R^2=0.46).

Stable atmospheric conditions lead to the accumulation of vehicular emitted pollutants and long range transport of plumes at night and in the early morning [2, 4, 43, 56]. Section 8 describes the extensions of freeway plumes during stable pre-sunrise hours were commonly observed across the SoCAB. The Richardson number (*Ri*) is a common indicator of atmospheric stability. It combines the vertical temperature gradient (static stability) with mechanical wind shear [57] as expressed in Eq. (12):

$$\text{Richardson number, } Ri \equiv \frac{g}{\overline{\theta}}\frac{d\theta}{dz}\cdot\left(\frac{dU}{dz}\right)^{-2} \qquad \text{(Eq. 12)}$$

where $\overline{\theta}$ is the mean potential temperature in the layer, $d\theta\cdot dz^{-1}$ is temperature gradient, $dU\cdot dz^{-1}$ is vertical wind shear, and g is the gravitational acceleration. $Ri > 0$ for stable, $Ri = 0$ for neutral, and $Ri < 0$ for unstable air.

The pre-sunrise periods for all transects had *Ri* values in the near neutral to stable ranges (Figure 29). Background UFP concentrations tend to increase when air is more stable (Figure 29a) as expected. However, decay rate coefficient β appears to decrease (plume dissipates fast)

when the nocturnal atmosphere is more stable (Figure 29b). We interpret this phenomenon as a result of *hypothesis 2*; larger $\Delta[UFP]_{peak}$ under more stable conditions leads to faster dissipation rate in a plume as discussed above.

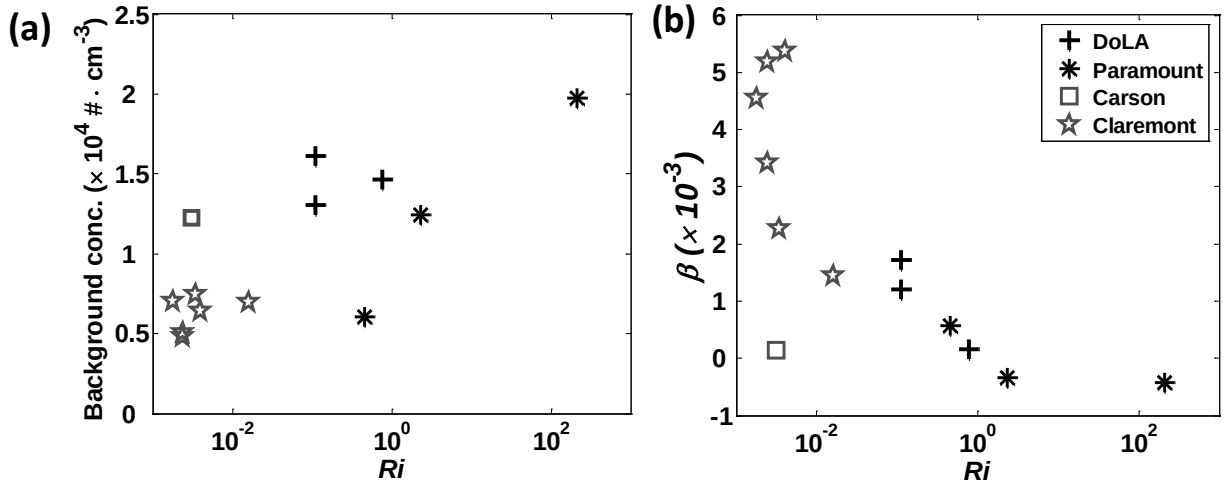

Figure 29. Dependencies of (a) background UFP concentrations and (b) dispersion coefficient, β on atmospheric stability which is represented by Richardson number (*Ri*).

Consequently, the effects of temperature and atmospheric stability on plume dissipation rates support the importance of *hypothesis 2* for plume decay rates. Nonetheless, we should emphasize that faster decay rates do not necessarily mean reduced plume impacts because faster dissipations were observed for higher $\Delta[UFP]_{peak}$ conditions, and higher peak concentrations eventually lead to more elevated UFP concentration in the far downwind areas (e.g., $\Delta[UFP]_{peak}$ shows a positive correlation with $\Delta[UFP]$ at 1,500 m downwind from the freeway; not shown).

9.6.3 Estimate of particle number emission factor (PNEF) and evidence for reductions in ultrafine particle emissions in recent years

Vehicular emissions from the freeways depend on traffic volumes, vehicle types and maintenance, driving conditions, and fuel composition (e.g., sulfur content) [38]. Emission rates estimated by a number of previous studies show considerable variability [38]. The freeways studied here have similar vehicle composition with modest contributions from heavy-duty vehicles (< 3–7%), and consistent traffic speeds due to light traffic density during the pre-sunrise periods. Thus, it is expected that traffic volume is a dominant factor in controlling the variations in emission rates from the freeways. Figure 30a shows a strong linear relationship between emission parameter, Q_c and traffic density (vehicles·5min^{-1}) during the measurement periods, at least when traffic flow ranged from 400 to 1,200 vehicles·5min^{-1} (Eq. 13):

$$Q_c = 227.72\times(\textit{Traffic density}) - 7.30\times10^4, \text{ when } 400 < \text{Traffic density} < 1{,}200 \quad (R^2 = 0.80) \qquad \text{(Eq. 13)}$$

This strong correlation further supports the effectiveness of the curve fit methods described here and also suggests that Q_c estimated from curve fits describes vehicular emission rates from the freeways during the measurement periods well.

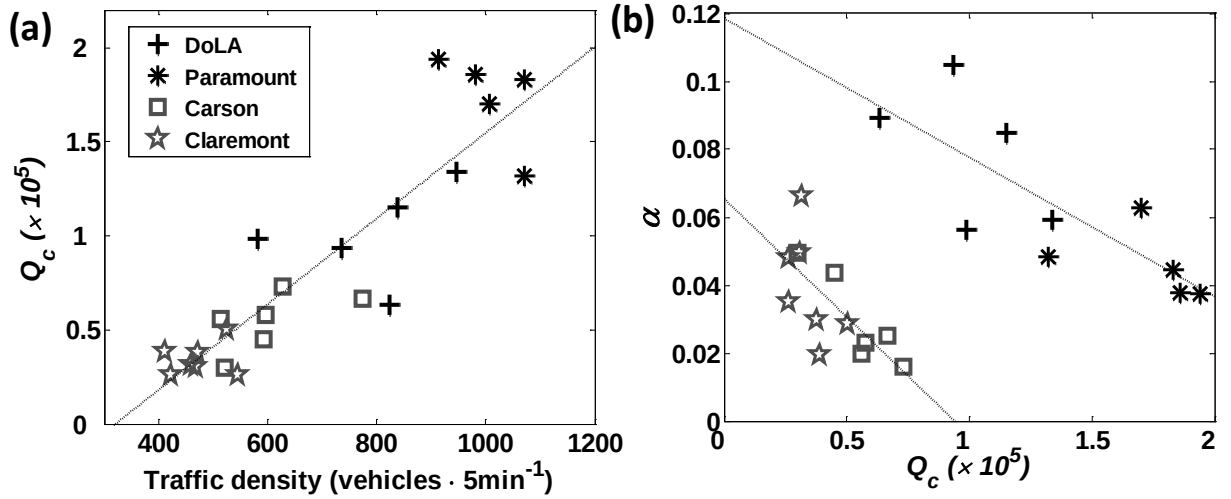

Figure 30. Emission parameter, Q_c as a function of traffic density (vehicles·5min^{-1}) in four sampling sites. Dotted line represents a linear fit to all data points in the plot: (a) Q_c=227.7×(Traffic) − 7.3×10^4 (R^2 = 0.80) and (b) α = -4.1×10^{-7}·Q_c+0.12 (R^2 = 0.63 for overpass freeways) and α = -6.9$_5$×10^{-7}·Q_c+0.065 (R^2 = 0.51 for underpass freeways).

With the mean Q_c (8.12×10^4 particles·m·cm^{-3}), observed wind speeds (0.64 m·s^{-1}), a wind speed correction factor suggested by Chock [50] for stable air (0.2 m·s^{-1}), and observed traffic flow on freeways, the mean particle number emission factor (PNEF), q_{veh} (particles·mi^{-1}·vehicle^{-1}), can be estimated as expressed in Eq. (14), which was derived from Eqs. (8) and (9):

$$q_{veh} = \frac{\sqrt{2\pi} Q_1 \cdot U_e}{(traffic\ density)} = \frac{\sqrt{2\pi} \times (8.12\times10^4) \times (0.64 + 0.2\ m/s) \times 10^6\ cm^3/m^3 \times 300\ s/5\min}{(680.2\ vehicles/5\min)} \quad \text{(Eq. 14)}$$

where the last two values of the numerator are unit conversion factors:

Averaged q_{veh} on the 101, 91, I-110, and I-210 freeways with consistent fleet speeds under stable pre-sunrise conditions was estimated as 1.2×10^{14} particles·mi^{-1}·vehicle^{-1}, which is smaller than the estimate (8.3×10^{14} particles·mi^{-1}·vehicle^{-1}) made by Zhu and Hinds [5] for the nearby I-405 freeway in 2001. In Section 11, we also report reduced peak UFP concentrations near freeways compared to the peak values observed in 2008 and 2005 by Hu et al. [2] and Zhu et al. [4], respectively, increasing the evidence for declining emission factors over the past decade in the SoCAB. In addition, Quiros et al. [58] reported similar value of PNEF (5.5–8.0×10^{13} particles·mi^{-1}·vehicle^{-1}) for the I-405 in 2011, suggesting an ~70% reduction in UFP emissions over the past decade.

9.6.4 Predicting plume behavior

A concern for human exposure to freeway emissions, as well as the utility of air quality studies, is how accurately the plume extension can be predicted with easily measurable data. Once we can properly estimate Q_c, α, and β in the analytical solution form of the Gaussian dispersion model (Eq. 9), the Gaussian line source model can accurately predict not only the peak concentration from the freeway emissions but also the extension of the plumes. This is shown by curve fits using the Gaussian dispersion model precisely describing our observed

concentration profiles during stable pre-sunrise periods. Q_c can be estimated from traffic flow data using Eq. (13). As noted, α and β showed strong positive correlations with freeway topography (Figure 24; Eqs. 15 and 16). Thus, from appropriately estimated α, we can also obtain β.

$\beta = 3.45\times10^{-2}\ \alpha - 1.64\times10^{-3}$ ($R^2 = 0.90$) for group *A* (overpass freeways) (Eq. 15)

$\beta = 1.37\times10^{-1}\ \alpha - 1.86\times10^{-3}$ ($R^2 = 0.74$) for group *B* (underpass freeways) (Eq. 16)

As discussed above, α is strongly related to both meteorology and $\Delta[UFP]_{peak}$. Thus, combining these relationships, it is possible to parameterize α with various statistical methods. In the present study, a multivariate linear regression method was used to reproduce α with observed meteorological and emission data. We assumed α can be expressed as Eq. (17):

$$\alpha_{0,j} = coef_1 \cdot Q_{c,j} + coef_2 \cdot \left|WD_{rel,j}\right| + coef_3 \cdot T_j + coef_4 \cdot WSR_j + C \qquad (j = 1,2,3,...,k) \qquad \text{(Eq. 17)}$$

where *j* indicates the j^{th} observation, Q_c, WD_{rel}, *T*, *WSR, and C* are the emission parameter, wind direction relative to the freeway orientation, ambient temperature, resultant wind speed, and correction factor (intercept), respectively.

Regressions were performed separately according to freeway topography: overpass (group *A*) and underpass freeways (group *B*) due to different dependencies of α on *WSR* and Q_c (Figure 26a and Figure 30b). In addition, the estimations for the DoLA and Paramount transects were also conducted separately because correlations between α and *WSR* were different between the two transects (Figure 26a). Calculated *coefs* are listed in Table 10. Estimated values for α show excellent agreement with observed values with R^2=0.95 (Figure 31a). We acknowledge, however, the perfect agreements for the DoLA and Paramount transects resulted from a limited number of observations (note that just five data points in each transects were used with five variables). Further measurements are needed to verify these results. β was estimated from Eqs. (8) and (9), and compared with observations in Figure 31b. Although the correlation between observations and estimates is somewhat scattered compared to those for α, the predicted values successfully reproduced the observed β values with R^2=0.70.

Table 10. Coefficients obtained from multivariate linear regression using Eq. (10). Bold fonts represent the dominant contributors in the analyses.

	$coef_1$	$coef_2$	$coef_3$	$coef_4$	C
Underpass freeways (Carson and Mountain)	-1.7×10^{-7}	-6.4×10^{-4}	1.2×10^{-3}	5.4×10^{-3}	6.8×10^{-2}
Overpass freeway1 (DoLA)	-2.6×10^{-6}	1.9×10^{-3}	-9.3×10^{-3}	-1.5×10^{-1}	4.4×10^{-1}
Overpass freeway2 (Paramount)	-1.2×10^{-6}	4.2×10^{-3}	9.2×10^{-2}	2.2×10^{-1}	-9.5×10^{-1}

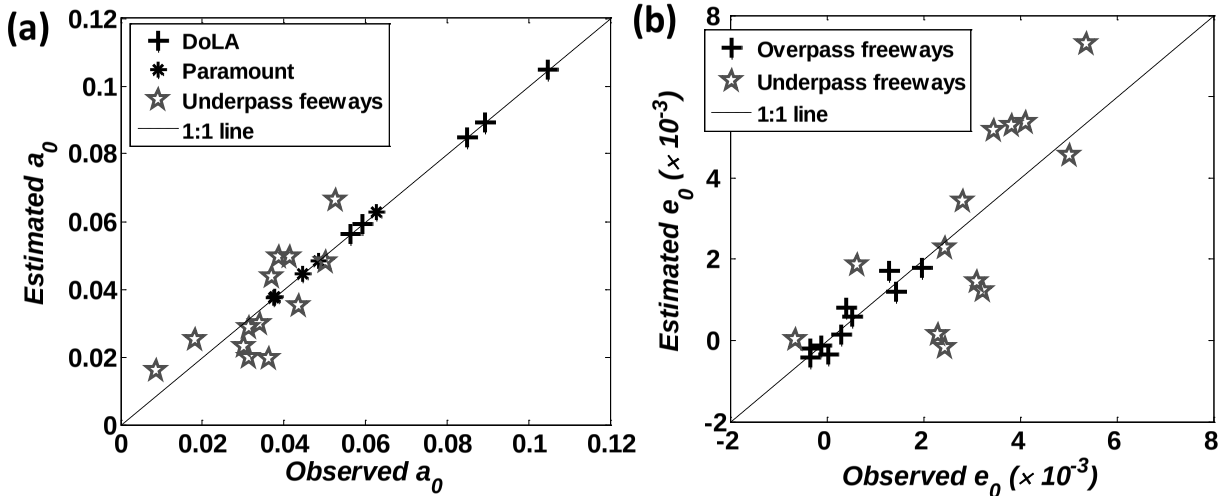

Figure 31. Comparisons of predicted dispersion coefficients (a) α and (b) β with observations.

Consequently, we believe this method provides a more efficient and precise tool to predict freeway plume profiles near major roadways under stable conditions compared with conventional formulas for dispersion coefficients. This study provides useful datasets and the potential to parameterize dispersion coefficients and emission factors for more sophisticated model simulations.

10. Particle Dynamics in the near-roadway region

The mobile measurement platform measurements equipped with Fast Mobility Particle Sizer (FMPS, TSI model 3091) provide a potential to investigate evolution of nanoparticles with distance plume travelled from the freeways with a fine spatial resolution. Figure 32 shows distinct differences in decay rates of each size bin: faster decay as particle size decreases. The previous studies concerning particle evolution were mainly based on particle dynamics models or limited to time scale analysis to our knowledge. In this study, we attempt to estimate the effects of particle dynamics on plume decays from the highly resolved UFP spatial profiles obtained with FMPS.

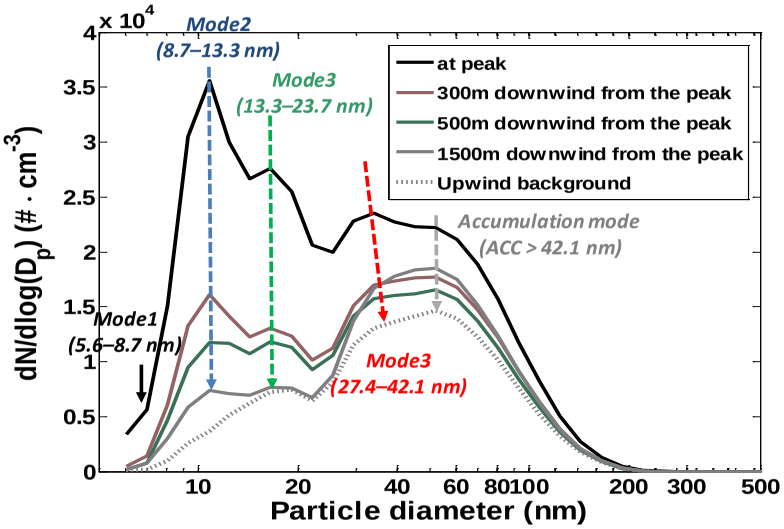

Figure 32. Variations in size distribution of UFP with distance from the 101 freeway at DoLA: the black line: at peak, light brown: at 300m downwind, green: at 500m downwind, gray solid: at 1500m downwind, and dotted gray line: background upwind of the freeway. Arrows represent size changes of 5 size bins with distance from freeway.

The major assumptions used in this study are that 1) variations in particles in largest size bin (> 42.1 nm) are determined solely by dilution, 2) particles in all size bins are diluted in the same way (with same dilution rate), and 3) coagulation occurs mainly through Brownian motion of particles. For the analysis, first, particle distributions were grouped into 5 size bins (5.6–8.7 nm, 8.7–13.3 nm, 13.3–23.7 nm, 27.4–42.1 nm, and >42.1 nm based on the shape of particle size distributions as shown in Figure 32). Second, dilution was corrected by the decay rate of largest particle bin, so that dilution corrected profiles were obtained for each size bin. Third, Brownian coagulation loss rates for each size bin were calculated. Finally, remaining variations in particle concentrations were considered to be caused by evaporation/condensation of gaseous organic compounds.

The very preliminary results for the downtown Los Angeles transect are shown in Figure 33 roughly 20–30% of total loss rate was attributable to particle dynamics: 2) within 50 m downwind from the plume peak, it appears that production dominates for all size bins, 3) Farther downwind than 300–400 m, particle dynamics effects appear to be negligible, and 4) changes in number concentration due to particle dynamics are more pronounced for smaller particles. Figure 33 shows that UFP production occurred in the vicinity to the freeways (< 50 m) before elevated UFP being diluted enough by either nucleation or growth of particles smaller than detection limit through condensation of semi-volatile gases (net gain region). In farther downwind areas (> 50 m; net losses region), particle dynamics yields net losses in particle number due to both coagulation and evaporation of semi-volatile compounds.

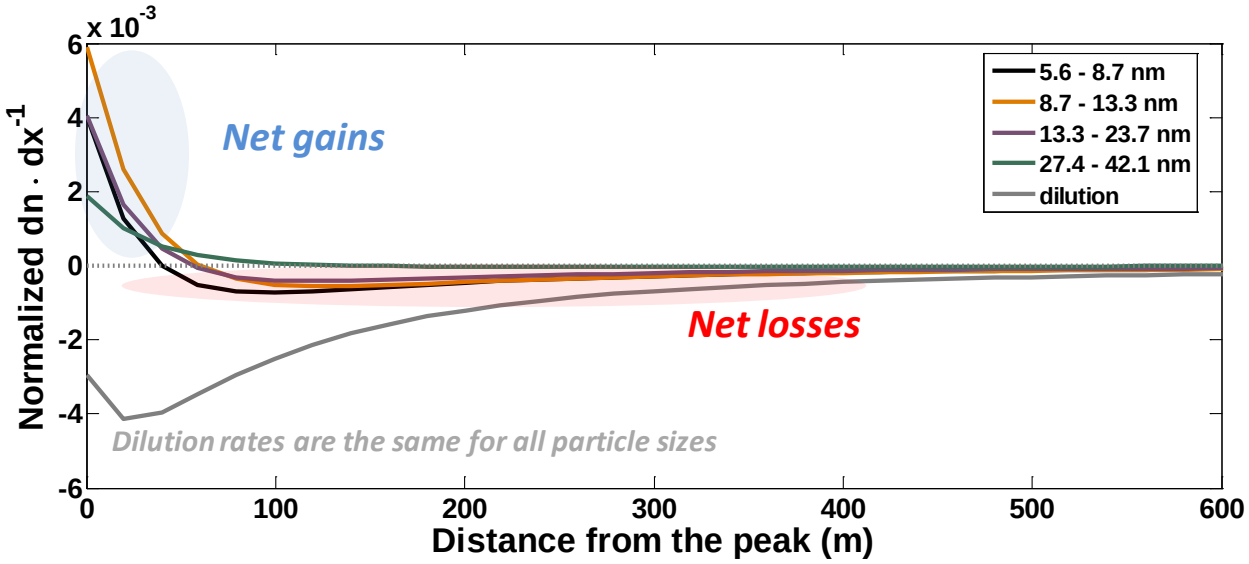

Figure 33. Normalized particle number variation with distance ($dN \cdot dx^{-1}$) with respect to dilution (gray line) and particle dynamics for each size bin.

11. Comparing measurements made on different days and different locations: Application of Classification and Regression Tree (CART) analysis

11.1 Introduction

Ultrafine particles, along with other traffic-related pollutants including nitrogen oxide (NO_x), carbon monoxide (CO), and various organic gases emitted near major roads, are of particular interest in metropolitan areas, including the California South Coast Air Basin (SoCAB) as well as many others. Numerous air quality studies have been conducted near major roads and freeways in this region [e.g., 2, 4, 30, 37, 59]. Because traffic-related pollutants are dependent on meteorological conditions, as well as emission rates, the atmospheric levels of these pollutants vary from day to day and by location, showing significant heterogeneity in temporal and spatial distributions [59-61]. Thus, correcting for time-variant differences in meteorology for pollutant time series data for the same area, as well as correcting for spatial differences in meteorology for the same time periods, is highly desirable.

To map highly resolved spatial and temporal variations in pollutant concentrations over a large area such as the SoCAB is challenging. In part for this reason, interest in making measurements with instrumented mobile measurement platforms has been growing in recent years as high time-resolution instrument capabilities have developed [2, 30, 62]. However, simultaneous measurements with multiple mobile measurement platforms in more than one area, comparing data from different areas obtained on different days present challenging because the high cost of an electrical vehicle fully equipped with sophisticated monitoring instruments makes it prohibitively expensive. Because of this to our knowledge such simultaneous measurements have never been reported in the literature. At present there appears to be no straightforward quantitative and systematic method to classify the degree of similarity or difference of meteorological conditions between days or locations.

Numerous efforts to investigate meteorologically-adjusted tropospheric ozone trends in urban areas have been made since the 1980's using a wide range of statistical methodologies such as linear or nonlinear regression approaches, tree-based or stratified model approaches, time-series filtering methods, and extreme value theory [63]. However, these attempts have been confined to secondary pollutants, mostly ozone, with a focus on predicting the ozone threshold excesses or investigating meteorologically-adjusted, long-term ozone trends. Because ozone is produced in the atmosphere through photochemical processes, the major meteorological factors affecting ozone concentrations are different from those for traffic-related primary pollutants such as UFP and CO [63, 64].

In contrast to the case for ozone, we are not aware of any studies that have produced systematic assessment criteria for meteorological adjustment of traffic-related primary pollutants. Here, we develop an objective classification scheme of meteorological conditions for the SoCAB using a classification and regression tree (CART) method. Since the CART approach was first developed in the 1960's [65], it has been applied to purposes as diverse as remote sensing data processing [66], ecological data analysis [67], medical causation analysis [68], and prediction of daily maximum ozone and $PM_{2.5}$ levels [64, 69]. Although the CART method has a predictive potential for atmospheric pollutant concentrations, the predictive power of this method is limited by the assumption of consistent emissions for the study period in this study. Thus, the ultimate purpose of this study is confined with quantitative classification of meteorological effects on pollutant levels. We expect this study may be applied to make more quantitative and systematic

comparisons of traffic-related pollutant concentrations between measurement days and locations in this area. Despite enormous progress in reducing air pollution over the past four decades, the California South Coast Air Basin (SoCAB) remains one of the most polluted regions in the U.S. In the SoCAB, which includes Los Angeles (LA) County, Orange County, and the western portions of Riverside and San Bernardino Counties, mobile sources account for 93% and 89% of the total annual emissions of CO and NO_x as of 2008 [70].

11.2 Classification and regression tree modeling approach and parameters for primary pollutants

11.2.1 Model description

The CART method explains distribution or variation of a target variable by a number of explanatory variables that have a linear or non-linear relationship with the target variable. The basic concept of the CART approach is to make a hierarchy of binary decisions, each of which splits distribution/variation of a target variable into two mutually exclusive branches (groups) based on one explanatory variable showing the largest reduction in variations in a target variable after split. Each split branch is then divided into two sub-branches by other variables or the same explanatory variable, until a set of terminal nodes (leaves) is reached. The details concerning how to determine the terminal nodes (to prune the overlarge splits) and theoretical underpinning of the CART approach are found in Breiman et al. [71] and supplementary material S1. A target variable is either categorical (classification trees) or numerical (regression trees), and a number of explanatory variables are also either categorical or numerical. Thus, the CART approach allows complicated links between a target variable and various explanatory variables to be clear, easier to interpret, and quantitatively compared.

CART is a statistical method to classify a variation or distribution of a numerical or categorical target data by a number of explanatory variables that can also be numerical or categorical. Because CART splits target data into two mutually exclusive groups using one explanatory variable at a time, it does not matter if the relationship between target data and predictor variable is linear or non-linear. In this study, a commercial software package, DTREG (www.dtreg.com; free demonstration version) was used to create regression trees. DTREG has been successfully adapted in other studies [66, 72].

In order to split the root node (entire dataset), CART, first divides each predictor variable into 100 groups based on numerical order (from lower 1% to upper 100%). Then it repeatedly makes splits moving the break point across all possible division points (e.g. lower 1% and upper 99%, lower 2% and upper 98%,…, lower 99% and upper 1%) until the best improvement is achieved. CART conducts this process with the other predictor variables and finds the best split variable and decisive value to divide the dataset into two exclusive sub-groups (branches). Each sub-group now splits into two additional sub-groups through the same process conducted for the first split until it reaches the terminal node (leaves).

In most applications, smaller trees have greater utility. In order to prune the overgrown branches with the best model efficiency, DTREG adopts *v*-fold cross-validation technique, which performs independent tree size tests, a method that has been demonstrated to produce accurate results [71]. First, the initial tree is constructed using all available learning dataset with intentionally overgrown leaves. The total learning dataset is, as the next step, randomly partitioned into v groups to create v independent sub-dataset for test. In this study, v=10 was used, and Breiman et al. [71] demonstrated that this value is good enough to assure accurate

results. Using *(v − 1)* groups (90% of the total dataset), a test tree is constructed. With the remaining one group (10% of the dataset), which is independent of the test tree because this group was not included in the tree construction, the classification error as a function of tree-size is computed. A different dataset with another *(v − 1)* groups is collected to perform the same test, and hence this classification error test is conducted *v* times with different test dataset, in total. Finally, the average classification error rates as a function of tree-size are obtained to determine the minimal tree-size with the minimal classification error. More details in regard to *v*-fold cross-validation are explained in Sherrod [73] and Breiman et al. [71].

11.2.2 Regional parameters

The SoCAB occupies a coastal plain surrounded by mountains on three sides (the San Gabriel, San Bernardino, and San Jacinto mountains). The predominant meteorological conditions in the SoCAB are characterized by mild winds and shallow boundary layer heights capped by low-altitude temperature inversions due to a semi-permanent Pacific High pressure cell. Prevailing winds dominated by a diurnal cycles of week off-shore breezes at night and stronger on-shore sea breezes during the day. The three mountains surrounding the SoCAB further enhance the pollutant-capping effects preventing air ventilation [74]. Less common weather patterns, occurring primarily in the winter, include storm fronts arriving largely from the north and west, and dry winds arising from high deserts to the east. The latter are referred to as Santa Ana's.

In this study, downtown LA (DTLA) monitoring site (N. Main St., 25 km from the coast, 34.07°N/118.23°W) was selected as a representative station to create and investigate the regression trees for traffic related primary pollutants and five additional monitoring sites were chosen to investigate the applicability of a representative regression tree for meteorological comparability with respect to air pollution by location (Figure 12, Figure 37): Long Beach (N. Long Beach, 7 km North from Port of Long Beach and 25 km south from DTLA, 33.82°N/118.19°W), Pomona (mid of the SoCAB, 45 km east from DTLA, 34.07°N/117.75°W), Upland (foothill area south of San Gabriel mountains, 55 km east from DTLA, 34.10°N/117.63°W), Rubidoux (an inland site, 78 km east from DTLA, 34.00°N/117.42°W), and San Bernardino (inland site closer to mountainous area, 88 km east from DTLA, 34.11°N/117.27°W). Details about these measurement sites, which are operated by the South Coast Air Quality Management District (SCAQMD), can be found in the California Air Resources Board's (CARB) air monitoring network description [42].

11.2.3 Vehicular emissions

Atmospheric levels of traffic-related primary pollutants also depend strongly on emission source strengths, which are a function of the vehicle fleet and its maintenance, as well as vehicle miles travelled and traffic patterns. Thus, if the modeling periods extend too long, results may be influenced by long-term changes in emission rates and the number of vehicles in the modeling area. Annual vehicle fuel consumption in the SoCAB gradually increased with time prior to 2005, but during 2005–08, fuel consumption reached a plateau [34] (Figure 34). In addition, the number of registered vehicles in the SoCAB remained nearly constant after 2007, decreasing slightly from 13,495,744 in 2007 to 13,278,657 in 2010 [33]. Thus, it is expected that vehicle fuel consumption and the emission source strength did not change significantly from 2007 to 2009, the period examined here. Indeed, Kolmogorov-Smirnov (KS) test showed that the annual distributions of both daily mean and max. NO_x at the DTLA monitoring site are statistically

identical during 2007–09 study period (p>>0.05) at 5% level (Figure 35). These results support the assumption that there had not been significant changes in traffic emissions during the study period.

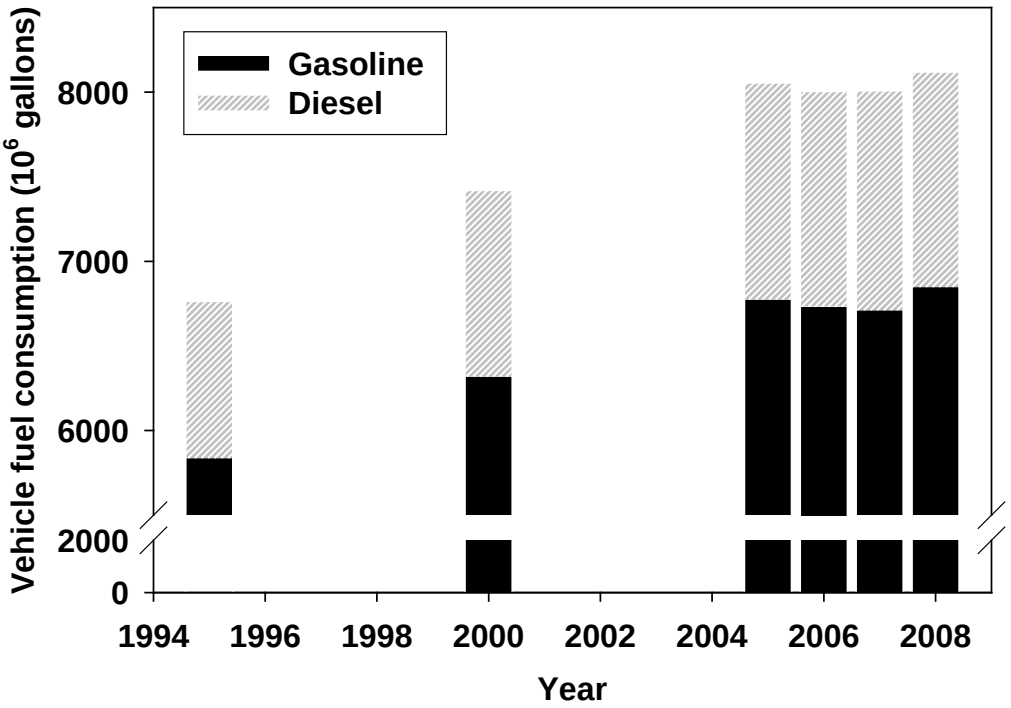

Figure 34. Sum of annual vehicle fuel consumption (in millions of gallons) in LA, Orange, Riverside, and San Bernardino counties. The black and grey bars indicate gasoline and diesel consumption, respectively. 2008 estimates are projected values [34]. Vehicle fuel consumption increased prior to 2005, at which point it roughly plateaued. Considering that the number of registered vehicles in SoCAB decreased slightly from 2007 to 2010 (from 13,495,744 to 13,278,657), vehicle fuel consumption is expected not to noticeably change during the study period (2007 – 2009). It is also notable that the ratio of diesel to total consumption has remained nearly constant between 2005 and 2008 at 15.9±0.3%.

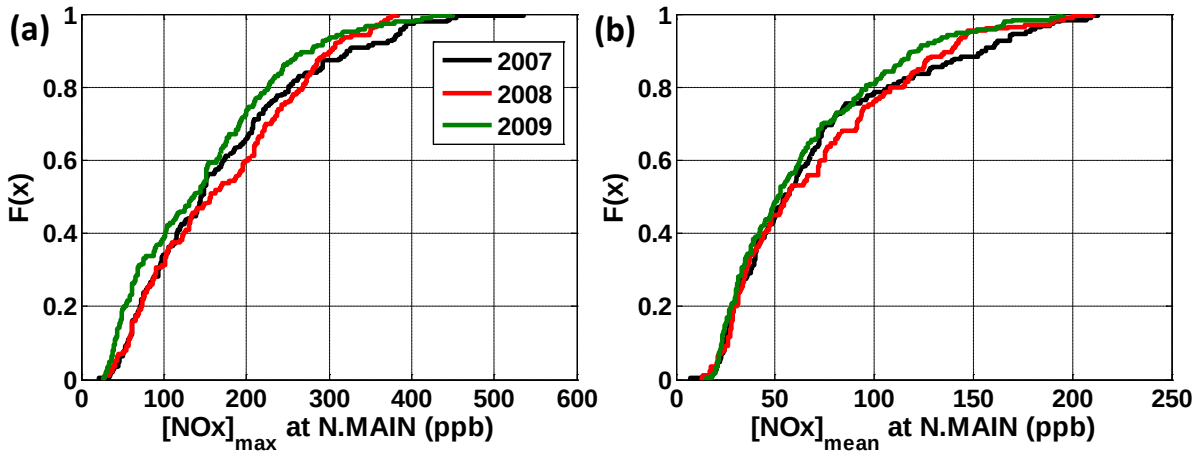

Figure 35. Empirical cumulative distribution function, F(x) as a function of (a) daily max. NOx and (b) daily mean NOx concentrations at the DTLA monitoring site for each year of 2007–2009 periods.

In addition, Zhu et al. [75] reported no seasonal variations in traffic flows, or in the ratio of vehicle types (heavy duty diesel vs. gasoline) on both the I-710 and I-405 freeways (north-south roadways in the western SoCAB, Figure 37). Moreover, the annual diurnal traffic patterns for the I-10 (east-west direction over the length of the SoCAB) and I-15 (north-south in the eastern SoCAB, Figure 37), show only small monthly variations (< 5% and < 13%, respectively, Figure 36). Thus, assuming traffic patterns on these freeways are representative of those in the entire SoCAB, it appears seasonal changes in the emissions were modest over the study period. We also note our analysis further assumes that stationary source emissions of oxides of nitrogen (NO_x) varied little over the relatively short study period of three years. Stationary sources contribute less than 5% of CO emissions in the SoCAB and hence any changes can be ignored [70].

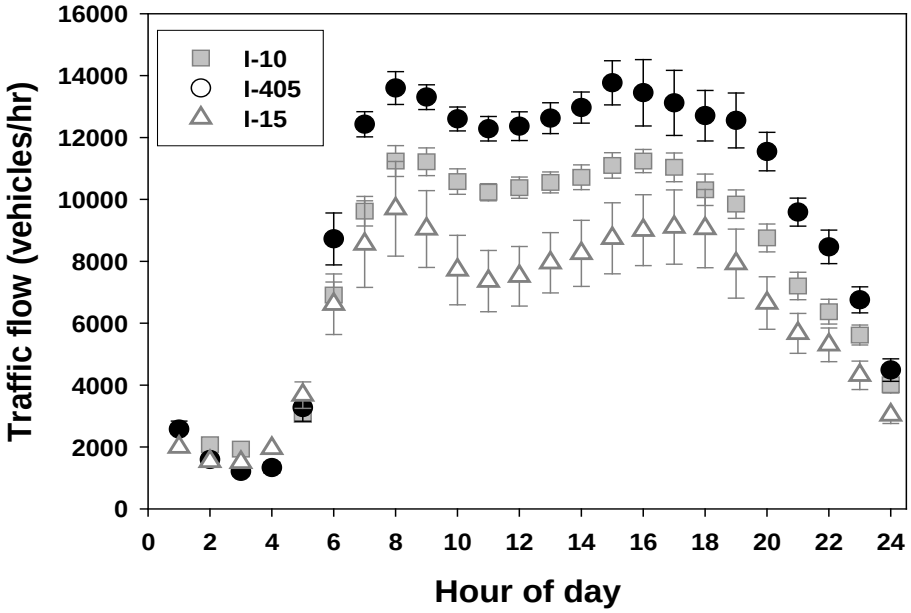

Figure 36. Mean diurnal profile of traffic flow rates (vehicles per hour) on I-405 (Normandie Ave. in the city of Los Angeles), I-10 (Central Ave. in LA), and I-15 (Jurupa St. in Ontario) freeways in 2009. I-405 and I-15 extend north-south of the west coastal region and east part of SoCAB, respectively, and I-10 proceeds east-west of SoCAB. Here, we make an implicit assumption that these three major freeways represent the general traffic patterns in the entire SoCAB. Data were collected from the Performance measurement system (PeMS) operated by the California Department of Transportation (http://pems.dot.ca.gov). Black circles, gray squares, and white triangles represent the mean value in I-405, I-10, and I-15, respectively, and vertical bars denote monthly standard deviation.

Figure 37. Map of the study area and locations of pollutant monitoring sites (white squares) and NCEP upper air meteorology data obtained (red circles). Map from Google Maps.

In contrast to the lack of variation in seasonal and annual mean emission rates from traffic sources as discussed above, significant diurnal variations in vehicular emissions clearly occur. The annual mean diurnal profiles of traffic flow rates on the I-405 freeway show consistent patterns through the entire year (Figure 36). Traffic flows reach a minimum around 03:00-04:00 and sharply increase with the onset of morning rush hours (04:30-07:00). This is followed by somewhat lower midday flows and a broad second peak in the late afternoon. Remarkably consistent diurnal patterns (scaled by total volume) have been observed for both the I-10 and I-15 freeways as well as several other freeways, indicating these are general traffic patterns throughout the majority of the SoCAB.

There are significant differences in travel patterns and traffic flows between weekdays and weekends. To avoid day-of-the-week effects in vehicular emissions, only Tuesday - Friday data were collected and analyzed in this study. Mondays were also excluded to avoid possible carry-over effects from the previous weekend and various Monday holidays.

Because emissions were not used as an explanatory variable in this analysis, the resulting regression trees have limitation in predicting absolute concentrations for days or locations of different emissions patterns (e.g., weekend/holidays and other years with significant changes in emissions). Nonetheless, we can apply regression tree results to investigate meteorological

comparability for years not in the study period because a regression tree is created solely with meteorological variables. We note that meteorology controls only the atmospheric dispersive power for emissions and is not influenced by human activities (e.g., emission changes). Developing an accurate model to predict absolute pollutant concentrations for all years and for other locations is beyond the scope of this study.

11.2.3 Primary pollutants as target variables

Of numerous pollutants emitted primarily from vehicular sources, the only species that are widely monitored are NO, NO_2 and CO. CO undergoes little reaction on time scales of hours, and for the purpose of this study is considered a conservative pollutant. Although NO is much more reactive particularly during daytime when ozone concentrations are elevated, NO_x ($NO+NO_2$) can be more conservative and a good indicator of vehicular emissions and atmospheric mixing, given that most important chemical reactions occur in a $NO\text{-}NO_2$ conversion loop in urban areas. Thus, as representative target pollutants emitted from traffic sources, daily max. CO and NO_x concentration ($[CO]_{max}$ and $[NO_x]_{max}$), and daily mean NO_x concentration ($[NO_x]_{mean}$) at the DTLA monitoring site were chosen. Due to the coarse resolution of CO measurements, daily mean CO concentration was not considered in this analysis.

Although in the SoCAB the nighttime traffic flow is only about 10% of daytime (Figure 36), meteorological conditions, such as a stably stratified boundary layer and calm winds, allow pollutants to accumulate within the nocturnal boundary layer, resulting in higher concentrations of primary traffic-related pollutants such as NO_x and CO. The leading edge of the morning rush hour also contributes to pollutant concentrations that accumulate in the early morning [2]. Frequency histograms of $[CO]_{max}$ and $[NO_x]_{max}$ clearly show the maxima between 5–7 A.M., demonstrating these pollutants accumulate in stable air (Figure 38). In the SoCAB, CO and NO_x concentrations also show strong seasonal variations, peaking in the winter season and reaching a minimum in summer (Figure 39a and b). This is likely due to lower boundary layer heights, lighter wind speeds in the winter compared to summer particularly during the morning rush hour emission period when the sun rises later in winter and thus delays the onset of thermally induced mixing [76].

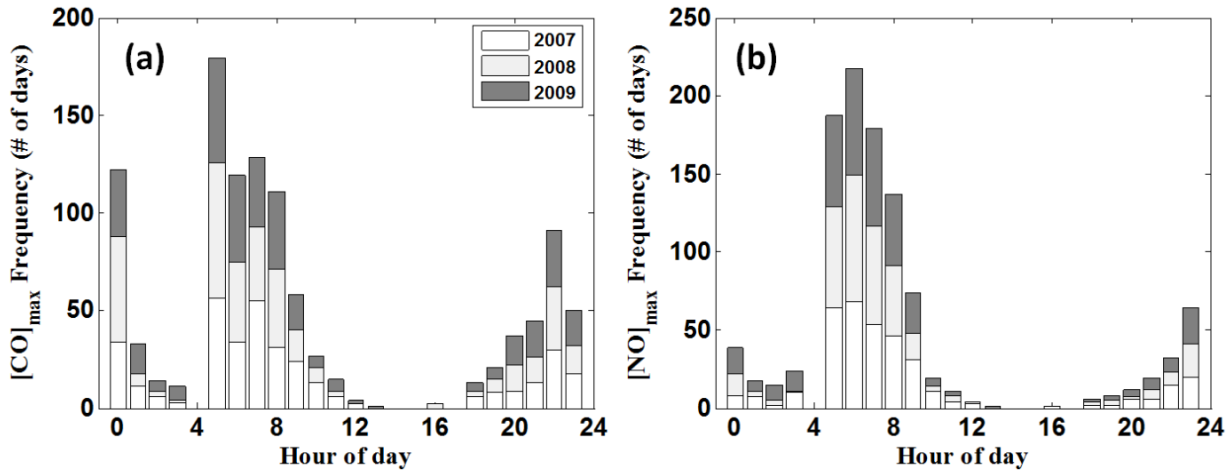

Figure 38. Histogram plot of the frequency of the daily maximum concentration as a function of hour of day. (a) Daily maximum CO ($[CO]_{max}$) and (b) daily maximum NO concentration ($[NO]_{max}$) for 2007 - 2009. White bars denote 2007, light gray bars 2008, and dark gray bars 2009.

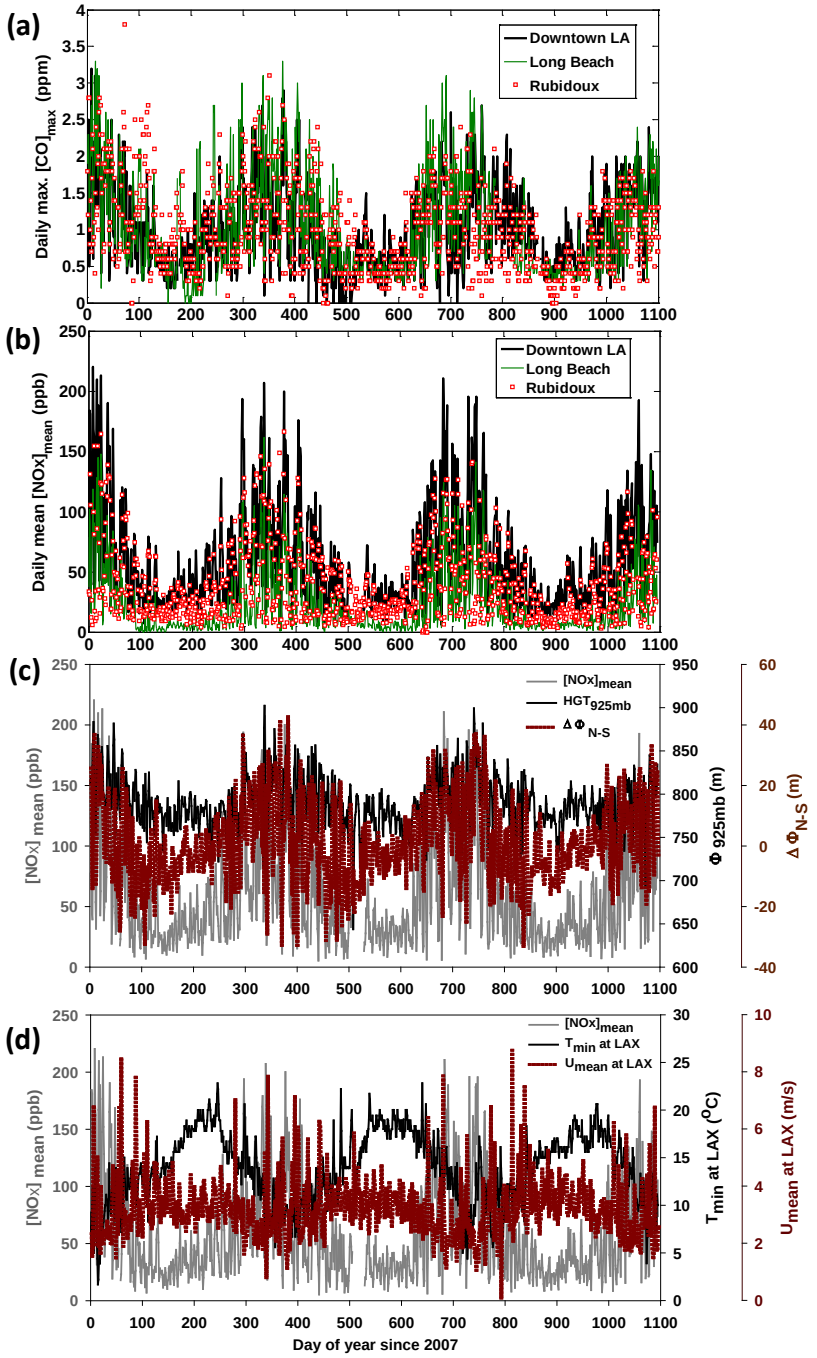

Figure 39. Time-series of (a) daily maximum CO (*[CO]$_{max}$*), (b) daily mean NO_x concentrations (*[NO_x]$_{mean}$*) at downtown LA (black line), N. Long Beach (green line), and Rubidoux (red squares), (c) geopotential height at 925 mbar pressure level over the SoCAB (black solid line) and north-south geopotential height gradient at 1000 mbar (brown dotted line), and (d) surface daily minimum temperature (black solid line) and daily mean wind speed (brown dotted line) observed at Los Angeles International Airport (LAX). Light gray solid lines in (c) and (d) represent daily mean *[NO]$_{mean}$* at downtown LA (N. Main St.) for a comparison. x-axis is day of year since 2007 (Jan. 1, 2007 equals to 1).

11.2.4 Meteorological variables as predictor variables

Most previous studies attempting to explain ozone or $PM_{2.5}$ concentrations with meteorological variables using statistical modeling methods found that fewer than 10 meteorological variables were significant predictors, among several tens of variables considered [63]. In the present study, a total of 29 upper-air and surface meteorological variables were used as inputs (Table 11), as follows: Geopotential height (Φ) represents the synoptic-scale weather pattern; temperature at 850 mbar is a measure of the strength and height of the subsidence inversion; temperature differences between layers provide information about atmospheric stability; and the geopotential height gradients ($\Delta\Phi_{N\text{-}S} = \Phi_{north} - \Phi_{south}$ and $\Delta\Phi_{W\text{-}E} = \Phi_{west} - \Phi_{east}$) at 1000 mbar are likely to be strongly related to regional wind fields, and hence ventilation effects [69, 77]. Air stability is likely related to surface temperature indirectly for nocturnal temperature inversions as well as for thermals in the convective boundary layer. Wind speeds are a measure of dispersion and ventilation strength and can affect boundary layer heights somehow indirectly through turbulence intensity. Besides these parameters, relative humidity and surface pressure were added in the analyses as indirect meteorological factors. Some variables listed in Table 11 were additionally divided into daily, morning, and afternoon mean values to investigate intra-day effects.

Table 11. Meteorological variables used as explanatory (predictor) variables in the CART model and their effects on atmospheric primary pollutant concentrations.

Meteorological variables		Importance on primary pollutant level
Upper-air (NCEP model)	• Geopotential heights (Φ) at 1000/925/850/500 mbar	Indicator of synoptic-scale weather pattern
	• Mean temperature (T) at 1000/925/850 mbar	A measure of the strength and height of the subsidence inversion
	• Stability ($T_{1000mbar} - T_{925mbar}$, $T_{1000mbar} - T_{850mbar}$)	Indicator of atmospheric stability
	• Thickness ($\Phi_{925mbar} - \Phi_{1000mbar}$)	Related to the mean temperature in the layer
	• Relative humidity at 1000 mbar ($RH_{1000mbar}$)	Indirect effect
	• Pressure gradient at 1000 mbar level ($\Phi_{north} - \Phi_{south}$, $\Phi_{east} - \Phi_{west}$)	Related to wind fields and/or synoptic-scale weather
Surface observations (LAX)	• mean/min./max. temperature (T_{mean}, T_{min}, T_{max})	Indirect effects on air stability and emission rates from the engine
	• mean/max. wind speed (U_{mean}, U_{max})	Related to dispersion/ventilation strength
	• Relative humidity (RH)	Indirect effect
	• Mean surface pressure	Indicator of synoptic-scale weather

Upper air meteorological variables were extracted from the "4-times daily" National Centers for Environmental Prediction (NCEP) reanalysis database [9]. Four data points (32.5°/35° N latitude and 117.5°/120°W longitude) around the SoCAB were selected and averaged to represent the upper air meteorological conditions above the SoCAB (Figure 36). Surface weather variables were obtained from the MesoWest website operated by the University of Utah (http://mesowest.utah.edu/index.html). Figure 39c shows a time-series of geopotential height at 925 mbar (Φ_{925mb}), and north-south pressure gradient at the 1000 mbar pressure level ($\Delta\Phi_{N\text{-}S}$). Also plotted are the surface meteorological variables, including daily mean wind speed (U_{mean}) and daily minimum temperature (T_{min}) at Los Angeles International Airport (LAX), with daily mean $[NO]_{mean}$ at Downtown LA as a reference in Figure 39d.

Both upper-air and surface meteorological variables show strong seasonal variations, similar to $[CO]_{max}$ and $[NO_x]_{mean}$ (Figure 39). Of the 18 upper air meteorological variables collected, pressure gradients ($\Delta\Phi_{N\text{-}S}$) and geopotential heights at 925 and 1000 mbar ($\Phi_{925mbar}$ and $\Phi_{1000mbar}$) show the best correlation with daily maximum $[NO_x]_{max}$, $[CO]_{max}$, and daily mean $[NO_x]_{mean}$ at the Downtown LA monitoring site (LA N. Main, Figure 36), with correlation coefficients (r) ranging from 0.42–0.61. *RH* at 1000 mbar shows a significant negative correlation (-0.38 – -0.41) although its effect is indirect. Correlations with upper air temperature and wind speeds are less significant compared to other variables, with absolute correlation coefficients below 0.2.

Of the surface meteorological variables obtained at LAX, daily mean wind speed (U_{mean}), minimum temperature (T_{min}), and surface *RH* are negatively correlated most strongly with NO and CO. Correlations coefficients for U_{mean}, T_{min}, and *RH* with $[NO_x]_{max}$, $[CO]_{max}$, and $[NO_x]_{mean}$ are -0.52 – -0.56, -0.36 – -0.40, and -0.34 – -0.42, respectively. Daily mean surface pressure shows significant positive correlations (r = 0.41–0.47). Daily mean and daytime temperature effects are insignificant.

11.3 Regression trees results

11.3.1 Regression trees for the entire year

Once rain days, weekends, and Mondays were excluded, the numbers of 2007-2009 data points input into the CART model were 553 and 549 for CO and NO_x, respectively. The regression trees explicitly show the effects of a specific meteorological parameter on pollutant levels. The CART analysis divided daily $[CO]_{max}$ into two subgroups based on the surface mean wind speed (U_{mean}) at the first split level, followed by geopotential height at 925 mbar ($\Phi_{925mbar}$), north-south Φ gradient ($\Delta\Phi_{N\text{-}S}$), daily minimum temperature (T_{min}), relative humidity at 1000mbar ($RH_{1000mbar}$), and stability ($S_{925mbar}$), to make 11 final nodes (Figure 40). For example, low U_{mean} generates less mechanical turbulence resulting in higher $[CO]_{max}$. Higher $\Phi_{925mbar}$ is related to the winter season (Figure 39c), during which primary pollutant levels are typically elevated because of lower boundary layer heights, weaker winds, and possibly less active chemical sinks. Although surface layer temperature is not a direct function of atmospheric stability, surface temperature can be representative of surface cooling or heating. Enhanced surface heating can produce a deeper boundary layer and stronger turbulent energy during daytime and enhanced surface cooling can affect nocturnal atmospheric stability, showing inverse correlation with pollutant concentrations.

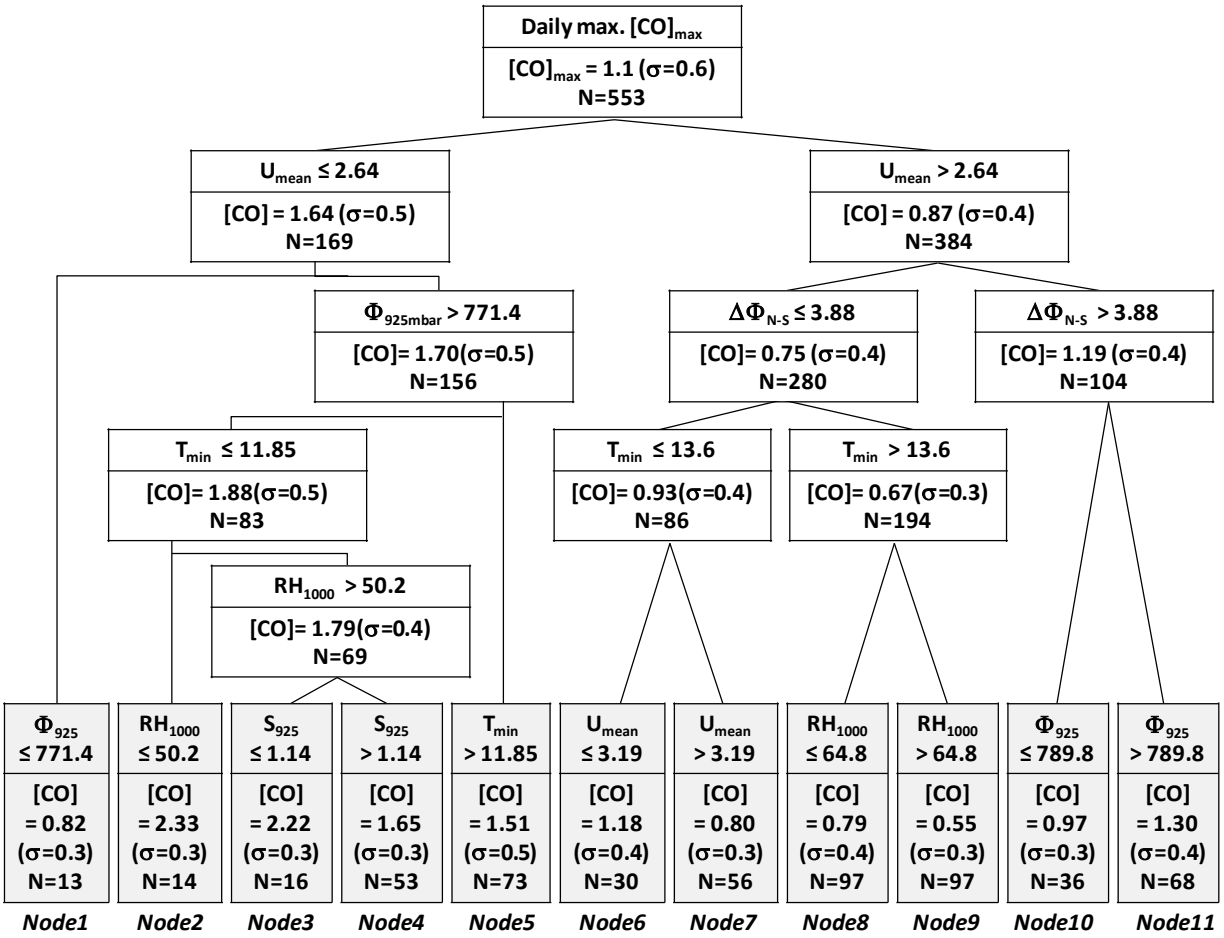

Figure 40. Regression trees for daily *[CO]$_{max}$* observed at downtown LA (N. Main St.) for 2007–2009. The split criteria of explanatory variables are shown at the top of each box (*node).* The bottom layer of each node indicates the mean *[CO]$_{max}$* and standard deviation (σ) as well as the number of data in the node (*N*). Gray boxes represent the terminal nodes.

S_{925mb} is defined as the temperature difference between 1000 mbar and 925 mbar pressures. A larger positive value of S_{925mb} represents less stable air due to warmer air below, likely implying enhanced mixing, and hence resulting in modest $[CO]_{max}$. Interestingly, strong $\Delta\Phi_{N\text{-}S}$ also appears to be closely related to lower $[CO]_{max}$ whereas west–east geopotential height gradient at 1000 mbar $\Delta\Phi_{W\text{-}E}$ showed a positive correlation with $[CO]_{max}$. Steeper pressure gradients generally correlate with strong winds. However, wind fields in the SoCAB are dominated by a west-east directional sea-breeze wind system. Thus, it is likely that prevailing westerlies or easterlies may be dampened by a strong north-south pressure gradient, establishing calm weather conditions with elevated primary pollutant concentrations. Otherwise, $\Delta\Phi_{N\text{-}S}$ may represent synoptic weather patterns related to calm meteorological conditions in the SoCAB. The regression tree for $[CO]_{max}$ at DTLA reproduces the observations well; the correlation coefficient between observations and representative nodal average values is 0.79. The mean absolute error is estimated to be 0.28 ppm, which is equivalent to a standard error of 28%.

Regression trees for $[NO_x]_{max}$ and $[NO_x]_{mean}$ were also successfully created (Figs. 4 and S6). The first two splits for $[NO_x]_{max}$ are based on U_{mean} (1st split) and $\Phi_{925mbar}$ and $\Delta\Phi_{N\text{-}S}$ (2nd splits)

exactly matching the initial split for $[CO]_{max}$. For higher winds regime (U_{mean} > 2.64 m/s) of the first split, final nodes are almost identical with those of $[CO]_{max}$ regression tree (Figure 41). Subsequent splits for $[NO_x]_{max}$ in the lower winds regime (U_{mean} < 2.64 m/s) are slightly different than for $[CO]_{max}$. In this regime, $[NO_x]_{max}$ were divided by wind speed at the 3rd level split, followed by RH_{LAX}, $\Delta\Phi_{W\text{-}E}$, and T_{min} where RH_{LAX} is the surface relative humidity at LAX. We also note that T_{min} is a common variable with that for $[CO]_{max}$ split in lower wind regime, although T_{min} is more important variable for $[CO]_{max}$ split (upper level split). The regression tree for $[NO_x]_{max}$ has 11 final nodes, almost identical with the $[CO]_{max}$ regression tree in major splits. This similarity in regression trees for $[NO_x]_{max}$ and $[CO]_{max}$ supports the validity of the CART model for traffic-related primary pollutants in urban areas. The correlation between observations and representative nodal average values (r=0.78) for $[NO_x]_{max}$ is comparable to that for $[CO]_{max}$, although the mean absolute error and standard error are slightly larger (48.7 ppb and 30%, respectively).

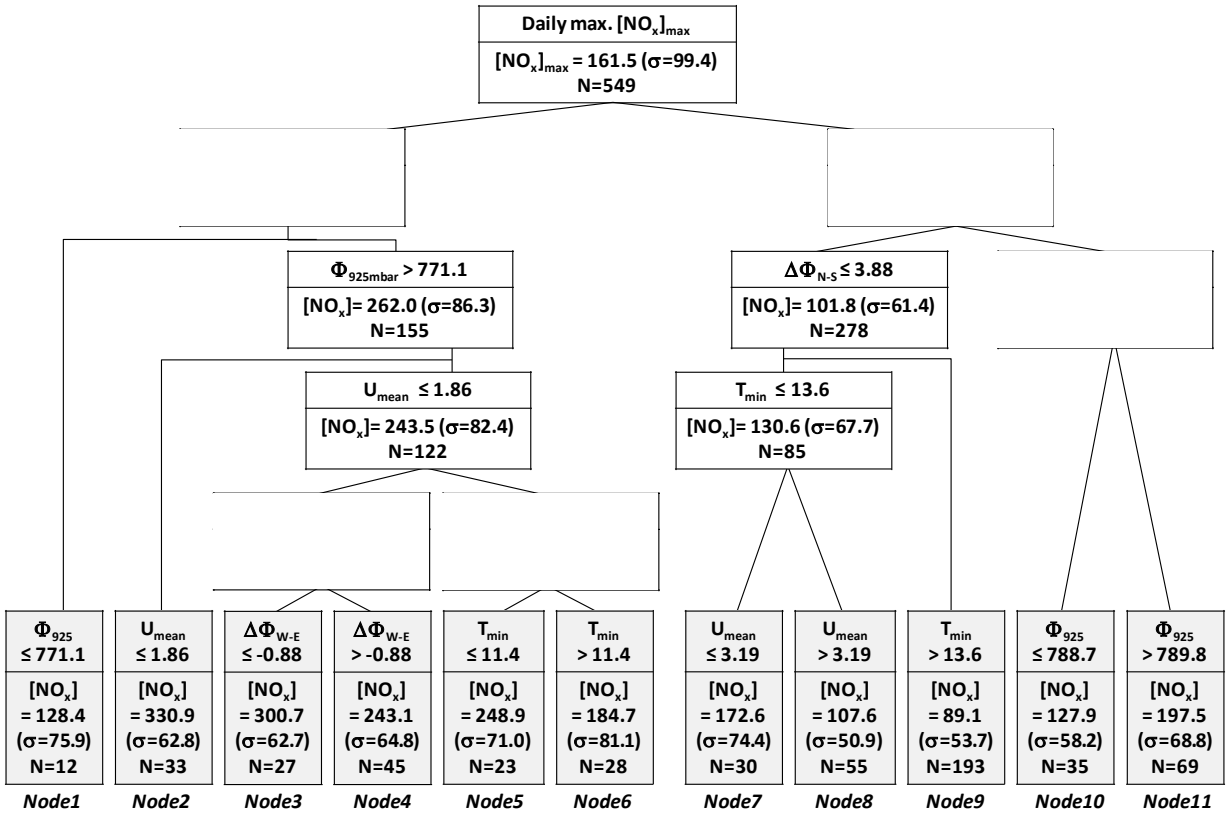

Figure 41. Regression trees for daily $[NO]_{max}$ observed at downtown LA (N. Main St.) for 2007–2009. See Figure 40 caption for an explanation of the notation.

Daily $[NO_x]_{mean}$ falls into 12 final nodes of its regression tree, first split by U_{mean} (2.64 m/s) and followed by U_{day}, $\Delta\Phi_{N\text{-}S}$ (2nd split), U_{mean}, Φ_{925mb} (3rd split), RH_{1000mb}, S_{925mb}, and RH_{LAX} where U_{day} is daytime (10:00-16:00) mean surface wind speed. The correlation coefficient between actual and representative nodal average values is excellent (r=0.87) and the mean absolute error is estimated by the model to be 16.8 ppb (25% standard error) (Figure 42). Note the $[NO_x]_{mean}$ regression tree also has several branches in common with the $[NO_x]_{max}$ regression tree.

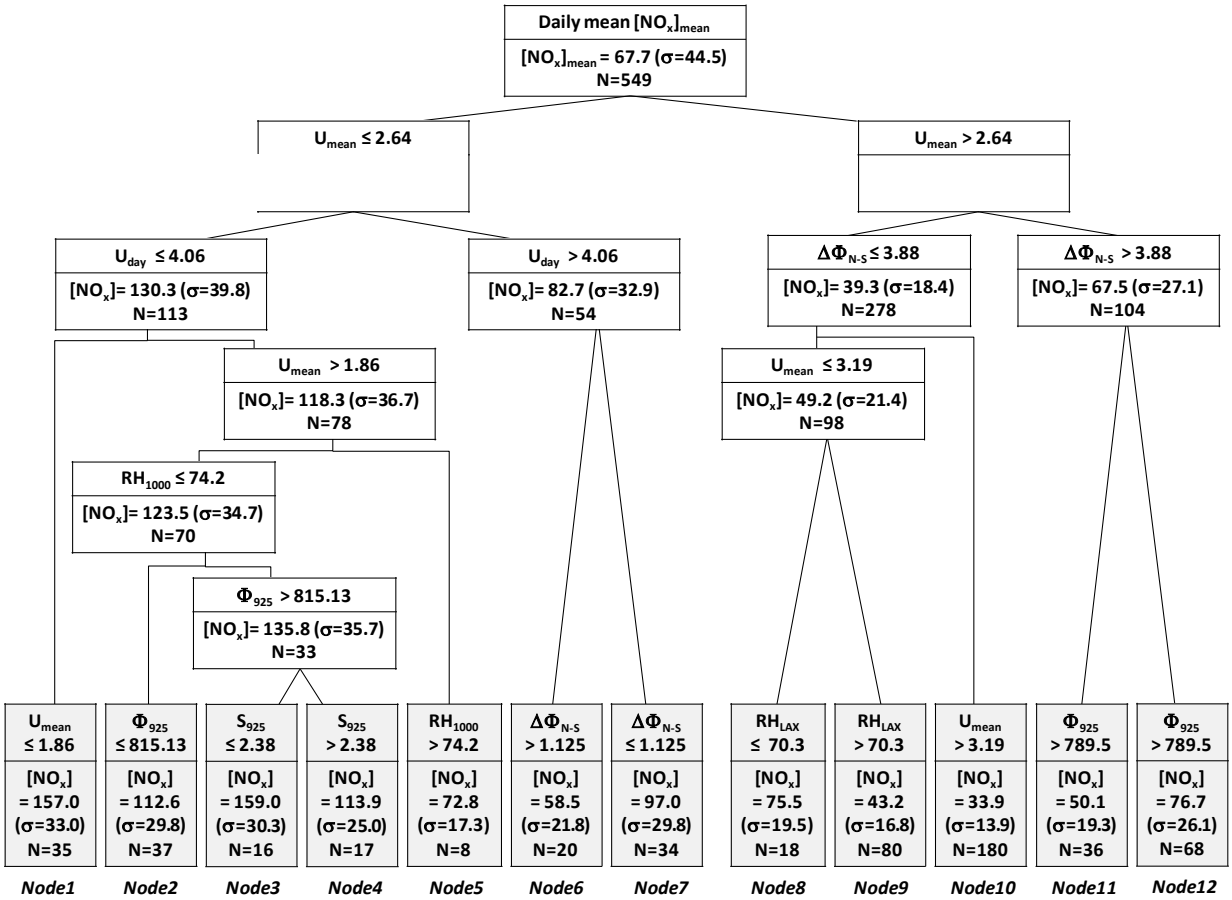

Figure 42. Regression tree for daily *[NO]mean* observed at Downtown LA (N. Main St.) for 2007 - 2009. The tree has 11 terminal nodes.

Meteorological variables tend to be related to each other. Thus, it is not surprising that different pollutants have somewhat different meteorological variables in their optimized regression trees. For example, wind fields arise primarily from pressure gradients, and hence one pollutant tree may be slightly better divided by wind speed while the other is better divided by pressure gradient, while the divisions are similar. In order to evaluate the comparability of the regression trees between the primary pollutants under consideration, mean $[NO_x]_{max}$ and $[NO_x]_{mean}$ were obtained for days that fall into each terminal node of the $[CO]_{max}$ regression tree. Excellent linear correlations between $[CO]_{max}$ and both $[NO_x]_{max}$ (r=0.99) and $[NO]_{mean}$ (r=0.97) (Figure 43a and b) imply that the $[CO]_{max}$ regression tree can also effectively split $[NO_x]_{max}$ and $[NO_x]_{mean}$, and that the $[NO_x]$ and $[CO]_{max}$ regression trees similarly classify meteorological conditions.

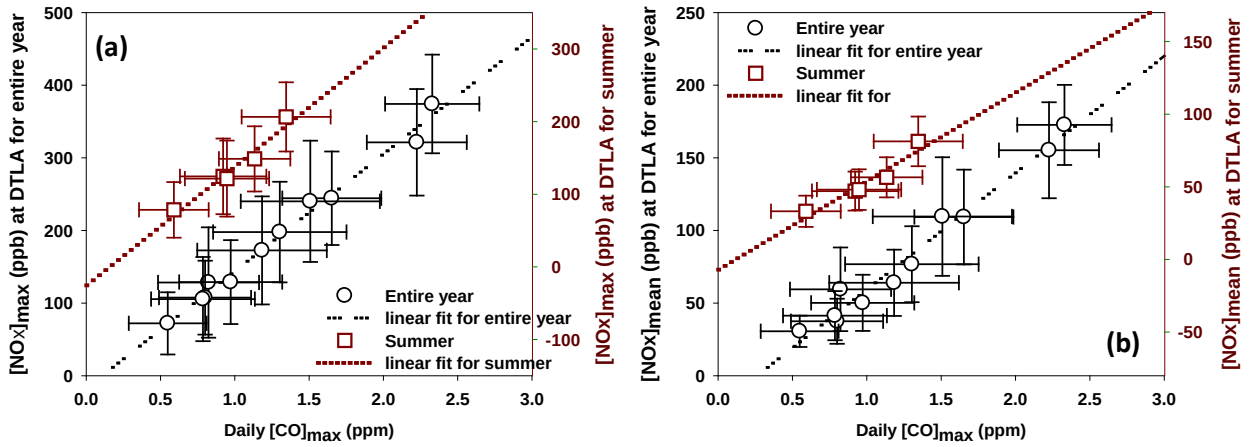

Figure 43. Comparison plots of the mean nodal $[CO]_{max}$ vs. (a) mean $[NO_x]_{max}$ and (b) $[NO_x]_{mean}$ for days that fall into the terminal nodes of the $[CO]_{max}$ regression tree at Downtown LA. Black circles represent the regression tree results for the entire year and dark red squares denote the seasonal regression trees for the summer (June 21st to September 21st). Horizontal and vertical bars denote standard deviation of $[CO]_{max}$ and $[NO_x]_{max}$ or $[NO_x]_{mean}$ in each terminal node, respectively. Black dash-dot line indicates linear fits for the entire year regression tree (r=0.99 and 0.97 for $[NO_x]_{max}$ and $[NO_x]_{mean}$, respectively). Summer season regression tree yielded r=0.97 and 0.92 for $[NO_x]_{max}$ and $[NO_x]_{mean}$, respectively.

11.3.2 Summer season regression trees

Concentrations of primary pollutants are lower and have lower variability in the summer season than those in the other periods of a year primarily due to deeper boundary layer heights providing more volume for mixing with ambient air, as well as stronger thermally induced turbulence and higher surface wind speeds. 84% of the total summer days fall into only three nodes (*node 8, 9, and 10*) of the entire-year regression tree. To examine this seasonal effect in detail and investigate if smaller standard deviations could be obtained with more focused regressions, summer season regression trees were created separately using the same explanatory variables as above. Summer was defined as 21 June to 21 September. Five final nodes were created for $[CO]_{max}$ and $[NO_x]_{max}$, and seven nodes for $[NO_x]_{mean}$.

Unlike the regression trees for the entire year, primary pollutant concentrations tend to be higher with higher surface temperature within the summer period. This inverse trend is likely due to the fact that higher temperature is generally linked to enhanced stagnation of air masses during the summer in the SoCAB [77]. Indeed, daily mean temperature was positively correlated with pollutant concentrations and negatively correlated with surface wind speeds for the summer season (Figure 44). The effects of other explanatory variables on concentration levels were similar to the entire year regression trees. Even for the summer, one predominant node appears, including more than 59% of the summer days. Nonetheless, standard deviations in each final node were notably reduced for all pollutants for the summer regression trees (Figure 43a and b). Although the summer regression trees were not conspicuously improved from those for the entire year, this analysis shows another advantage of the CART method, namely that a specific period of year can be separately considered.

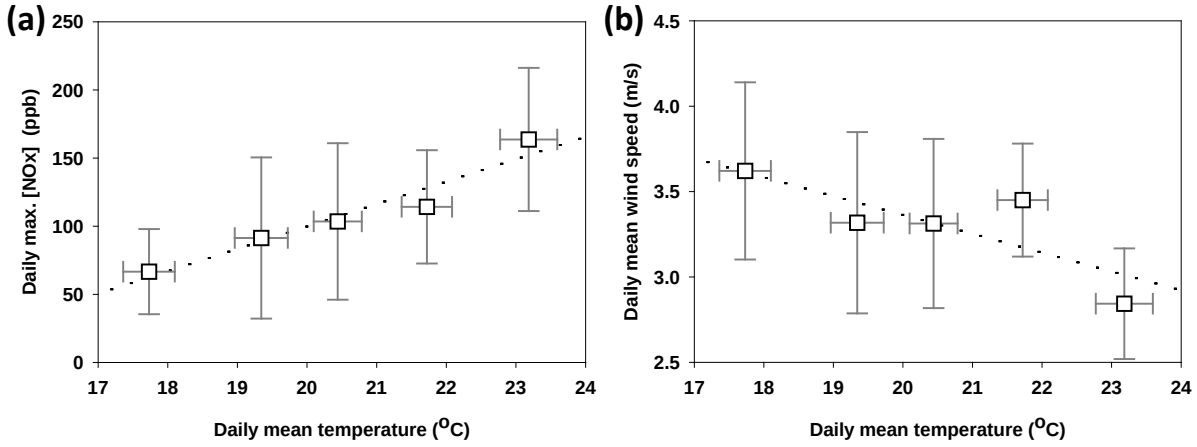

Figure 44. Correlation of daily mean surface temperature (℃) with (a) Daily max. $[NOx]_{max}$ (ppb) at DTLA and (b) daily mean wind speeds (U_{mean}).

12. Neighborhoods, roadways, and airports: Air quality benefits of emissions reductions from mobile sources

12.1 Introduction

Vehicular emissions are known to be a dominant source of UFP in urban areas, commonly accounting for ~80% of total number concentrations [78, 79]. Although UFP number concentrations tend to rapidly decline within 100–500 m from major roadways during daytime [28], dense networks of roadways in cities increase neighborhood UFP concentrations along with other pollutants [62]. Under stable atmospheric conditions such as nocturnal inversions, traffic-related pollutants tend to be more elevated and have much wider impacts downwind of roadways, reaching about 2 km [2, 6, 43].

Effective implementation of traffic interventions, stringent emission regulations, and/or improvements in engine efficiency and fuel composition can help mitigate air pollutant concentrations of combustion related pollutants including UFP, NOx, and CO. Wählin [80] and Wang et al. [81] reported significant decreases in nucleation mode particle concentrations after fuel regulations for lower sulfur content were adopted. Friedman et al. [82] found 1-hour peak ozone concentrations were 13% lower due to decreased traffic counts during the 1996 Summer Olympic Games in Atlanta, Georgia, accompanied with 16%, 18%, and 7% reductions in PM_{10}, CO, and NO_2 concentrations, respectively, although only weekday morning peak traffic flows near the downtown were noticeably decreased. Several studies reported significantly decreased air pollutants concentrations, including CO (-33%), NOx (-42%), sulfur dioxide (SO_2) (-60%), black carbon (BC) (-26 – -74%), and surface area $PM_{1.0}$ (-37%) during the 2008 Summer Olympics in Beijing urban areas due to stringent traffic interventions and emission controls on industrial sources [83, 84]. Those trends were also found in a rural area 100 km downwind of the Beijing urban center with 23%, 60%, 32%, and 36% reductions of ozone (O_3), SO_2, CO, and NOx, respectively [85].

To date, only a handful of studies have investigated improvements in UFP-related air quality due to temporary suspension of traffic, based on curbside measurements at closed roadways. Whitlow et al. [86] observed 58% lower UFP concentrations during the "Summer Streets"

campaign in New York City, in which vehicular traffic was not allowed on Park Ave. in the morning of three consecutive Saturdays. Quiros et al. [87] reported 83% and 39% decreases in UFP and $PM_{2.5}$ concentrations, respectively, 50m downwind of the I-405 freeway in West Los Angeles, California. This work occurred from July 15 at 20:00 to July 17 at 1200, a period in which the road was closed due to the demolition of an overpass bridge in 2011.

In the present study, we also focused on airport impacts on UFP levels in nearby neighborhoods; inter- and intra-community variations in traffic-related air pollutants both in residential neighborhoods and on arterial roadways; as well as variations in pollutants levels over a period of years in these same neighborhoods. In addition, the I-405 closure event provided a rare opportunity to investigate the effects of reduced traffic emissions on air pollutant distributions at both near-roadway [87] and neighborhood scales (this study).

12.2 General Meteorological Comparability

The mean air temperature, relative humidity (RH), wind speeds and direction during measurement periods are shown in Table 12. In general, higher air temperature, lower RH, and lower wind speeds were observed in DTLA than in WLA. Prevailing winds were consistently from the southwest strongly influenced by sea-breezes in both DTLA and WLA.

The CART analysis allowed us to investigate day-by-day meteorological comparability on a more regional scale. Summer season regression trees for daily maximum CO concentrations ($[CO]_{max}$) classify five specific meteorological conditions (*nodes*) to explain observed $[CO]_{max}$ [36]. Of the total 15 measurement days, 13 days were classified to be under meteorologically comparable conditions for primary pollutant dispersions (*node 2; most typical summer conditions*). Only two days (7/8/2008 and 7/16/2011 WLA) fell into meteorologically different nodes (*node 1* and *5*, respectively) (Table 12). *Node 1* represents the identical meteorological conditions to *node 2* except weaker winds. *Node 5* represents meteorologically less common summer conditions with stronger north-south pressure gradients which cause more stable conditions with weaker winds fields over the region, but higher humidity that is statistically related to lower concentrations in this group. Meteorological conditions for *node 2* are linked to the lowest $[CO]_{max}$ (0.6 ppm), and *nodes 1* and *5* are related to modest $[CO]_{max}$ (0.9 and 1.0 ppm, respectively). However, we note that all three nodes for the sampling dates are the lower three *nodes* of a total of five nodes with respect to pollutant concentrations. The regression trees for daily maximum and mean NO_x concentrations also showed similar classifications, all sampling days represented typical summer days related to the lowest primary pollutant concentrations of the whole summer season.

Table 12. Measurement dates, mean surface meteorological conditions, and the CART classification results for meteorological comparability.

Area	Measurement Date (Time)	Day of week	Temp. (°C)	Relative humidity (%)	Wind speeds ($m \cdot s^{-1}$)	Wind direction (°)	CART final node[a]
DTLA	07/14/2008 (14:00 – 17:00)	Mon.	27.6	41	2.6	240	2
	07/16/2008 (14:00 – 17:00)	Wed.	26.7	49	2.4	260	2
	07/18/2008 (14:00 – 17:00)	Fri.	24.6	61	2.9	250	2
	Mean (Std.)		26.3 (1.5)	50 (9)	2.6 (0.7)	250 (10)	
WLA	06/30/2008 (14:00 – 16:30)	Mon.	21.9	60	4.1	243	2
	07/08/2008 (14:00 – 16:30)	Tue.	20.7	73	5.1	240	5
	07/10/2008 (14:00 – 16:30)	Thu.	23.4	63	4.4	227	2
	07/12/2008 (14:00 – 16:30)	Sat.	23.9	63	4.3	240	2
	Mean (std.)		22.5 (1.5)	65 (5)	4.5 (0.6)	238 (13)	
WLA	07/08/2011 (12:00 – 14:00)	Fri.	22.6	70	3.9	240	2
	07/09/2011 (12:00 – 13:30)	Sat.	21.5	72	3.8	233	2
	07/10/2011 (12:00 – 13:30)	Sun	21.8	68	4.1	240	2
	07/15/2011 (13:30 – 15:00)	Fri.	21.3	57	4.6	247	2
	07/16/2011 (14:30 – 16:00)	Sat.	20.3	67	5.1	245	1
	07/17/2011 (13:15 – 14:45)	Sun	20.9	68	4.3	240	2
	07/22/2011 (14:20 – 16:00)	Fri.	20.9	66	4.8	233	2
	07/23/2011 (13:30 – 15:00)	Sat.	21.1	66	4.4	245	2
	Mean (std.)		21.3 (0.7)	67 (4)	4.4 (0.4)	240 (5)	

[a] CART classifications were made based on daily maximum CO data obtained at N. Main monitoring station operated by South Coast Air Quality Management District as described in detail in Section 11.

12.3 Traffic on the freeways in WLA and DTLA

Average traffic flows (*vehicle·5min*$^{-1}$) for the measurement periods are shown in Table 13. Although traffic flows (a sum of both directions) were consistent or showed slowly decreasing trends beginning in early afternoon (Figure 45a), we note that vehicle speeds (particularly for the north-bound) significantly dropped after 2 or 3 p.m. (Figure 45b). Traffic jams reduce the number of vehicles passing by the sensor due to slower speeds, but the numbers of vehicles on a given length of roads can be much larger at slower traffic speeds. Thus vehicle density (*vehicle·km*$^{-1}$), defined as traffic flow divided by vehicle speed, is more representative of traffic conditions, particularly for morning and late afternoon rush hours (Figure 45c).

Table 13. Mean traffic flows (veh·5min^{-1}) and densities (veh·km^{-1}) on the surrounding freeways of DTLA and WLA routes during sampling periods. Percent values are relative increase or decrease rates with respect to WLA 2008 values.

	Freeway	WLA 2008		WLA 2011			DTLA 2008
		Weekdays	Sat.	Fri.	Sat.	Closure day (Sat.)	Weekdays
Traffic Flow (Truck flow) (veh·5min^{-1})	I-405	1231 (41)	1252 (16)	1214 (33) -1%	1454 (54) +16%	106 (8) -92%	
	I-10	848 (10)	735 (3)	827 (33) -2%	814 (22) +11%	502 (2) -32%	1171 (30) +38%
	I-110						1293 (58)
	101						927 (95)
Traffic density (std. dev.) (veh·km^{-1})	I-405	319 (±44)	247 (±20)	269 (±26) -16%	268 (±24) +9%	10 (±2) -96%	
	I-10	123 (±10)	73 (±10)	171 (±21) +39%	148 (±21) +103%	52 (±3) -29%	195 (±29)
	I-110						293 (±72)
	101						156 (±18)

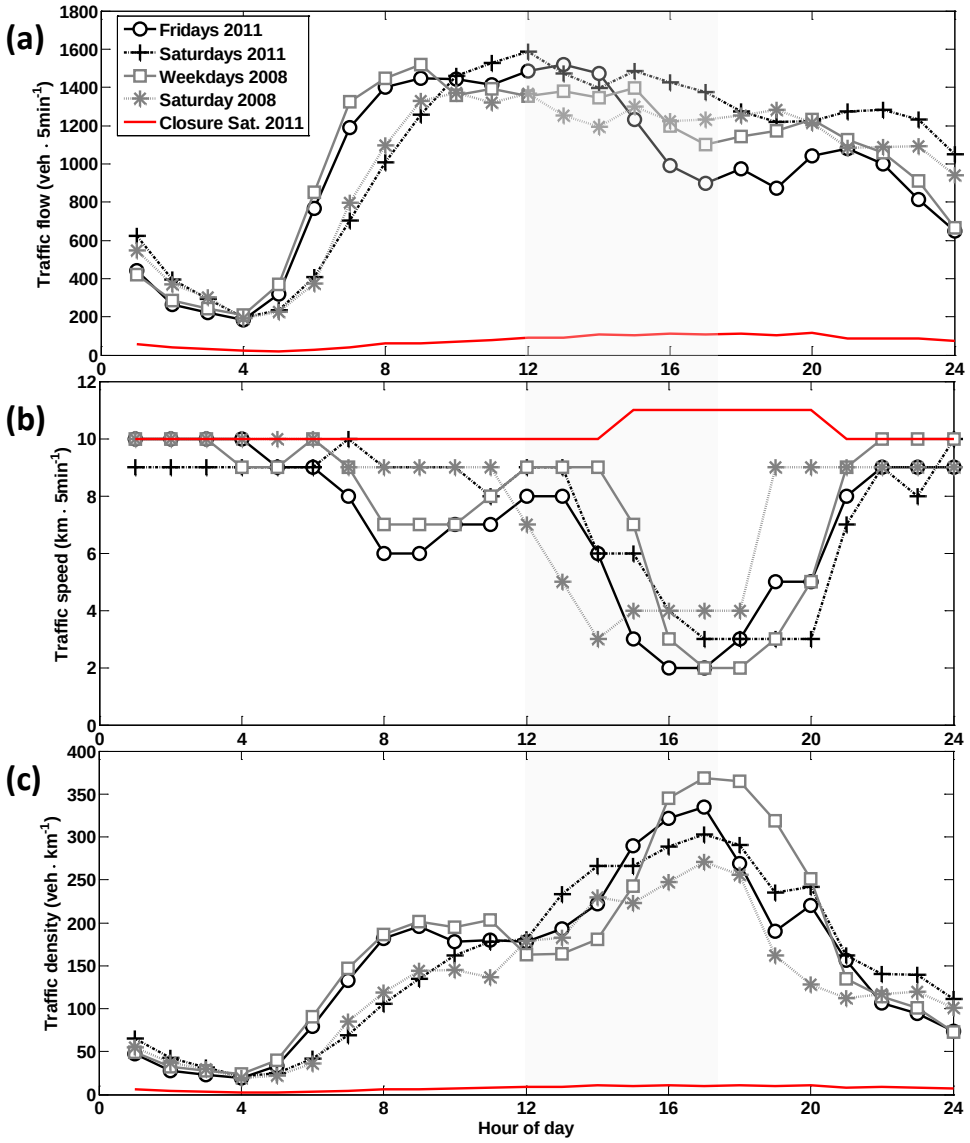

Figure 45. Mean diurnal variations of traffic data obtained at Pico-station sensors on I-405 freeway: (a) traffic flows (vehicles·5min^{-1}), (b) vehicle speeds (km·5min^{-1}), and (c) traffic density (vehicles·km^{-1}). Black circles are for Fridays in 2011 data, black crosses for non-closure Saturdays in 2011, gray squares for weekdays in 2008, gray asterisks for Saturday in 2008, and red lines for I-405 closure Saturday. Gray-shaded area represents measurement a period of day.

In general, traffic emissions are likely to be enhanced in the DTLA area which is intersected by five busy freeways and congested arterial streets (e.g., the I-10 freeway had 59% more vehicles per km and 38% more traffic flows in the DTLA area than in WLA. In WLA, Fridays traffic flows in 2011 were comparable to those in 2008 for both the I-405 and I-10 freeways, but vehicle densities in 2011 were 16% lower on the I-405 and 39% higher on the I-10 freeway than those in 2008. Traffic on Saturdays significantly increased in 2011 on both the I-405 and I-10 compared to 2008. More noticeably, both traffic flows and densities on the I-405 closure day (7/16/2011) were less than 10% of 2008 Saturday measurements for the I-405, and about 30%

lower compared to 2008 Saturday traffic for the I-10 freeway. Traffic flows and densities on the I-10 on the I-405 closure day decreased by 38% and 65%, respectively, compared to normal 2011 Saturdays. In addition to freeways, significant traffic reductions on nearby arterial streets were observed during I-405 closure measurement periods, although these were not quantified.

12.4 Inter-community variations in pollutant concentrations in residential neighborhoods

Significant differences in traffic-related pollutants concentrations in residential neighborhoods were observed between Boyle Heights (BH), DTLA, and WLA (Figure 46). BH data from 2008 were obtained from Hu et al. [62] whose measurements were conducted during the same periods as DTLA measurements. The mean UFP concentrations in the neighborhoods of BH, DTLA, and WLA in 2008 were $3.3\pm2.2\times10^4$, $2.2\pm1.7\times10^4$, and $1.1\pm1.4\times10^4$ particles·cm^{-3}, respectively. However, we note that standard deviations are large due to strong impacts from individual high emitting vehicles (HEV). The Kolmogorov-Smirnov (KS) test after removing the local spikes from high emitting vehicles (HEV) encountered during the measurements, verified the inter-community variations in UFP concentrations are statistically significant ($p<<0.01$) at 99% confidence level (see supplementary material S1 for the details of identification for HEV spikes).

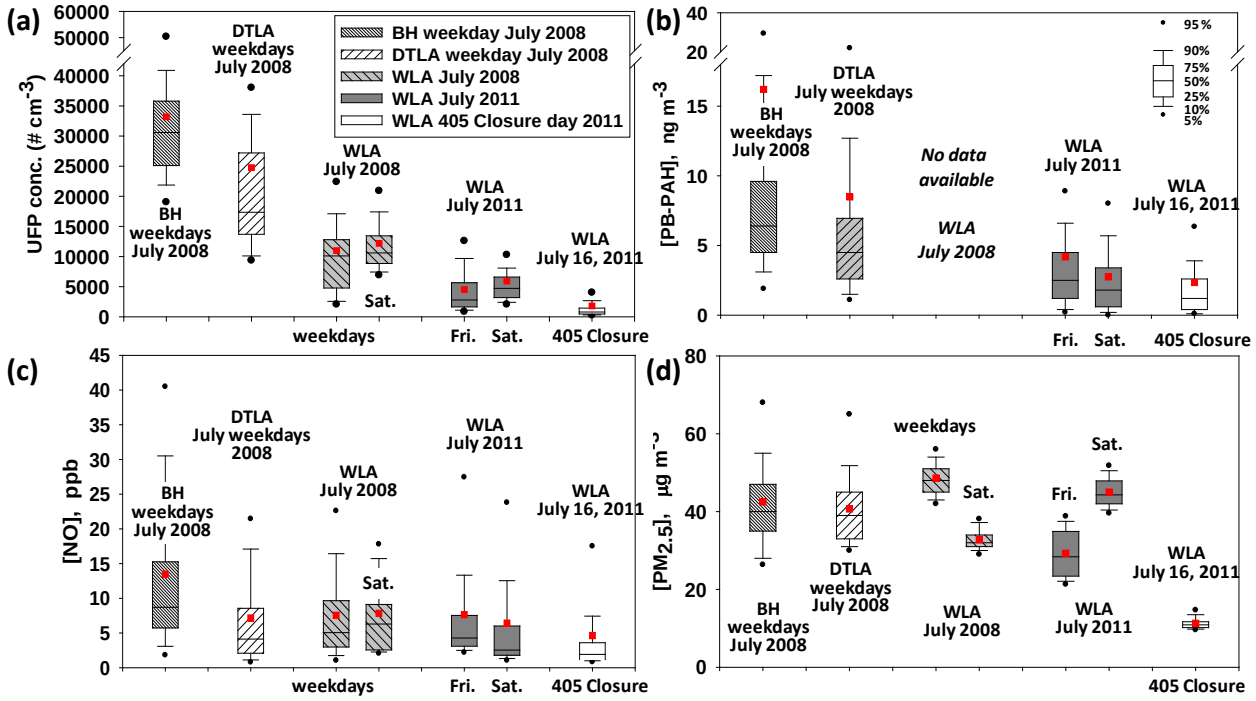

Figure 46. Box plots of pollutant concentration variations sampled in residential neighborhoods of Boyle Heights (BH; black fine slant lines), Downtown LA (DTLA; black coarse slant lines), West LA in 2008 (WLA; gray coarse slant lines), WLA in 2011 (simple gray boxes), and WLA on I-405 closure Saturday (white simple boxes): (a) Ultrafine particles (particles·cm^{-3}), (b) PB-PAH (ng·m^{-3}), (c) NO (ppb), and (d) particle mass less than 2.5 µm diameter ($PM_{2.5}$, µg·m^{-3}). Red squares represent the mean values.

Similarly, PB-PAH concentrations were highest in BH (16±58 $ng \cdot m^{-3}$), followed by DTLA (8±23 $ng \cdot m^{-3}$) and WLA (4±10 $ng \cdot m^{-3}$ in 2011) (Figure 46b). Nitric oxide concentrations were comparable between DTLA (7.2±10 ppb) and WLA (7.5±6.8 ppb), but higher in BH (13.5±12.7 ppb) (Figure 46c). Although daytime NO is rapidly converted to NO_2 by ozone, O_3 concentrations during measurement periods varied little by site (44 ppb in BH and DTLA, and 38 ppb and 41 ppb in WLA 2008 and 2011, respectively). Thus, assuming O_3-NO-NO_2 photochemical processes are comparable in these areas (spatial scales of ~ 20 km), higher NO concentrations in BH were likely to result from more emissions from denser traffic networks in BH.

$PM_{2.5}$ did not show noticeable heterogeneous spatial distributions on an inter-community scale (Figure 46d). Relatively homogeneous distributions of fine particles are likely due to a large fraction of $PM_{2.5}$ being formed secondarily through regional photochemical processes [88]. Thus, differences in direct emissions of fine particles from vehicular sources are relatively insignificant within these study areas (~ 20 km). Recent near-roadway studies also showed relatively insignificant elevations of $PM_{2.5}$ from major roadways [6, 87]. Hu et al. [62] attributed elevated concentrations of traffic-related pollutants in BH to relatively higher traffic density compared to other regions of the Southern California [89], combined with substantial numbers of HEV and a high density of stop signs and traffic lights with short block lengths. We found the percent of times HEV encountered are not significantly different between BH and DTLA, and hence we concluded more elevated UFP concentrations in BH are attributed to mainly denser traffic networks.

No significant differences in UFP and other pollutant concentrations were observed between weekdays and weekend days in WLA either in 2008 or 2011 (e.g., 1.1 vs. 1.2×10^4 in 2008 and 0.5 vs. 0.6×10^4 $particles \cdot cm^{-3}$ in 2011 for UFP, and 7.5 vs. 7.8 in 2008 and 7.6 vs. 6.4 ppb in 2011 for NO).

12.5 Intra-community variations in pollutant concentrations in residential neighborhoods

WLA residential neighborhoods were divided into four sub-areas to investigate intra-community variations in traffic related pollutants: *A* (upwind from freeways), *B* (intermediate between I-405 and I-10 freeways), *C* (downwind from freeways), and *SMA* (adjacent downwind of Santa Monica Airport) (Figure 13b). Increases in pollutant concentrations were observed as air masses travel from *A* through *C* (prevailing winds during the afternoon are consistent southwesterlies in both WLA and DTLA) (Figure 13b and Figure 47). As an air mass travels from area *A* to *C*, it experiences emissions from surface streets as well as freeways (e.g. area *A* is influenced only by surface streets, whereas *B* by surface streets and the I-10 freeway, and *C* additionally by the I-405 freeway). The increments of additional vehicle-related pollutants during the north-eastward air parcel transport were more readily observed in median concentrations than mean values because mean values are likely more strongly influenced by intermittent encounters with high-emitting vehicles.

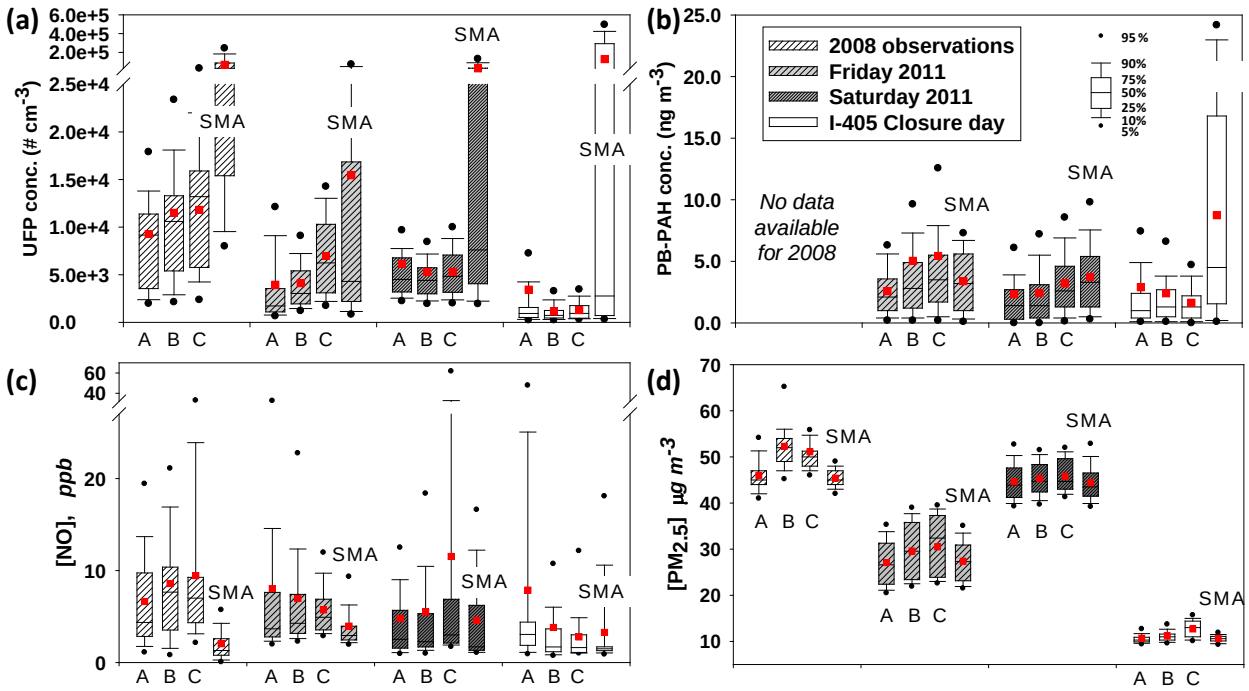

Figure 47. Box plots of pollutant concentrations observed in residential sub-areas (*A*, *B*, *C*, and *SMA*) of WLA for weekdays in 2008 (coarse slant lines in white boxes), Fridays in 2011 (fine slant lines in light gray boxes), non-closure Saturdays in 2011 (fine slant lines in dark gray boxes), and I-405 closure Saturday in 2011 (simple white boxes): (a) UFP, (b) PB-PAH, (c) NO, and (d) $PM_{2.5}$. Red squares represent the mean values.

The median concentrations of UFP in area *B* and *C* were 16% and 39% higher, respectively, compared to *A* in 2008 (weekdays), and 76% (*B*) and 262% (*C*) higher in 2011 (Fridays). The mean UFP concentrations removing spikes from HEV (supplementary material) showed the similar distributions; 25% (*B*) and 40% (*C*) higher in 2008, and 42% (*B*) and 158% (*C*) higher in 2011, compared to area *A*. The KS test showed the intra-community UFP variations were statistically significant at 99% confidence level ($p<<0.01$) in both 2008 and 2011. These trends in spatial distributions were consistently observed for other pollutants during weekdays (Table 14).

Table 14. Median pollutant concentrations obtained in the sub-areas (*A*, *B*, and *C*) of residential neighborhoods in West LA, and % increments of median values as an air mass travels *A* through *C*.

		Median Concentrations (% increase compared to *A*)		
		A	*B*	*C*
UFP	Weekdays in 2008	9,165	10,600 (+16%)	12,700 (+39%)
	Fridays in 2011	1,725	3,040 (+76%)	6,245 (+262%)
	Saturdays in 2011	4,510	4,410 (-2%)	4,840 (+7%)
	Sunday (07/10/2011)	1,440	3,385 (+135%)	4,350 (+202%)
NO	Weekdays in 2008	4.4	7.7 (+76%)	7.1 (+64%)
	Fridays in 2011	3.7	4.3 (+17%)	4.9 (+34%)
	Saturdays in 2011	2.5	2.3 (-9%)	3.0 (+20%)
	Sunday (07/10/2011)	1.4	2.5 (+82%)	2.0 (+48%)
PAH	Fridays in 2011	2.1	2.8 (+33%)	3.5 (+67%)
	Saturdays in 2011	1.4	1.4 (0%)	2.6 (+86%)
	Sunday (07/10/2011)	1.6	1.0 (-38%)	1.8 (+13%)
CO	Fridays in 2011	0.49	0.50 (+3%)	0.56 (+14%)
	Saturdays in 2011	0.53	0.52 (+-3%)	0.58 (+9%)
	Sunday (07/10/2011)	0.43	0.45 (+4%)	0.50 (+16%)
$PM_{2.5}$	Weekdays in 2008	45	52 (+16%)	50 (+11%)
	Fridays in 2011	27	30 (+11%)	33 (+22%)
	Saturdays in 2011	44	45 (+2%)	45 (+2%)
	Sunday (07/10/2011)	27	33 (+24%)	30 (+13%)

Elevations of pollutant levels in area *C* were normally observed for the entire sampling periods, whereas increments in area *B* were somewhat variable by pollutant and sampling period (e.g. concentrations of UFP, NO, and CO were slightly lower in area *B* than *A* on Saturdays in 2011). However, we note that the UFP intra-community variations on Saturdays in 2011 are not statistically significant with KS and T-tests. Areas *A* and *B* are expected to experience similar pollutant contributions from the upwind areas except for the I-10 freeway that is likely a dominant contributor to pollutant levels in area *B*. Given that prevailing winds are somewhat parallel to the I-10 freeway orientation (240° vs. 252°), the instantaneous variations in wind direction during sampling might dampen the intra-community differences between areas *A* and *B*. Changes in traffic activities over WLA for weekend days might also contribute to intra-community variations in weekend pollutant levels (e.g., larger traffic in the beach areas, which are ~3 km upwind of the study areas, is expected for leisure activities on the weekend,). For example, during the I-405 closure period, median concentrations of UFP and NO were highest in area *A* (Figure 47) due to massive decreases in traffic density around the sampling route but possibly less of a decrease in the upwind coastal areas.

12.6 Santa Monica Airport (SMA) impacts on locally elevated UFP concentrations

Another interesting feature in intra-community variations in pollutant levels is found in the neighborhood immediately downwind of the Santa Monica Airport (SMA), particularly for UFP concentrations. Hu et al. [90] reported UFP concentrations that were about a factor of 10 higher 100 m downwind of SMA over background levels. The SMA residential area in this study covered 120–480 m downwind of the north end of the airstrip (Figure 13). Figure 47a shows a remarkable increase in UFP levels in the SMA residential area with extremely wide variations. The mean UFP concentrations in the SMA residential area were 6.8, 1.5, 3.0, and 1.3×10^4 particles·cm^{-3} for weekdays in 2008, and Fridays, Saturdays, and the I-405 closure day in 2011, respectively. These values are factors of 7, 4, 5, and 37, respectively, higher compared to those in area *A* for the above sampling periods. In addition, the ratios of mean to median values of UFP concentrations ranged from 2 to 46 (dimensionless ratio) through the measurement periods, implying exceedingly high levels of UFP appeared intermittently, associated with idling and takeoff of aircraft [90]. Over all measurement days, 2–7 takeoffs of jet and reciprocal engine aircraft (81% reciprocal engine and 19% jet) were observed for each of the SMA sampling periods. Upper 90% quantile UFP concentrations in SMA neighborhoods were one order of magnitude higher than those in area *A* over the sampling periods.

On the I-405 closure day, UFP concentrations around SMA were comparable to those of other sampling periods, whereas exceptionally low concentrations were observed in other residential areas due to significantly reduced traffic densities in WLA (Figure 47a). This is consistent with aircraft impacts on elevated UFP levels in the neighborhood downwind of the airport. Although we cannot quantify UFP emissions from an individual aircraft due for the sampling design of this study (we measured UFP concentrations with a moving mobile platform, and hence peak concentrations were encountered at different locations from the SMA and different angles to prevailing winds), qualitatively, the highest UFP peak concentrations were associated with mid-size jet takeoffs (the largest aircraft using SMA), followed by small jets and smaller reciprocal-engine aircraft (not shown quantitatively in Figure 48a). These results are consistent with Hu et al. 's [62] observations and calculation of fuel consumption rates at SMA.

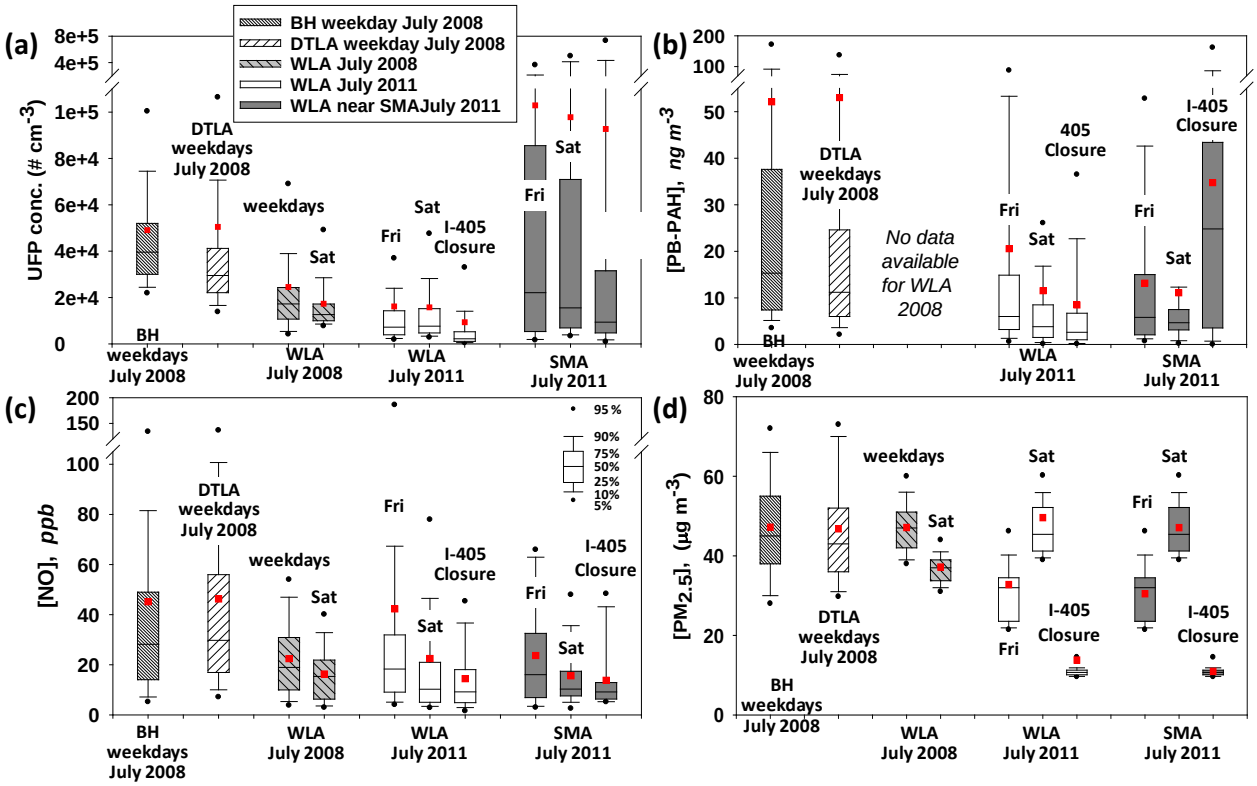

Figure 48. Box plots of pollutant concentrations measured on arterial roadways in BH in 2008 (fine slant lines in white boxes), DTLA in 2008 (coarse slant lines in white boxes), WLA in 2008 (coarse slant lines in gray boxes), WLA in 2011 (simple white boxes), and WLA adjacent to SMA in 2011 (simple dark gray boxes): (a) UFP, (b) PB-PAH, (c) NO, and (d) $PM_{2.5}$. Red squares represent the mean values.

PB-PAH in the SMA neighborhood slightly increased on Fridays and Saturdays compared to the other residential areas, whereas a relatively conspicuous peak was observed on the I-405 closure day. We note there were two jet takeoffs (one small and one mid-size) during the sampling periods around SMA on the closure day. Given that PB-PAH spikes are associated with transitory jet takeoffs [90], and measurement periods around the SMA neighborhood were short (two times for 5–10 minutes per day), day-to-day variations in PB-PAH concentrations due to airport activities are expected (Figure 47b). Similar but less dramatic trends were observed for CO concentrations (not shown). Concentrations of other pollutants in the SMA neighborhood, such as NO and $PM_{2.5}$, were comparable to or lower than those in sub-area *A* where the lowest pollutants concentrations were observed. These results are also consistent with Hu et al.'s [90] interpretation of pollutant concentrations they measured in the vicinity of SMA.

12.7 Comparisons of pollutant concentrations on arterial roadways

Pollutant concentrations on arterial roadways were compared between BH, DTLA, and WLA in 2008 and WLA in 2011 (Figure 48). Although on-road measurements are influenced strongly by vehicles ahead of the MMP (because we did not try to change lanes to avoid HEV), these results are valuable for several applications: on-road in-vehicle exposure assessments; many people are active adjacent to arterial roadways, e.g. walking and waiting at bus stops; and many commercial stores are densely located on arterial roadways. In general, pollutant

concentrations were highest in BH, followed by DTLA and then WLA, as expected. Median UFP concentrations were 4.0, 3.0, 1.7, and 0.8×10^4 particles·cm^{-3} in BH, DTLA, WLA in 2008, and WLA in 2011, respectively. The KS test with data removing transient spikes from HEV also showed the differences in UFP distributions by location are statistically significant at 99% confidence level ($p<<0.01$). UFP concentrations on an arterial roadway adjacent to SMA (S. Bundy Dr.) showed the highest extreme and mean values with exceptionally wide variations, consistent with aircraft activities as discussed earlier (Figure 48a) and in Hu et al. [90].

PB-PAH showed on-road distributions similar to UFP on arterial roadways (median concentrations of 15, 11, 6, 4, and 3 ng·m^{-3} in BH and DTLA in 2008, and Fridays, Saturdays, and closure Saturday in WLA 2011, respectively). However, HEV contributions to observed PB-PAH concentrations were more pronounced in BH and DTLA than at SMA compared with HEV contribution to UFP distributions (Figure 48b). NO concentrations were higher in BH and DTLA (28–30 ppb median) compared to WLA (14–18 ppb median), with no significant difference around SMA (Figure 47c). No observable spatial and temporal differences in $PM_{2.5}$ were found during the measurement periods. Airport effects on $PM_{2.5}$ mass were negligible (Figure 47d).

12.8 High emitting vehicles (HEV) impacts on observed UFP concentrations

Percent of time HEV encountered and total UFPs from HEV were calculated as in Hu et al. [62], but in this study the threshold values were determined statistically (supplementary material) instead of arbitrary values used in Hu et al. [62]. As summarized in Table 15, percent of time HEV encountered was usually higher on arterial roadways than in residential areas as expected, but no distinct differences between BH/DTLA and WLA were found (10–13% vs. 7–10% on arterials and 4–7% vs. 4–5% in residential neighborhoods in BH/DTLA and WLA, respectively). Nonetheless, as Hu et al. [62] discussed, larger fraction of total UFP resulted from relatively smaller HEV numbers. For example, 7–13% of time HEV encountered accounted for 29–48% of total UFP observed on arterial roadways, and 4–7% of time of HEV encountered contributed 13–18% of total UFP concentrations. Larger HEV impacts on observed UFP concentrations were found in relatively cleaner WLA areas both on arterials and in residential neighborhoods due to lower baseline concentrations of UFP. These results suggest how effectively UFP air quality can be improved, if we reduce HEV successfully through a retrofit on or early-retirement of HEV.

Table 15. The effects of HEV on UFP concentrations on arterial roadways and residential areas in BH, DTLA, and WLA (2008 and 2011).

	Sites (data #)	Mean (all data)	STD (all data)	Mean (HEV removed)	STD (HEV removed)	Threshold	% of time HEV encountered	% of total UFP from HEV
On-arterial roads	BH (1,192)	49,100	55,900	39,100	12,800	64,700	10%	29%
	DTLA (3,051)	50,500	181,700	29,300	11,900	53,000	13%	49%
	WLA `08 (1,158)	24,500	38,800	16,400	8,600	33,600	10%	40%
	WLA `11 (2,116)	16,200	58,300	9,000	7,000	23,000	7%	48%
Residen-tial Area	BH (766)	33,200	22,200	29,900	6,600	43,000	7%	16%
	DTLA (1,152)	21,600	17,100	19,500	8,200	36,000	4%	13%
	WLA `08 (1,451)	12,600	13,200	10,800	6,200	23,100	5%	18%
	WLA `11 (3,592)	4,500	5,200	3,800	3,100	10,000	4%	18%

12.9 UFP emission reductions over time

Significant decreases in UFP concentrations both in residential neighborhoods and on arterial roadways in WLA were observed between 2008 and 2011 (Figs. 3 through 5). The median and mean concentrations of UFP were reduced approximately 70% and 60%, respectively, in residential neighborhoods for weekdays compared to observations in 2008 (1.1 to 0.3 $\times 10^4$ particles$\cdot$cm^{-3} for median and 1.2 to 0.5$\times 10^4$ particles$\cdot$cm^{-3} for mean values). Compared to values in 2008, the median and mean UFP Saturday concentrations decreased ~55% and ~50%, respectively, in 2011 in WLA neighborhoods. Similar reductions of median UFP concentrations were also observed on arterial roadways (~60% and ~40% on weekdays and Saturdays, respectively), although the declines in the mean UFP concentrations were less pronounced (~35% for weekdays and ~10% for Saturdays). This relatively smaller reduction in the mean concentrations resulted from more frequent encounters with high emitters during sampling periods (standard deviation is about a factor of two larger in 2011). Given that both local and regional meteorological conditions were similar between the sampling periods in 2008 and 2011 (as discussed earlier), and traffic densities on the I-10 and I-405 freeways were generally increased in 2011 (Table 13), this suggests that reduced UFP concentrations in WLA resulted from reductions in emissions of UFP from on-road vehicles. However, no noticeable changes in $PM_{2.5}$ concentrations were observed in neighborhoods and on arterial roadways between 2008 and 2011. A slight decline in median NO concentrations was found in residential neighborhoods and on arterial roadways between 2008 and 2011 but mean NO did not follow a declining trend.

Several recent studies have also reported significant decreases in vehicular UFP emissions. Quiros et al. [87] reported a 67% reduction in UFP concentrations from measurements in the vicinity of the I-405 freeway during the same period of this study in 2011, compared to 2001

measurements [3], and estimated an ~70% decrease in UFP emissions over a decade. In section 8 we qualitatively reported reduced UFP peak concentrations from freeway plumes under pre-sunrise stable atmospheric conditions in the South Coast Air Basin in 2011 compared to observations for pre-sunrise hours in 2008 [2] and nighttime measurements (22:30 – 05:00) in 2005 [4] in the WLA area. Near-roadway studies in other geographical areas have reported similar findings, including a distinct declining trend in nucleation mode particles in Rochester, New York from 2002–2005 to 2005–2007 [81]; a 21% decrease in UFP number concentrations (< 50 nm) for five years (2006–2010) in Toronto, Canada [91]; and a 27% reduction in UFP (particularly for < 30 nm) between 2002–2004 and 2005–2007 in Copenhagen, Denmark [80]. One of the major contributors to these reductions was stringent regulation of sulfur content in gasoline and diesel fuels [80, 81]. In California, Quiros et al. [87] attributed the conspicuous reductions in UFP emissions over time to a combination of several factors, including retirement of older vehicles, adoption of more stringent regulations of particle emissions and fuel composition [92-94], and increased use of smaller and more fuel-efficient engines [95]. We also note that as of 2011, statewide net taxable sales gasoline and diesel gallons have declined ~8% (~1.5%/yr) and ~15% (-4%/yr) since 2006 and 2007, respectively, in California [96]. In addition, fleet fuel economy has significantly improved in the United States (e.g., from 19.9 MPG in 2004 to 23.2 MPG in 2010 [97]).

12.10 Air quality benefits of traffic emission reductions

A striking and valuable feature from the present study is that the 36-hour I-405 closure event provided a superb opportunity to investigate the air-quality benefits of traffic emission reductions on a larger neighborhood scale (several kilometers) not just at near-roadway scales (several hundred meters). During the I-405 closure Saturday, more than 95% and 65% reductions in traffic densities were observed on the I-405 and I-10 freeways, respectively, compared to the preceding and following non-closure Saturdays. Although not quantitatively measured, significant drops in vehicle numbers on nearby arterial roads were also observed during the closure Saturday. Quiros et al. [87] reported a 20% decrease in traffic flows on the closure day on Sepulveda Blvd., a surface street running parallel to, and near, the I-405 freeway, concluding there was no spillover of freeway traffic onto alternative surface streets. Based on available evidence, we conclude voluntary restraints on vehicle-use occurred extensively throughout the WLA area in response to the intensive and long-running warnings of potential chaotic congestion, i.e. "Carmageddon".

Dramatic decreases in both particle number and mass concentrations were observed on the closure day accompanied by relatively smaller reductions in gaseous pollutants and PB-PAH (Table 16 and Figs 3 through 5). The median UFP number and $PM_{2.5}$ concentrations were 800 particles·cm^{-3} and 11 μg·m^{-3}, respectively, in residential neighborhoods of WLA on the I-405 closure Saturday, which were only 30% and 25% of non-closure Saturday UFP and $PM_{2.5}$ levels, respectively. Even on arterial roadways, similar reductions in UFP number and $PM_{2.5}$ concentrations were observed throughout the WLA area. We note that $PM_{2.5}$ on non-closure Saturdays in 2011 was much higher than that on Fridays, which appears an inverse trend compared to 2008 observations. To validate data quality of $PM_{2.5}$ on 2011 Saturdays, we have compared $PM_{2.5}$ with $PM_{0.5}$ obtained from FMPS size distribution data with a density of 1.2 g·cm^{-3}. Mean $PM_{2.5}$ and $PM_{0.5}$ in the residential areas showed an excellent agreement (Supplementary material, S3), and hence we concluded the variations in $PM_{2.5}$ during the

campaign are reliable, supporting a significant reduction in $PM_{2.5}$ during the I-405 closure period.

Table 16. Median concentrations of pollutants measured in residential neighborhoods and on arterial roadways of WLA in 2011 for I-405 closure Saturday and non-closure Saturdays, and concentration reduction rates (%) on closure Saturday compared to non-closure Saturdays.

Median conc. and reduction rates		UFP (#·cm^{-3})	$PM_{2.5}$ (μg·m^{-3})	PB-PAH (ng·m^{-3})	NO (ppb)	CO (ppm)
Residential neighbor-hoods	Non-closure Saturdays	4720	44	1.8	2.5	0.53
	Closure Saturday	800	11	1.2	1.9	0.39
	% Reduction	-70%	-75%	-33%	-25%	-26%
Arterial roadways	Non-closure Saturdays	7660	48	3.8	10.3	0.64
	Closure Saturday	2200	12	2.6	9.2	0.49
	% Reduction	-71%	-74%	-32%	-10%	-25%

Gaseous pollutants and PB-PAH also showed modest drops during the closure event both in residential neighborhoods and on arterial roadways (~25% – ~33%) with the exception of NO on arterial roadways (only ~10% reduction). Simultaneous measurements of UFP and $PM_{2.5}$ at a fixed site on Constitution Ave. (located 2 km north of WLA route) also found 84% and 55% reductions in daily median UFP and $PM_{2.5}$ concentrations, respectively [87].

While we recognize there are likely no near-term prospects for significant reductions in traffic densities in urban locations such as Los Angeles, our findings from the closure of the I-405 freeway, and the trends we have observed in pollutant concentrations over several years, provide evidence that reductions of vehicle emissions through practical and achievable strategies can improve local and regional air quality, particularly for particulate matter in urban areas. Clearly, the atmospheric responses of traffic-related particulate pollutants to the dramatic traffic reductions resulting from the I-405 closure were immediate and conspicuous. With the assumption that observed traffic flows on the I-10 freeway and Sepulveda Blvd. on the I-405 closure Saturday represent overall traffic patterns throughout the WLA areas, a 30–40% reduction in traffic flows accomplished about a 70% decrease in UFP and $PM_{2.5}$ concentrations both in the neighborhoods and on arterial major roads. Although the elevation of $PM_{2.5}$ directly from major roadways is insignificant compared to UFP, PB-PAH, and NO [6, 87], area-wide reductions in traffic densities can decrease direct $PM_{2.5}$ emissions as well as its precursors for secondary production, achieving improvements in $PM_{2.5}$ levels.

We also note that heavy-duty diesel trucks (HDDT) on the I-10 freeway virtually disappeared (10% of non-closure Saturday's truck flows). This case study makes clear the potential benefits for public health of achieving significant vehicle emission reductions through strategies such as HDDT retrofits, and transition to electric vehicles and alternative fuels such as natural gas, and reducing vehicular travel demand. This study also showed the significant impact of HEV on total UFP concentrations, and hence, retrofits or earlier retirement of high-emitting vehicles can help

improve urban air quality. The findings of this study should provide a useful data-set for cost-benefit analyses of such strategies.

13. Freeway Plumes during "Carmageddon"

Average pollutant concentration profiles obtained with high spatial resolution (~10 m) around the 405 freeway before, during and after the I-405 closure are displayed in Figure 49. Daily profiles of pollutants show that pollutant concentrations peaked ~60 m downwind from the freeway median. As discussed in detail in Section 8 above, this peak location is likely caused by freeway geometry. Because the I-405 is elevated above the surface of Constitution Ave., the crossing street on which measurements were made (and the surrounding ground surface), freeway plumes are transported farther downwind before reaching the ground. Higher peak concentrations of UFP, NO, and PAH were observed on pre-closure Saturday than for the post-closure Saturday, accompanied by higher far downwind (> 250 m) concentrations. Given I-405 traffic flow was similar on both Saturdays (Table 6), weaker prevailing winds on Saturday July 9 are likely the explanation for the increase in relative concentrations of pollutants between the pre- and post-closure Saturdays.

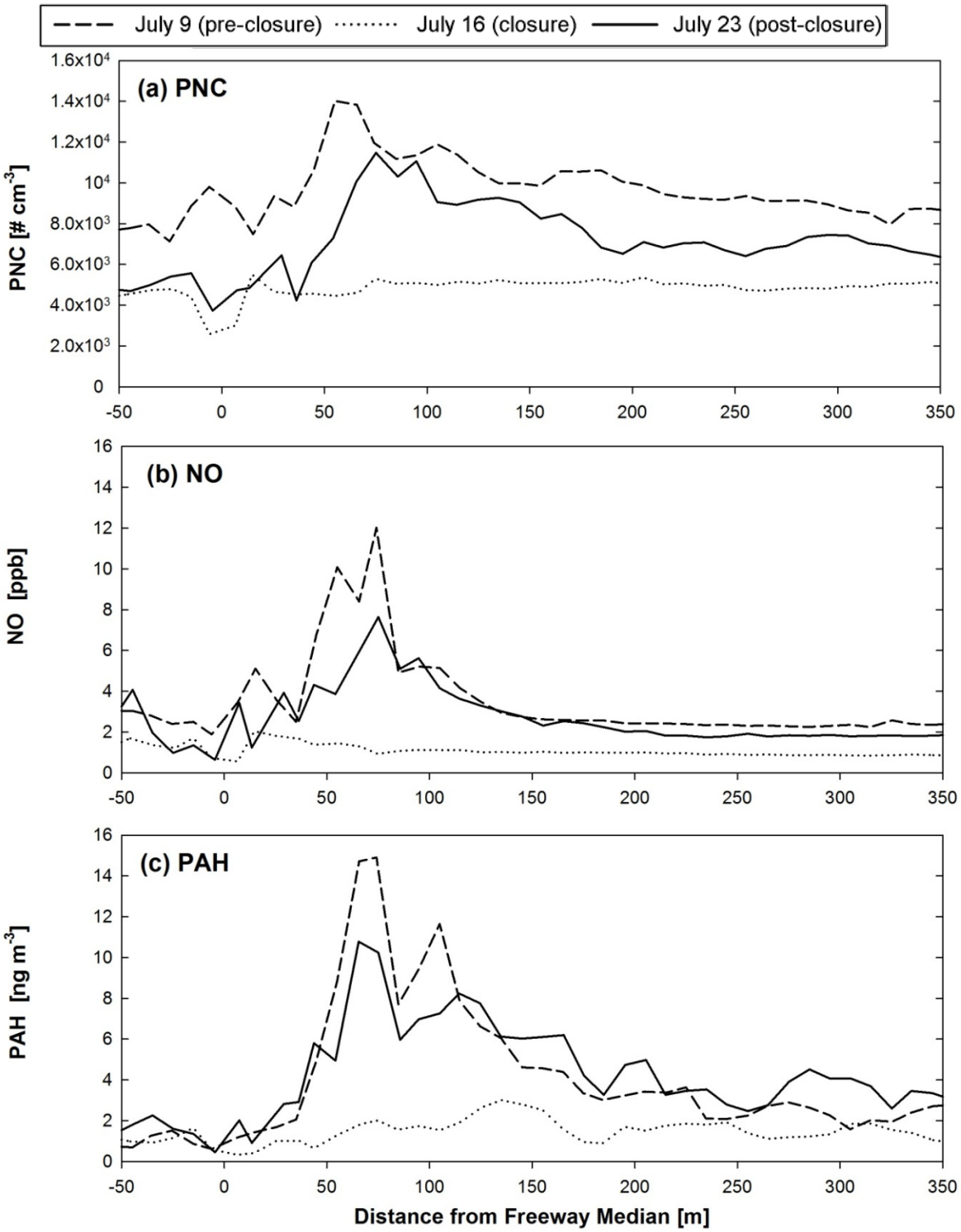

Figure 49. Concentrations of (a) PNC, (b) NO, and (c) PAH at several distances from I-405 median.

Figure 50 shows contour plots of size distribution concentration, where the x-axis indicates the distance from freeway median, the y-axis indicates the particle diameter (log scale), and the color intensity indicates normalized particle number concentration ($dN/dLogD_p$). In both the upwind and downwind areas (>150 m), a unimodal particle mode was measured at ~52 nm. The surge of nucleation mode particles disappeared much more quickly than accumulation mode particles for distances < 150 m downwind due to dilution with air containing lower concentrations of nucleation mode particles but higher concentrations of accumulation mode particles, and coagulation losses to larger particles [3, 98]. However, around the freeway peak, distinct spikes in nucleation mode particles (~11 nm) were observed on both the pre- and post-closure Saturdays. Given that nucleation mode particles were not observed during closure (Figure 49b), it is clear that vehicular UFP emissions dominate nucleation mode particles as discussed above for the fixed site measurements. Another interesting feature of the size distribution (Figure 50) is that the accumulation mode was measured at ~52 nm on both pre- and post-closure Saturdays compared to measurement at ~40 nm during the closure Saturday. This is likely due to the absence of freshly emitted organic vapors and/or nucleation mode particles from the freeway that serve as condensation/coagulation agents to allow accumulation mode particles to effectively grow. A detailed investigation of particle dynamics to prove this hypothesis is, however, beyond the scope of this study.

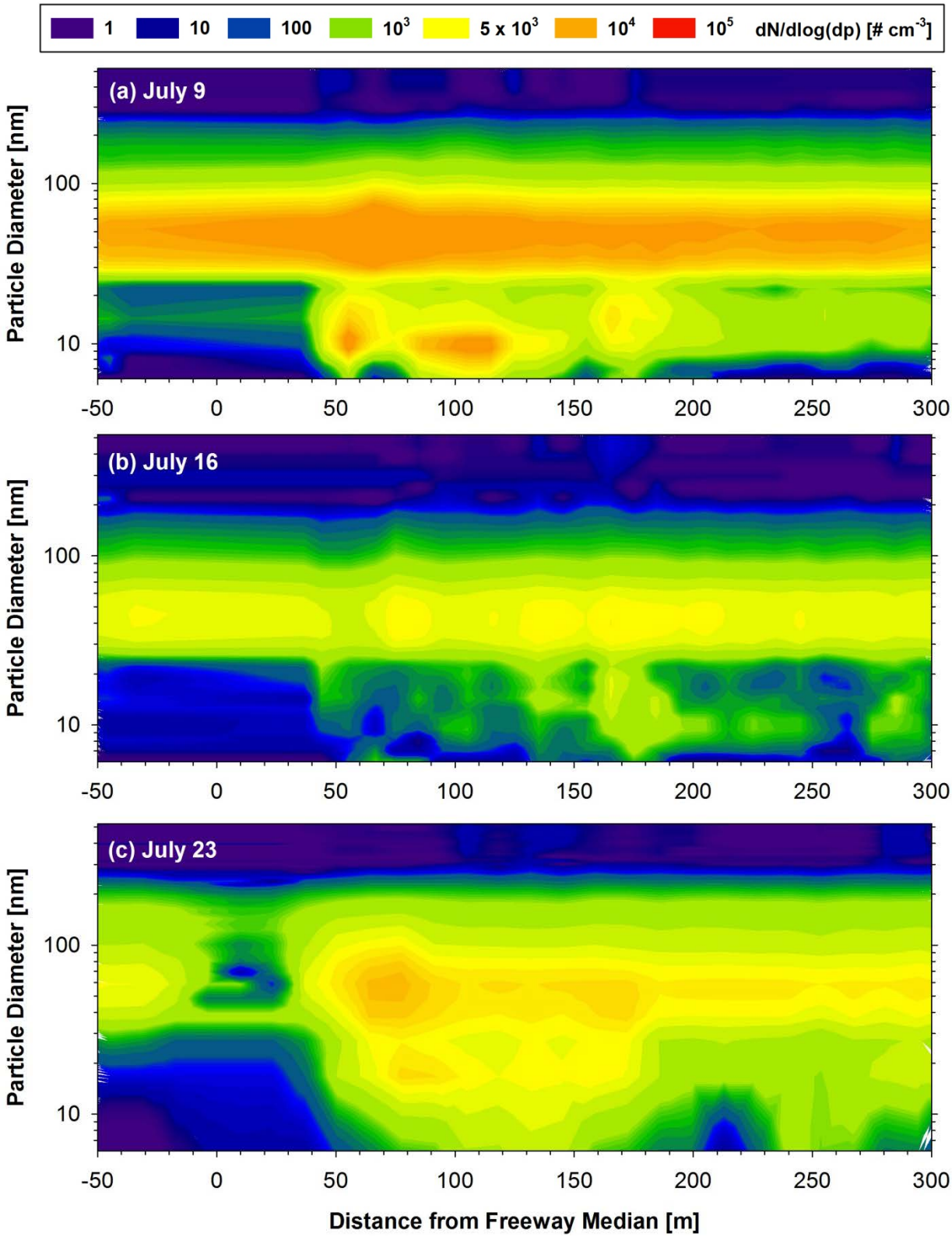

Figure 50. Contour plots of particle size distributions as a function of distance from I-405 on Saturday (a) July 9 (pre-closure), (b) July 16 (closure) and (c) July 23 (post-closure).

14. Concluding Remarks

We have conducted air-quality studies with a focus on ultrafine particles (UFP) distributions and concentration decays with distance from major roadways using an electric mobile measurement platform (MMP) with no pollution of its own (Toyota RAV4 electric sub-SUV). Major findings are as below:

For pre-sunrise measurements,

1) Pre-sunrise (or nocturnal) extension of freeway plumes far downwind (> 2 km) compared to daytime plume length (<300 m) is a general phenomenon in the SoCAB.
2) The plume peak UFP concentrations were strongly related to traffic density on the freeway under stable air conditions.
3) Freeway geometry (underpass or overpass freeway) is an important parameter to determine the position of the plume peak concentration.
4) Plume decay rate constants near freeways were one order of magnitude slower for pre-sunrise hours compared to those of daytime.
5) Decay rates of UFP with distance from freeway increase as particle size decreases.
6) A curve fit using a Gaussian dispersion model solution described excellently the observed UFP profiles both at the peak and far downwind (> 2 km) with R^2 ~0.9 or larger for all measurement sites.
7) Factors controlling pollutant plume length downwind of freeways under stable conditions were background-subtracted peak concentration (which is a function of traffic flows and temperature) as well as meteorological parameters, such as wind direction and speeds. Vertical stability (Richardson number) plays a minor role in dispersion coefficient variations within stable boundary layer conditions.
8) Estimated particle number emission factor (PNEF) using a curve fit method was 7.5×10^{13} particles·vehicle^{-1}·km^{-1}, which is 7 times smaller than an estimate (5.2×10^{14} particles·vehicle^{-1}·km^{-1}) made in 2001 for the I-405 freeway by Zhu et al. [5].

For daytime neighborhoods measurements in West LA (WLA), Downtown LA (DoLA), and Boyle Heights (BH),

9) As a As a supplementary study for MMP measurements, we developed an objective and systematic classification scheme of meteorological conditions affecting atmospheric primary pollutant levels for the South Coast Air Basin. We then used in this as a quantitative framework with which to control for variations in meteorology from measurements made on different days at different locations.
10) Daytime UFP concentrations in neighborhoods showed strong inter-community variations between WLA (1.1×10^4 particles·cm^{-3}), DoLA (2.2×10^4 particles·cm^{-3}) and BH (3.3×10^4 particles·cm^{-3}) in 2008.
11) Intra-community pollutant variations were less intense but significant as an air mass experiences emissions from major freeways (I-405 and I-10).
12) Santa Monica Airport (SMO) impacts on locally elevated UFP distributions were significant.
13) Impacts of high emitting vehicles on UFP distributions both on arterial roadways and in neighborhoods were significant.
14) About 70% reductions of UFP and $PM_{2.5}$ were observed during the I-405 closure event (so called "Carmageddon") in 2011 with about 20 to 70 % decrease (depending on location) in traffic flows in WLA.

15) A drop in ultrafine particle concentrations in West Los Angeles between 2008 and 2011 was also observed.

While 4.4% of the SoCAB population lives within 100 m of freeways, 50% of the SoCAB population lives within 1.5 km of freeways [27]. Because particle concentrations can be several times greater in the pre-sunrise and early morning, exposures in this period can dominate total daily exposure depending on individual time-activity patterns. A much greater population of downwind residents may be exposed to vehicle-related pollutants during the early morning hours, because people are generally in their homes in the early morning, and penetration of outdoor UFP and related pollutants is reasonably efficient, although infiltration factors for outdoor pollutants are strongly influenced by house characteristics as well as air-exchange rates and indoor deposition rates [e.g., 1, 99]. A more quantitative evaluation of the exposure implications of our findings is desirable.

15. Acknowledgements

The authors gratefully acknowledge support for this study by the California Air Resources Board, Contract No. 09-357. We also thank Southern California Edison (SCE) for the use of electric charging facility and for providing security, James Murakami at UCLA for assistance with local meteorological characteristics and data, and Dr. Sioutas' group at University of Southern California for the use of particle instrumentation unit (PIU) and electric charging facility. Data for the 405 freeway closure daytime plume study is part of a collaboration with Prof. Y. Zhu and Mr. D. Quiros at UCLA, and data for traffic on Sepulveda Blvd. was collected by Prof. Zhu's research group.

16. Expected publications from this project

Accepted/Published

1. Choi, W., M. He, V. Barbesant, K. Kozawa, S. Mara, A.M. Winer and S.E. Paulson (2012) Prevalence of Wide Area Impacts Downwind of Freeways under Pre-sunrise Stable Atmospheric Conditions. *Atmos. Environ.*, **62**, 318-327 (In press).

2. Choi, W., S.E. Paulson, J. Cassmassi and A.M. Winer (2013) Evaluating meteorological comparability in air quality studies: Classification and regression trees for primary pollutants in California's South Coast Air Basin, *Atmos. Environ.*, **64**, 150-159 (In press).

3. Quiros, D.C, Q. Zhang, W. Choi, M. He, S.E. Paulson, A.M. Winer, R. Wang, and Y. Zhu (2012) Air quality impacts of a scheduled 36-hour closure of a major highway, *Atmos. Environ.* (In press).

In Preparation

4. Choi, W., S.S. Hu, A.M. Winer, M. He, K. Kozawa, S. Mara, and S.E. Paulson (2012) Neighborhoods, roadways, and airports: Air quality benefits of emissions reductions from mobile sources.

5. Choi, W., A.M. Winer and S.E. Paulson (2012) Factors controlling pollutant plume length downwind of major roadways in nocturnal surface inversions.

6. Choi, W. and S.E. Paulson (2012) Ultrafine particle dynamics downwind of major roadways.

17. References

1. Zhu, Y.F., et al., *Penetration of freeway ultrafine particles into indoor environments.* Journal of Aerosol Science, 2005. **36**(3): p. 303-322.

2. Hu, S.S., et al., *A wide area of air pollutant impact downwind of a freeway during pre-sunrise hours.* Atmospheric Environment, 2009. **43**(16): p. 2541-2549.

3. Zhu, Y.F., et al., *Concentration and size distribution of ultrafine particles near a major highway.* Journal Of The Air & Waste Management Association, 2002a. **52**(9): p. 1032-1042.

4. Zhu, Y.F., et al., *Comparison of daytime and nighttime concentration profiles and size distributions of ultrafine particles near a major highway.* Environmental Science & Technology, 2006. **40(8)**: p. 2531-2536.

5. Zhu, Y.F. and W.C. Hinds, *Predicting particle number concentrations near a highway based on vertical concentration profile.* Atmospheric Environment, 2005. **39**: p. 1557-1566.

6. Choi, W., et al., *Development of a classification system for air pollution meterology applied to primary pollutants in the Los Angeles Air Basin.* in prep., 2012.

7. Morawska, L., et al., *Quantification of particle number emission factors for motor vehicles from on-road measurements.* Environmental Science & Technology, 2005. **39**(23): p. 9130-9139.

8. Kittelson, D.B., W.F. Watts, and J.P. Johnson, *Nanoparticle emissions on Minnesota highways.* Atmospheric Environment, 2004. **38**(1): p. 9-19.

9. Kalnay, E., et al., *The NCEP/NCAR 40-year reanalysis project.* Bulletin of the American Meteorological Society, 1996. **77**(3): p. 437-471.

10. Brunekreef, B., *Air pollution and life expectancy: is there a relation?* Occupational And Environmental Medicine, 1997. **54**(11): p. 781-784.

11. Knox, E.G. and E.A. Gilman, *Hazard proximities of childhood cancers in Great Britain from 1953-80.* Journal Of Epidemiology And Community Health, 1997. **51**(2): p. 151-159.

12. Pearson, R.L., H. Wachtel, and K.L. Ebi, *Distance-weighted traffic density in proximity to a home is a risk factor for leukemia and other childhood cancers.* Journal Of The Air & Waste Management Association, 2000. **50**(2): p. 175-180.

13. vanVliet, P., et al., *Motor vehicle exhaust and chronic respiratory symptoms in children living near freeways.* Environmental Research, 1997. **74**(2): p. 122-132.

14. Venn, A.J., et al., *Living near a main road and the risk of wheezing illness in children.* American Journal Of Respiratory And Critical Care Medicine, 2001. **164**(12): p. 2177-2180.

15. Janssen, N.A.H., et al., *The relationship between air pollution from heavy traffic and allergic sensitization, bronchial hyperresponsiveness, and respiratory symptoms in Dutch schoolchildren.* Environmental Health Perspectives, 2003. **111**(12): p. 1512-1518.

16. Li, S., et al., *Asthma exacerbation and proximity of residence to major roads: a population-based matched case-control study among the pediatric Medicaid population in Detroit, Michigan.* Environmental Health, 2011. **10**: p. 10.

17. Hoek, G., et al., *Association between mortality and indicators of traffic-related air pollution in the Netherlands: a cohort study.* Lancet, 2002. **360**(9341): p. 1203-1209.

18. Williams, L.A., et al., *Proximity to Traffic: Inflammation, and Immune Function among Women in the Seattle, Washington, Area.* Environmental Health Perspectives, 2009. **117**(3): p. 373-378.

19. Puett, R.C., et al., *Are Particulate Matter Exposures Associated with Risk of Type 2 Diabetes?* Environmental Health Perspectives, 2011. **119**(3): p. 384-389.

20. Medina-Ramon, M., et al., *Residential exposure to traffic-related air pollution and survival after heart failure.* Environmental Health Perspectives, 2008. **116**(4): p. 481-485.

21. Tonne, C., et al., *A case-control analysis of exposure to traffic and acute myocardial infarction.* Environmental Health Perspectives, 2007. **115**(1): p. 53-57.

22. Volk, H.E., et al., *Residential Proximity to Freeways and Autism in the CHARGE Study.* Environmental Health Perspectives, 2011. **119**(6): p. 873-877.

23. Ritz, B., et al., *Effect of air pollution on preterm birth among children born in Southern California between 1989 and 1993.* Epidemiology, 2000. **11**(5): p. 502-511.

24. Ren, C., et al., *Association Between Local Traffic-generated Air Pollution and Preterm Delivery in the South Coast Air Basin of California.* Epidemiology, 2008. **19**(6): p. S158-S159.

25. Hoek, G., et al., *Concentration Response Functions for Ultrafine Particles and All-Cause Mortality and Hospital Admissions: Results of a European Expert Panel Elicitation.* Environmental Science & Technology, 2010. **44**(1): p. 476-482.

26. Brugge, D., J.L. Durant, and C. Rioux, *Near-highway pollutants in motor vehicle exhaust: A review of epidemiologic evidence of cardiac and pulmonary health risks.* Environmental Health, 2007. **6: 23**.

27. Polidori, A., et al., *Effect of proximity to a freeway with heavy-duty diesel traffic on the ambient concentrations of criteria and air toxic pollutants*, in *2009 National Ambient Air Monitoring Conference*2009, the US Environment Protection Agency: Nashville, TN.

28. Karner, A.A., D.S. Eisinger, and D.A. Niemeier, *Near-Roadway Air Quality: Synthesizing the Findings from Real-World Data.* Environmental Science & Technology, 2010. **44**(14): p. 5334-5344.

29. Capaldo, K. and S. Pandis, *Lifetimes of ultrafine diesel aerosol*, in *Report for the University of Minnesota and the coordinating research council under the E-43 project diesel aerosol sampling methodology*2001, Carnegie Mellon University: Pittsburgh, PA.

30. Kozawa, K.H., S.A. Fruin, and A.M. Winer, *Near-road air pollution impacts of goods movement in communities adjacent to the Ports of Los Angeles and Long Beach.* Atmospheric Environment, 2009. **43**(18): p. 2960-2970.

31. Westerdahl, D., et al., *Mobile platform measurements of ultrafine particles and associated pollutant concentrations on freeways and residential streets in Los Angeles.* Atmospheric Environment, 2005. **39**(20): p. 3597-3610.

32. CARB, *2008 Estimated Annual Average Emissions*, 2009, California Air Resources Board: Sacramento, CA.

33. DMV, *Estimated fee-paid vehicle registrations by county, California*, 2011, DMV forecasting unit, California Department of Motor Vehicles.

34. CALTRANS, *2008 California motor vehicle stock, travel and fuel forecast, Appendix C Vehicle fuel consumption by county and fuel type*, 2009, California Deartment of Transportpation: Sacramento.

35. Quiros, D.C., et al., *Near-Roadway Air Quality Impacts of a Scheduled 36-hour Closure of a Major Highway.* . submitted 2012.

36. Choi, W., et al., *Evaluating meteorological comparability in air quality studies: classification and regression trees for primary pollutants in California's South Coast Air Basin.* Atmospheric Environment, 2012: p. under review.

37. Zhang, K.M., et al., *Evolution of particle number distribution near roadways. Part II: the 'road-to-ambient' process.* Atmospheric Environment, 2004. **38**(38): p. 6655-6665.

38. Kumar, P., et al., *Dynamics and dispersion modelling of nanoparticles from road traffic in the urban atmospheric environment-A review.* Journal of Aerosol Science, 2011. **42**(9): p. 580-603.

39. Jacobson, M.Z. and J.H. Seinfeld, *Evolution of nanoparticle size and mixing state near the point of emission.* Atmospheric Environment, 2004. **38**(13): p. 1839-1850.

40. Dillon, M.B., et al., *Chemical evolution of the Sacramento urban plume: Transport and oxidation.* Journal of Geophysical Research-Atmospheres, 2002. **107**(D5-6).

41. !!! INVALID CITATION !!!

42. CARB. *Quality Assurance Air Monitoring Site Information* 2011 [cited 2011 4/28]; Available from: http://www.arb.ca.gov/qaweb/siteinfo.php.

43. Kerminen, V.M., et al., *Development of particle number size distribution near a major road in Helsinki during an episodic inversion situation.* Atmospheric Environment, 2007. **41**(8): p. 1759-1767.

44. Hussein, T., et al., *Meteorological dependence of size-fractionated number concentrations of urban aerosol particles.* Atmospheric Environment, 2006. **40**(8): p. 1427-1440.

45. Sharma, P. and M. Khare, *Modelling of vehicular exhausts - a review.* Transportation Research Part D-Transport and Environment, 2001. **6**(3): p. 179-198.

46. Gramotnev, G., et al., *Determination of average emission factors for vehicles on a busy road.* Atmospheric Environment, 2003. **37**(4): p. 465-474.

47. Chen, H., et al., *Predicting Near-Road PM(2.5) Concentrations Comparative Assessment of CALINE4, CAL3QHC, and AERMOD.* Transportation Research Record, 2009(2123): p. 26-37.

48. Briant, R., I. Korsakissok, and C. Seigneur, *An improved line source model for air pollutant dispersion from roadway traffic.* Atmospheric Environment, 2011. **45**(24): p. 4099-4107.

49. Pasquill, F., *The estimation of the dispersion of windborne material.* The Meteorological Magazine, 1961. **90**(1063): p. 33-49.

50. Chock, D.P., *Simple line-source model for dispersion near roadways.* Atmospheric Environment, 1978. **12**(4): p. 823-829.

51. Briggs, G.A., *Diffusion estimation for small emissions*, 1973, NOAA: Oak Ridge, TN.

52. Sharan, M. and A.K. Yadav, *Simulation of diffusion experiments under light wind, stable conditions by a variable K-theory model.* Atmospheric Environment, 1998. **32**(20): p. 3481-3492.

53. Luhar, A.K. and R.S. Patil, *A GENERAL FINITE LINE SOURCE MODEL FOR VEHICULAR POLLUTION PREDICTION.* Atmospheric Environment, 1989. **23**(3): p. 555-562.

54. LaFranchi, B.W., A.H. Goldstein, and R.C. Cohen, *Observations of the temperature dependent response of ozone to NO(x) reductions in the Sacramento, CA urban plume.* Atmospheric Chemistry and Physics, 2011. **11**(14): p. 6945-6960.

55. Kittelson, D.B., W.F. Watts, and J.P. Johnson, *Fine particle (nanoparticle) emissions on Minnesota Highways., Final Report*, 2001, Minnesota Department of Transportation.

56. Durant, J.L., et al., *Short-term variation in near-highway air pollutant gradients on a winter morning.* Atmospheric Chemistry and Physics, 2010. **10**(17): p. 8341-8352.

57. Stull, R.B., *An Introduction to Boundary Layer Meteorology*1988, Dordrecht, Netherland: Kluwer Academic Publishers.

58. Quiros, D.C., et al., *Near-roadways air quality impacts of a scheduled 36-hour closure of a major highway.* Environmental Science & Technology, 2012. **under review**.

59. Moore, K., et al., *Intra-Community Variability in Total Particle Number Concentrations in the San Pedro Harbor Area (Los Angeles, California).* Aerosol Science and Technology, 2009. **43**(6): p. 587-603.

60. Krudysz, M., et al., *Intra-community spatial variability of particulate matter size distributions in Southern California/Los Angeles.* Atmospheric Chemistry and Physics, 2009. **9**(3): p. 1061-1075.

61. Turner, J.R. and D.T. Allen, *Transport of atmospheric fine particulate matter: Part 2 - Findings from recent field programs on the intraurban variability in fine particulate matter.* Journal of the Air & Waste Management Association, 2008. **58**(2): p. 196-215.

62. Hu, S., et al., *Observation of elevated air pollutant concentrations in a residential neighborhood of Los Angeles California using a mobile platform.* Atmospheric Environment, 2012: p. in press.

63. Thompson, M.L., et al., *A review of statistical methods for the meteorological adjustment of tropospheric ozone.* Atmospheric Environment, 2001. **35**: p. 617-630.

64. Horie, Y., *Air Quality Management Plan 1988 Revision, Appendix V-P: Ozone episode representativeness study for the South Coast Air Basin*, 1988: El Monte, CA.

65. Morgan, J.N. and J.A. Sonquist, *PROBLEMS IN ANALYSIS OF SURVEY DATA, AND A PROPOSAL.* Journal of the American Statistical Association, 1963. **58**(302): p. 415-&.

66. Tooke, T.R., et al., *Extracting urban vegetation characteristics using spectral mixture analysis and decision tree classifications.* Remote Sensing of Environment, 2009. **113**(2): p. 398-407.

67. De'ath, G. and K.E. Fabricius, *Classification and regression trees: A powerful yet simple technique for ecological data analysis.* Ecology, 2000. **81**(11): p. 3178-3192.

68. Hess, K.R., et al., *Classification and regression tree analysis of 1000 consecutive patients with unknown primary carcinoma.* Clinical Cancer Research, 1999. **5**(11): p. 3403-3410.

69. Dye, T.S., et al., *Guidelines for developing an air quality (ozone and PM2.5) forecasting program*, in *EPA-456/R-03-002*2003, Environmental Protection Agency, NC, U.S.A.

70. CARB. *2008 Estimated Annual Average Emissions*. 2009 [cited 2011 4/23]; Available from: http://www.arb.ca.gov/app/emsinv/emseic1_query.php?F_DIV=0&F_YR=2008&F_SEASON=A&SP=2009&F_AREA=AB&F_AB=SC&F_DD=Y.

71. Breiman, L., et al., *Classification and regression trees*1984: Wadsworth International Group, Belmont, California, USA.

72. Xu, M., et al., *Decision tree regression for soft classification of remote sensing data.* Remote Sensing of Environment, 2005. **97**(3): p. 322-336.

73. Sherrod, P.H., *DTREG predictive modeling software, Users manual*, 2010, www.dtreg.com/DTREG.pdf.

74. SCAQMD, *2012 Air Quality Management Plan (AQMP)*, 2012, South Coast Air Quality Management District: Diamond Bar, CA.

75. Zhu, Y.F., et al., *Seasonal trends of concentration and size distribution of ultrafine particles near major highways in Los Angeles.* Aerosol Science and Technology, 2004. **38**: p. 5-13.

76. Fujitani, T., *SEASONAL-VARIATION OF THE STRUCTURE OF THE ATMOSPHERIC BOUNDARY-LAYER OVER A SUBURBAN AREA.* Atmospheric Environment, 1986. **20**(10): p. 1867-1876.

77. Stoeckenius, T.E. and A.B. Hudischewskyj, *Adjustment of ozone trends for meteorological variation*, 1990, U.S. Environmental Protection Agency: Research Triangle Park, NC.

78. Pey, J., et al., *Source apportionment of urban fine and ultra-fine particle number concentration in a Western Mediterranean city.* Atmospheric Environment, 2009. **43**(29): p. 4407-4415.

79. Kumar, P., et al., *A review of the characteristics of nanoparticles in the urban atmosphere and the prospects for developing regulatory controls.* Atmospheric Environment, 2010. **44**(39): p. 5035-5052.

80. Wahlin, P., *Measured reduction of kerbside ultrafine particle number concentrations in Copenhagen.* Atmospheric Environment, 2009. **43**(22-23): p. 3645-3647.

81. Wang, Y.G., et al., *Long-term study of urban ultrafine particles and other pollutants.* Atmospheric Environment, 2011. **45**(40): p. 7672-7680.

82. Friedman, M.S., et al., *Impact of changes in transportation and commuting behaviors during the 1996 Summer Olympic Games in Atlanta on air quality and childhood asthma.* Jama-Journal of the American Medical Association, 2001. **285**(7): p. 897-905.

83. Wang, X., et al., *Evaluating the air quality impacts of the 2008 Beijing Olympic Games: On-road emission factors and black carbon profiles.* Atmospheric Environment, 2009. **43**(30): p. 4535-4543.

84. Wang, M., et al., *Use of a mobile laboratory to evaluate changes in on-road air pollutants during the Beijing 2008 Summer Olympics.* Atmospheric Chemistry and Physics, 2009. **9**(21): p. 8247-8263.

85. Wang, Y., et al., *Ozone air quality during the 2008 Beijing Olympics: effectiveness of emission restrictions.* Atmospheric Chemistry and Physics, 2009. **9**(14): p. 5237-5251.

86. Whitlow, T.H., et al., *Impact of local traffic exclusion on near-road air quality: Findings from the New York City "Summer Streets" campaign.* Environmental Pollution, 2011. **159**(8-9): p. 2016-2027.

87. Quiros, D.C., et al., *Near-roadways air quality impacts of a scheduled 36-hour closure of a major highway.* Atmospheric Environment, 2012. **under review**.

88. Zheng, M., et al., *Source apportionment of PM2.5 in the southeastern United States using solvent-extractable organic compounds as tracers.* Environmental Science & Technology, 2002. **36**(11): p. 2361-2371.

89. Houston, D., et al., *Structural disparities of urban traffic in Southern California: Implications for vehicle-related air pollution exposure in minority and high-poverty neighborhoods.* Journal of Urban Affairs, 2004. **26**(5): p. 565-592.

90. Hu, S., et al., *Aircraft Emission Impacts in a Neighborhood Adjacent to a General Aviation Airport in Southern California.* Environmental Science & Technology, 2009. **43**(21): p. 8039-8045.

91. Sabaliauskas, K., et al., *Five-year roadside measurements of ultrafine particles in a major Canadian city.* Atmospheric Environment, 2012. **49**: p. 245-256.

92. CARB, *The California diesel fuel regulations*, 2004, California Air Resources Board: Sacramento.

93. CARB, *Amendments to adopt more stringent emission standards for 2007 and subsequent model year new heavy-duty diesel engines*, 2008, California Air Resources Board: Sacramento.

94. Ristovski, Z.D., et al., *Influence of diesel fuel sulfur on nanoparticle emissions from city buses.* Environmental Science & Technology, 2006. **40**(4): p. 1314-1320.

95. Snyder, J., *They could've had a V8 - but more opt for 4*, in *Autoweek*2011, Crain Communications, Inc.

96. BOE, *Fuel Taxes Statistics & Reports*, 2012, The California State Board of Equalization: Sacramento. p. http://www.boe.ca.gov/sptaxprog/spftrpts.htm.

97. Schoenberger, R. *Upcoming fuel economy regulations expected to drive car prices higher through 2016*. 2011 2/13/2012]; Available from: http://www.cleveland.com/business/index.ssf/2011/04/upcoming_fuel_economy_regulati.html.

98. Choi, W.S., M. He, V. Barbesant, K. Kozawa, S. Mara, A.M. Winer, S.E. Paulson *Prevalence of Wide Area Impacts Downwind of Freeways under Pre-sunrise Stable Atmospheric Conditions.* 2012.

99. Long, C.M., et al., *Using time- and size-resolved particulate data to quantify indoor penetration and deposition behavior.* Environmental Science & Technology, 2001. **35**(10): p. 2089-2099.